UNIVERSITY OF LIVERPOOL

# MASS CYTOMETRY ANALYSIS OF B CELL RECEPTOR SIGNALING IN NORMAL B AND CHRONIC LYMPHOCYTIC LEUKAEMIA CELLS IN PERIPHERAL BLOOD

Thesis submitted in accordance with the requirements of the University of Liverpool for the degree of

Doctor in Philosophy

By

Faten Yasin

April,2021

# Dedication

To my Father, ‘**Captain Mansoor Yasin’**, who has always supported me throughout my life and pushed me to achieve my higher studies.

To my Mother, ‘**Eman Rashad’**, has and will always be by my side supporting me to reach my goals.

# Abstract

Chronic Lymphocytic Leukaemia (CLL) is the most common form of adult leukaemia and is characterised by accumulation of CD5+ B cells in peripheral blood (PB) and lymphoid tissues. B cell receptor (BCR) engagement plays an important role in the progression of this disease by affecting both proliferation and survival of the malignant clone. Typically, studies of BCR signaling in CLL cells have only considered whole populations of cells, and whether, or how, individual clones react has been largely ignored because of technical constraints. Mass cytometry solves these constraints with its ability to simultaneously measure more than 40 different parameters, including both cell surface and internal antigens, thereby permitting single cell resolution. The aim of this study was to use this technique to study BCR signaling in CLL with the purpose of providing insight into the relationship between such signals and individual clones. A further aim was to investigate how BCR pathway inhibitors such as ibrutinib [an inhibitor of Bruton's tyrosine kinase (BTK)] and idelalisib [an inhibitor of phosphatidylinositol 3 kinase δ (PI3Kδ)] affect BCR signaling at the single cell level. I optimised a panel of 13 surface antigens to differentiate B cells from other peripheral blood cells and examined these B cells for induced signaling using antibodies to 8 internal phospho-protein antigens. I first characterised B cell populations in peripheral blood from healthy individuals and patients with CLL; finding in the first instance that I was able to observe the normal counterpart of malignant CLL cells, the $CD5^+$ B cell, and in the second instance different subpopulations of CLL cells, including previously described older quiescent $CXCR4^+$ /$CD5^-$ (OQ cells) and newly emerged $CD5^+$/ $CXCR4^-$ (NE cells) phenotypes. I next investigated signaling in normal B and CLL cells, first by modelling my approach using Maver-1 cells, and then using primary cells. Analysis of BCR signaling in normal B cells showed that the way naïve and memory

B cells responded after anti-IgM stimulation were different, with the former having weaker responses compared to the latter. As control, class switched B cells and T cells were included in the analysis, no strong signals were recorded in these cell types despite the presence of anti-IgM antibody used to stimulate cells. FlowSOM was used to understand the relationship between expression of surface IgM and signal induction at the single cell level. This analysis showed a strong correlation between surface IgM expression and induction of protein phosphorylation. Thus, those cells with high levels of expression of surface IgM, such as memory B cells, had intense signals, whereas cells with lower levels of surface IgM had weaker. Cells which did not express surface IgM, class switched memory B cells, did not signal at all. I next investigated BCR signaling in CLL cells and found a similar relationship between surface IgM and signaling intensity. Comparison of BCR signaling between newly emerged (NE) and older quiescent (OQ) cells based on expression of CD5 and CXCR4 subclones showed that surface IgM expression was highest on CLL cells strongly expressing $CXCR4^{+}/CD5^{+}$ and $CD5^{+}/ CXCR4^{-}$ (NE cells). These were the same cells which responded to BCR engagement. In contrast, cells which were weak for CD5 (OQ cells) also had weak expression of surface IgM and did not readily respond to BCR stimulation. In my thesis I concentrated to study sIgM in both normal B and CLL B cells, first it is expressed in early formation of B cell differentiation in immature B cells after VDJ recombination and it is highly expressed in most CLL cases, UM-CLL compared to M-CLL. Studies have shown, surface IgM expression is more variable than IgD expression. This variance is correlated more with the clinical and biologic outcome response in CLL. sIgM promotes to increase survival and proliferation of mature B cells in the germinal centre and has found to be integrated with CXCR4 and IL-4, that results in BCR signaling to be the main driver to disease outcome.

Investigation of the effects of ibrutinib showed that selected nodes within subclones, $CXCR4^{+}/CD5^{+}$ and $CD5^{+}/ CXCR4^{-}$ populations could be identified where BCR signals were not impaired by the presence of this inhibitor, pointing to the usefulness of mass cytometry as a tool to study clonal evolution and disease resistance to therapy in CLL. Taken together, these results demonstrate my ability to use mass cytometry to measure BCR signaling in individual B cells. My findings therefore provide a foundation with which to study this phenomenon as well as others (such as gene transcription) in normal and malignant haemic cells in health and disease.

# Declaration

I, Faten Yasin declare that the entire data presented in this thesis is a result of my own work and effort and was generated from the experiments that I have performed during my work in this project. This was carried out in the laboratory of Professor Joseph Slupsky, Department of Molecular and Clinical Cancer Medicine, Institute of Translational Medicine, University of Liverpool, Liverpool, UK.

Faten Yasin
2021

# Acknowledgements

First, I want to thank my primary supervisor Professor Joseph Slupsky for giving me the chance to join his research team. He has provided me a lot of support, guidance and knowledge throughout my study.

Second, I thank Dr Andrew Duckworth and Professor Nagesh Kalakonda for continuous support, encouragement and supervision through my PhD laboratory work. Also, Dr Kathleen Till, Professor Andrew Pettit, Dr Ke Lin and all the Haematology and Leukaemia department, loads of appreciation for all the kind support and guidance that helped me till the end of my PhD.

Last, I want to thank Dr Sandra Cachinho for her unconditional help and support during my PhD studies.

# Table of Contents

# List of Figures

# List of Tables

# Abbreviations

| | |
|---|---|
| **ACCENSE** | Automatic Classification of Cellular Expression by Nonlinear Stochastic Embedding |
| **AID** | Activation-induced cytosine deaminase |
| **AKT** | Activation of Kinase Protein B |
| **ANN** | Artificial neural network |
| **APS** | Ammonium persulphate |
| **BAD** | BCL2 associated agonist of cell death |
| **BAFF** | B cell-activating factor |
| **BAFF-R** | B-cell activating factor receptor |
| **BC** | Barcoding |
| **BCL10** | B-cell Lymphoma/Leukaemia 10 |
| **BCR** | B cell receptor |
| **BFCA** | Bi-functional chelating agent |
| **BLNK** | B cell-linker |
| **BM** | Bone marrow |
| **BS3** | bis(sulfosuccinimidyl)suberate |
| **BSA** | Bovine serum albumin |
| **BTK** | Bruton's tyrosine kinase |
| **CARD11** | Caspase recruitment domain-containing protein 11 |
| **CITRUS** | Cluster identification, characterization, and regression |
| **CLL** | Chronic Lymphocytic Leukaemia |
| **CLP** | Common Lymphoid progenitor cells |
| **CML** | Chronic Myeloid Leukaemia |
| **CMP** | Common Myeloid progenitor |
| **$CO_2$** | Carbon dioxide |
| **CSR+** | Class-switch recombination |
| **CXCL12** | C-X-C motif chemokine 12 |
| **CXCR4** | C-X-C chemokine receptor type 4 |
| **CyTOF** | Cytometry by Time Of Flight |
| **DAG** | Diacylglycerol |
| **DMSO** | Dimethyl sulfoxide |
| **DNA** | Deoxyribonucleic acid |
| **DOTA** | Dodecane tetraacetic acid |
| **DTPA** | Diethyl-enetriaminepentaacetic acid |
| **Dy** | Dysprosium |
| **EDTA** | Ethylenediaminete-traacetic acid disodium salt dihydrate |
| **EMT** | Elemental mass tags |
| **Er** | Erbium |

| | |
|---|---|
| **ERK** | Extracellular Signal-Regulated kinases |
| **Eu** | Europium |
| **FCB** | Fluorescent cell barcoding |
| **FcγRIIb** | Fc gamma receptor II b |
| **FCS** | Fetal calf serum |
| **FCS file** | Flow Cytometry Standard |
| **FITC** | Fluorescein isothiocyanate |
| **FL** | Fetal liver |
| **FO** | Follicular |
| **FoxP3** | forkhead box P3 |
| **FSC** | Forward side scatter |
| **GC** | Germinal center |
| **Gd** | Gadolinium |
| **GL** | Germline layer |
| **GSK3beta** | Glycogen synthase kinase 3 beta |
| **GTP** | Guanosine-5'-triphosphate |
| **H** | Hour |
| **$H_2O$** | 2 hydrogen and 1 oxygen |
| **$H_2O_2$** | Hydrogen Peroxide |
| **Ho** | Holmium |
| **HRP** | Horseradish peroxidase |
| **HSC** | Haematopoietic stem cells |
| **ic-CSB** | ice cold cell staining buffer |
| **ICP** | Inductively coupled plasma |
| **Ig** | Immunoglobulin |
| **IgA** | Immunoglobulin A |
| **IgD** | Immunoglobulin D |
| **IgE** | Immunoglobulin E |
| **IgG** | Immunoglobulin G |
| **IGHV** | Immunoglobulin variable heavy chain |
| **IgM** | Immunoglobulin M |
| **IL4** | Interleukin 4 |
| **IP3** | Inositol trisphosphate |
| **Ir** | Iridium isotopes |
| **ISH** | In situ hybridization |
| **ITAM** | Immunomodulatory tyrosine activation motifs |
| **iwCLL** | International workshop on Chronic Lymphocytic Leukaemia |
| **JNK** | c-Jun N-terminal kinases |
| **KNN** | k-nearest neighbor graphing |
| **KU** | Thousand Units |

| | |
|---|---|
| **LCA** | Leukocyte antigen |
| **Ln** | Lanthanide |
| **Lu** | Lutetium |
| **LYN** | Lck/Yes novel tyrosine kinase |
| **M-CLL** | Mutated CLL |
| **MALT1** | Mucosa-associated lymphoid tissue lymphoma translocation protein 1 |
| **MAPK** | Mitogen-activated protein kinase |
| **MCB** | Mass tag cell barcoding |
| **mg** | Milligram |
| **μg** | Microgram |
| **$MgSO_4$** | Magnesium sulphate |
| **MHC II** | MHC class II major histocompatibility complex II |
| **min** | Minutes |
| **ml** | millilitre |
| **mM** | milli Molar |
| **mRNA** | Messenger Ribonucleic acid |
| **MSAPK** | Mitogen stress-activated protein kinase |
| **MST** | Minimal spanning tree |
| **mTOR** | Mammalian target of rapamycin |
| **MZ** | Marginal zone B cells |
| **Nabs** | Natural antibodies |
| **Nd** | Neodymium |
| **NE** | Newly emerged |
| **NF-κB** | Nuclear factor kappa-light-chain-enhancer of activated B cells |
| **NHS** | National Health Service |
| **NK** | Natural Killer cells |
| **nM** | Nanomolar |
| **OQ** | Older quiescent |
| **PBMCs** | Peripheral blood mononuclear cells |
| **PBS** | Phosphate-buffered saline |
| **PCA** | Principle components analysis |
| **Pd** | Palladium |
| **PDK1** | Pyruvate dehydrogenase lipoamide kinase isozyme 1 |
| **PE** | Phycoerythrin |
| **PFA** | Paraformaldehyde |
| **PH** | Pleckstrin homology domain |
| **PI3Kδ** | Phosphoinositide 3-kinase delta |
| **PIP2** | Phosphatidylinositol 4,5 bisphosphate |
| **PIP3** | Phosphatidylinositol 3,4,5 trisphosphate |
| **PKC** | Protein kinase C |

| | |
|---|---|
| **PLAYR** | Proximal Ligation Assay for RNA |
| **PLCγ2** | phospholipase Cγ2 |
| **Pr** | Praseodymium |
| **pS6** | Ribosomal protein phospho S6 |
| **Pt** | Platinum isotope |
| **PTP-1** | Phosphatases tyrosine phosphatase-1 |
| **PTPN22** | Protein tyrosine phosphatase nonreceptor type 22 |
| **PVDF** | Polyvinlydiene diflouride |
| **Raf** | Rapidly Accelerated Fibrosarcoma |
| **RAG** | Recombination activation gene |
| **RasGRP1** | Guanyl nucleotide-releasing protein guanyl-releasing protein |
| **RCA** | Rolling circle amplification |
| **RNA** | Ribonucleic acid |
| **RPMI** | Roswell Park Memorial Institute |
| **RT** | Room temperature |
| **SDS-PAGE** | Sodium dodecyl sulphate polyacrylamide gel electrophoresis |
| **SFKs** | Src-family kinases |
| **SH2** | Src homology 2 |
| **SHM** | Somatic hypermutation |
| **SHP-1,2** | SH2 domain-containing phosphatidyl 5-phosphatase -1 and -2 |
| **Sm** | Samarium |
| **SNE** | Stochastic neighbor embedding |
| **SOM** | Self-Organizing Map |
| **SPADE** | Spanning-tree Progression Analysis of Density-normalised Events |
| **SSC** | Side-scattered light |
| **SYK** | Spleen tyrosine kinase |
| **T-BST** | Tween-Tris saline buffer |
| **TAK1** | Transforming growth factor-beta-activated kinase 1 |
| **Tb** | Terbium |
| **TCEP** | Tris-(2-carboxyethyl)phosphine hydrochloride |
| **TEMED** | Tetramethylethylenediamine |
| **TOF** | Time Of Flight |
| **tSNE** | t-distributed stochastic neighbor embedding |
| **UK** | United Kingdom |
| **UM-CLL** | Unmutated CLL |
| **USA** | United States of America |
| **viSNE** | Visualization stochastic neighbour embedding |
| **VJD** | Variable(V), Joining (J) and Diversity (D) genes |
| **Yb** | Ytterbium |
| **ZAP-70** | zeta-chain associated protein kinase 70 |

| | |
|---|---|
| **µl** | Micro litre |
| **µM** | Micro molar |

# Chapter 1: Main Introduction

## 1.1 Overview

In the process of tumorigenesis factors such as genetic mutation, epigenetic change and microenvironment combine to create heterogeneous populations of malignant cells where outgrowth of a dominant clone is governed by favourable conditions created by these factors [1, 2]. Such heterogeneity within tumours contributes to the resistance of cancers to therapy because as the conditions that favour the growth of one population of malignant cells changes, new conditions that are created may favour the outgrowth of another [3]. For example, mutations within TP53 can confer resistance to DNA damaging therapies, such as fludarabine and cyclophosphamide, or enhance metabolic switch to glycolysis on to CLL cell clones to give them growth advantage [4]. Outgrowth of dominant clones in CLL can have a different phenotype that is based on particular genetic mutations that potentially could be detected using flow cytometry and other tools that include lineage tracing to understand the dynamics of this outgrowth. This is particularly applicable to the malignant cells of chronic lymphocytic leukaemia (CLL), a haemic cancer that has no conventional cure because of this adaptability. Understanding clonal heterogeneity in CLL requires ability to analyse the malignant cells of this disease at single cell resolution. Here I offer multidimensional (phenotype/signalling) characterisation with unprecedented parallelisation[5]. Conventional flow cytometry is one tool where light is used to discriminate single cells, which is by only forward scatter (FSC) and side scatter (SSC) and for the rest its fluorescently labelled antibodies and detect the presence of features such as cell size, surface antigen expression, markers of cell division, *et cetera*. The power of conventional flow cytometry is demonstrated by its use a “gold

standard” technique in the study of immune cells in health and disease[6]. However, conventional flow cytometry is burdened with limitations based on the fluorochromes that are used for detection reagents where physical properties, such as spectral overlap, result in the need to perform compensation algorithms that can lead to significant background noise and generate inaccurate results. This limitation becomes increasingly cumbersome when the dimensionality of a given experiment also increases. Thus, at the beginning of this thesis the most advanced conventional flow cytometer, the Becton Dickinson LSR-Fortessa™, was only able to measure 18 parameters on a simultaneous basis. Mass cytometry, the basis of which will be discussed later in this Chapter, was developed to address this problem of limited dimensionality. The use of heavy metal conjugated reagents allows this technique the ability to expand detection to over 40 biomarkers to allow more precise ability to examine single cell phenotype without the constraints of significant spectral overlap. This thesis applies mass cytometry to the study of normal and CLL B cell phenotypes to study clonal heterogeneity among single cells and build a basis for the understanding of evolution in cancer.

## 1.2 B cell development

### 1.2.1 B cell differentiation

Our body has several defence mechanisms to defend us against foreign pathogens pathogens in the environment [7]. These defence mechanisms, our immunity, are either innate and respond immediately to foreign antigen, or are adaptive where initial semi-specific activation is followed by more exact targeting of the offending body so that it can be efficiently removed. Importantly, this adaptive immunity also records memory against any foreign antigen so that repeat infections can be minimised [8]. Making up our immunity is a complex of five different cell types which work together

to create a defence shield against any pathogen. Known as white blood cells, these five cell types are made up of neutrophils, monocytes, eosinophils, basophils, and lymphocytes (Figure 1.1). The former four cell types have an innate immunity function, whereas lymphocytes can also take on the adaptive immune function.

Regardless of their differing function in the immune system, neutrophils, monocytes, megakaryocyte, eosinophils, basophils, and lymphocytes can be identified on the basis of surface antigen expression where antibodies can be used as reagents to accomplish this task. Nevertheless, these cells originate, indeed like all cells of the blood, from haematopoietic stem cells which are pluripotent (Figure 1.1). These cells reside in the bone marrow where they differentiate into common myeloid or lymphoid progenitor (respectively CMP and CLP) cells, and from this point on lose the ability to self-renew in terms of reconstituting the blood. In terms of myeloid lineage cells, differentiation to neutrophils, monocytes, eosinophils, basophils, red blood cells and platelets from CMP cells occurs along pathways that are described elsewhere [9] as this is not relevant to this thesis. Lymphoid cells, such as B, T and Natural Killer (NK) cells, derive from CLP cells (Figure 1.1) where expression of Ig genes coding for the B or gene coding for $\alpha/\beta$ or $\gamma/\delta$ chains of T cell receptors dictate differentiation of CLP to pro-B and pro-T cells, respectively [10]. This thesis is focussed on B cells, both normal and the malignant cells of CLL, and therefore differentiation of B cells will be more fully described. Differentiation of T and NK cells is not relevant to this thesis and is described elsewhere [11].

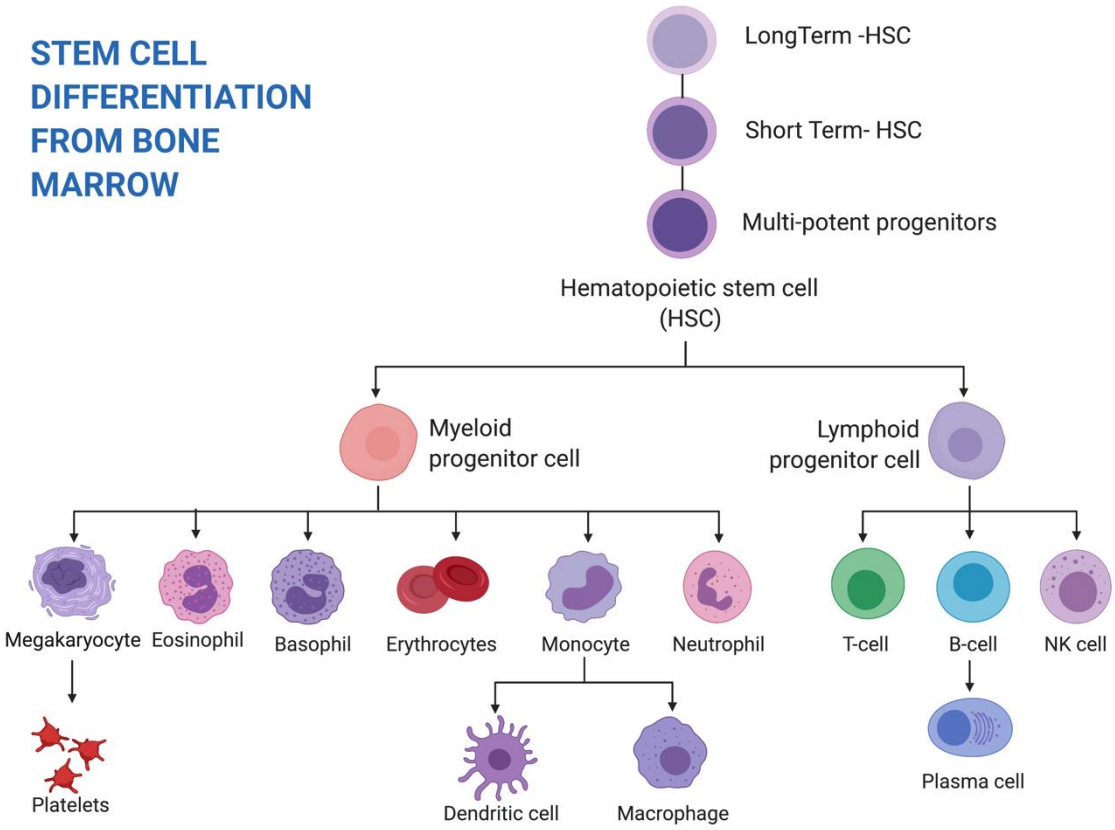


**Figure 1. 1 Stem cell differentiation diagram.** The normal development of hematopoietic stem cell and differentiation in normal healthy individuals. This figure was created using Biorender.com.

B cell differentiation begins with expression of the immunoglobulin (Ig) gene coding for the heavy chain of the B cell receptor within CLP cells [12]. These cells now become pro-B cells and concomitant expression of recombination-activation genes (RAG) stimulate recombination of the Ig gene such that the parts coding for the antigen-binding domain, the variable(V), Joining (J) and Diversity (D) genes, recombine to create an intact protein that is expressed as the pre-BCR that ultimately forms surface IgM[13, 14]. Once intact heavy chain Ig is expressed by pro-B cells, differentiation is then allowed to progress to pre-B cells [15-17]. Where Ig gene responsible for the light chain of the BCR are expressed and undergo the recombination as the heavy chain Ig [18]. The appearance of surface IgM, as the BCR,

on the surface of developing B cells in the bone marks them as immature B cells. Here BCR engages with the environment and where strong stimulation occurs, the B cells undergo apoptosis in order to remove self-reactive cells. This is known as the first immunological checkpoint. If BCR on immature B cells engages weakly with the environment, these cells become anergic and eventually die in the periphery. Finally, those cells which receive no signal from their BCR emerge from the bone marrow as naïve transitional B cells that go to the spleen and other secondary lymphoid organs where contact with foreign antigen stimulates further differentiation.

Peripheral B cells “see” antigen in two contexts; the first being in peripheral circulation or tissues where cognate foreign antigen is recognised by their BCR, the second context is when B cells naturally transit the lymphoid organs and come into contact with antigen-presenting cells that they then recognise by their BCR. Regardless of this context, BCR with antigen is internalised by the B cell, and then antigen is re-expressed as a peptide for display in conjunction with the MHC class II proteins. Activated B cells move to/remain in lymphoid organs where they come into contact with cognate CD4+ T cells which recognise the antigen-MHC class II configuration that is displayed by the B cell. These CD4+ T cells become themselves activated and are induced to express CD40 ligand (CD154) and interleukin 4 (IL4), which together act to stimulate the B cell to proliferate and further differentiate [19]. B cell interaction with CD154 and IL4 induces expression of activation-induced cytosine deaminase (AID) which then acts to mutate nucleotide residues coding for the antigen-binding domains of both heavy and light chain Ig genes in a process called somatic hypermutation. The ultimate goal of this process is to generate highly-specific antigen recognition (so-called affinity maturation) by the BCR through selection of reactive clones and then AID causes class switch of the gene coding for heavy chain Ig so that the IgM/IgD

configuration present on follicular B cells changes to IgG, IgA or IgE to diversify immune response to pathogen. Once affinity maturation is complete, B cells can then further differentiate into memory cells, or to the soluble antibody-producing plasma cells.

Each of these stages of B cell development through germinal centres is marked by change in expression of surface antigens on differentiating cells as is illustrated in Figure 1.2. Thus, transitional B cells enter germinal centres and differentiate to either follicular (FO) or marginal zone (MZ) B cells depending on the strength of BCR engagement they experience. MZ B cells ultimately differentiate to short-lived plasma cells for provide innate antibodies for immune defence, whereas FO B cells undergo affinity maturation as described above to generate memory B cells and long-lived plasma cells so that adaptive immune memory is maintained. Analysing this change in surface antigen expression requires ability to measure in multiple dimensions. For example, FO B cells have the phenotype $IgM^{low}$ $IgD^{+}$ $CD21^{+}$ $CD23^{+}$, MZ B cells are characterized with a phenotype of $IgM^{+}$ $IgD^{low}$ $CD27^{+}$ $CD21^{+}$ $CD23^{-}$, and class-switched memory B cells have a phenotype of $IgG^{+}$/$IgA^{+}$ $CD27^{+}$ $CD21^{+}$ $CD23^{-}$. The type of measurement that is required is typically performed using flow cytometry, and this technique will be described later in this thesis. Nevertheless, simultaneous measurement of all B cell phenotypes is not generally done because of limitations of conventional equipment to perform this analysis.

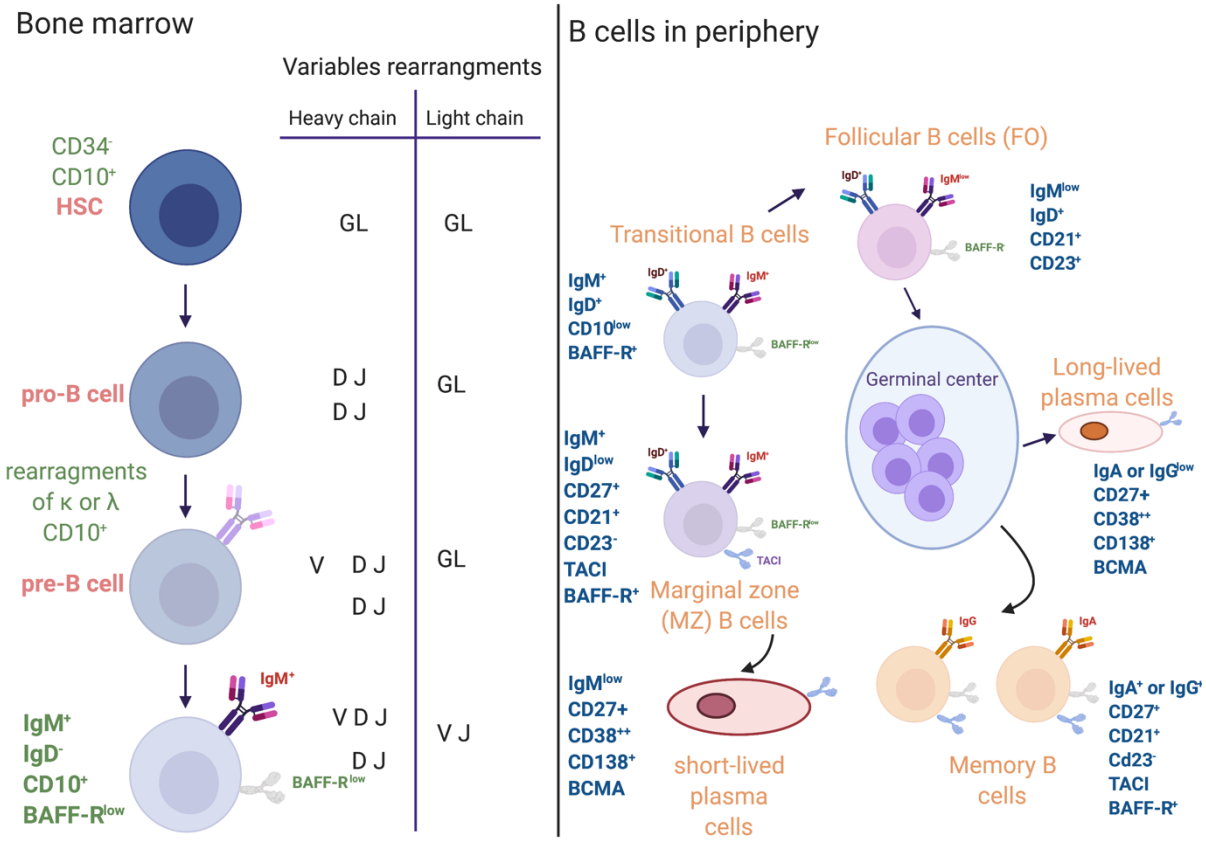


**Figure 1. 2 B cell differentiation and B cell subsets.** B cell differentiation and B cell subsets. B cells develop in the bone marrow from haematopoietic stem cells (HSC). Rearrangement of variable, joining and diversity genes by recombination activated genes (RAG) starts at the pro-B cell stage. After RAG rearrangement is successfully done, this leads to the pre-B cell stage where intact IgM is formed and expressed on the surface of the developing B cell. This process repeats for the immunoglobulin light chain, completion of this process promotes differentiation to the immature B cell stage. Here B cells expressing auto-reactive BCR are removed or altered by the mechanisms of immunological tolerance. Finally, naïve, transitional, B cells emerge from the bone marrow and move to the secondary lymphoid organs (spleen and lymph nodes) in the periphery to find cognate antigen. Recognition of cognate antigen promotes activation and further differentiation into MZ B cells or FO B cells depending on the BCR signal and T cell help. MZ B cells can develop into short-lived plasma cells to secrete antibody, and FO B cells develop in the germinal center (GC) with the support of T helper cells, undergoing affinity maturation and immunoglobulin class switch, and eventually emerge as either memory B cells or long-lived plasma cells. This figure was created using Biorender.com and was inspired by Pieper *et al* [20].

### 1.2.2 Origins of CD5+ B cells in mice and humans.

In mice there are two distinct B cell subsets, B-1 and B-2 cells. Whereas B-2 cells are recognised for their role in adaptive immunity, the differentiation of which is described above, B-1 cells have a role in innate antibody response to pathogen. A further difference between B-1 and B-2 cells is the former reside mainly in pleural and peritoneal spaces where they provide their innate immune function. As such the origin of B-1 B cells is controversial; on one hand, this B cell type develops during embryogenesis when haematopoiesis takes place within the fetal liver so that it becomes the most prevalent B cell type at birth [21]. After birth, B-1 cell populations decrease as adaptive immunity and B-2 cell populations expand. On the other hand, B-1 B cell populations can be reconstituted from bone marrow transplant, suggesting that these cells can arise during normal haematopoiesis in adults. Figure 1.3 illustrates the development pathway of B-1 and B-2 B cells where the former arises during embryogenesis.

In literature mouse B-1 cells have two distinct phenotypes, B-1a and B-1b. The difference between them is the expression of the T cell marker CD5; this is expressed on B-1a but not on B-1b cells [22]. B-1 B cells are responsible for the production of polyreactive natural antibodies (Nabs) which play a major role in protection against specific pathogens such as commensal bacteria and provides systemic homeostasis[23]. As such, the antigen-binding region of BCR expressed on B-1 cells arises from distinctive “stereotypic” IGHV genes and particular D-J rearrangements to yield polyreactive specificity [21]. B-1 cells derived from the fetal liver are said to have self-renewing capability within the pleural and peritoneal cavities [24] where they account for 35-70% of total lymphocytes. In the blood B-1 cells make up 0.3-0.5% of

total lymphocytes [24] and of 0.2-1% of total lymphocytes in the spleen and other lymphoid organs[25].

The B-1 cell phenotype has been identified: in mice this phenotype is marked by $CD19^{hi}$ $CD23^{-}$ $CD43^{+}$ $IgM^{hi}$ $IgD^{dim}$ and $CD5^{\pm}$ [26], in humans the phenotype is similar being $CD19^{+}$ $CD20^{+}$ $CD43^{+}$ $IgM^{hi}$ $IgD^{dim}$ where CD5 positivity is necessary to clearly identify this B cell subpopulation in peripheral blood. Recently, a connection has been made between human CD5+ B cells and CLL, where the malignant cells of this disease show gene expression patterns that resemble the former [27]. This paper also identified a new CD5+ B cell subset, one that is also CD27+, suggesting that, in humans, these CD5+ B cells can also hold memory [28, 29].

In human adults CD5+ B cells account for less than 1% of total B cells in peripheral blood [30]. However, this proportion changes with age and there is a propensity after the $5^{th}$ decade of life for clonal expansion of CD5+ B cells, a condition known as monoclonal B lymphocytosis [31, 32]. Since CLL in humans and mice develops from an expansion of CD5+ B cells [33], understanding the function of CD5+ B cells may give insight into the origins of CLL cells. At the beginning of this thesis, were only a few studies which isolate CD5+ B cells for study, so our understanding of how these cells respond to BCR crosslinking is limited. Moreover, there are populations of circulating B cells that are responsible for some types of autoimmune disease [34]. These B cells emerge from bone marrow and are not responsive to BCR engagement because of anergy. Phenotypically these cells have been shown to down regulate sIgM and CD22. Functionally, these cells can be released from anergy by contact with BAFF and can contribute to the development of autoreactive naïve B cells in SLE [35]. Moreover, we also do not understand how these cells are affected by new treatments for malignant disease such as ibrutinib and idelalisib which I will discuss later in this

thesis when I describe the pathogenesis of CLL. A potential solution would be to use techniques for study which do not rely on purification of CD5+ B cells for study, such a technique could involve flow cytometry as I will discuss later.

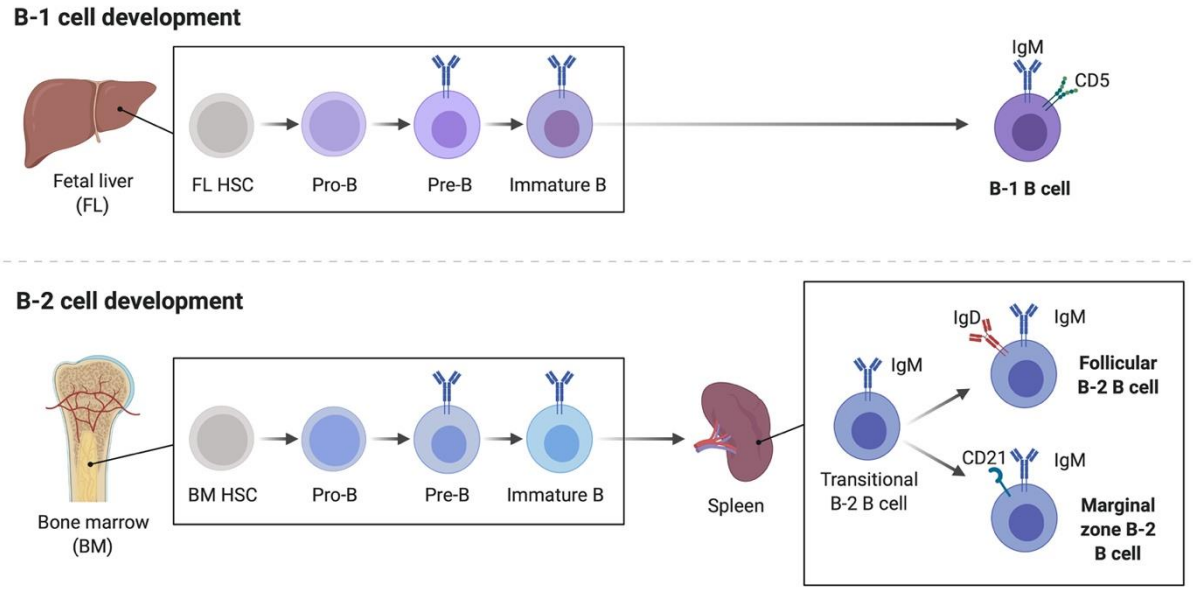


**Figure 1. 3 B cell development demonstration differentiation in B-1 and B-2 systems.** The B-1 differentiation occurs in the fetal liver (FL) lineage pathway that starts from the FL hematopoietic stem cell (HSC) and continue to maturate to pro-B cell, pre-B cell and immature B cells where IgM is formed at that stage. B-1 B cells are developed after leaving the FL which have an activated surface IgM and $CD5^{+}$ cells. B-2 cells are differentiated from the bone marrow (BM) and are further differentiate into the spleen to maturate into transitional B-2 B cells, into FO B cells and MZ B cells.

### 1.3 Chronic Lymphocytic Leukaemia (CLL)

Chronic Lymphocytic Leukaemia (CLL) is the most common leukaemia in the western world. The disease affects elder individuals, diagnosis of this condition occurs mainly in individuals who are 70 years and above [36], and results from the detection of abnormal numbers of mature B lymphocytes in blood bearing a phenotype of $CD19^{+}$, $CD5^{+}$, $CD23^{+}$, $CD22^{-}$, $CD79B^{-/+}$, surface immunoglobulin $^{-/+}$ of IgM/IgD and $FMC7^{-/+}$[37].

#### 1.3.1 Pathogenesis of CLL

CLL is a heterogeneous disorder where some patients have disease that remains stable for many years, so-called indolent disease, whereas others have disease which is progressive and succumb quickly to suppression of lymphoid and bone marrow function by the expanding malignant clone [38]. Based on the phenotypic diagnosis as per the international workshop on Chronic Lymphocytic Leukaemia (iwCLL) guidelines TP53 mutation, molecular cytogenetic and immunoglobulin variable heavy chain (IGHV) should always be part of the baseline evaluation in every CLL patient so that potential prognosis can be assessed [39]. Sequencing of the IGHV genes is an important feature in the determination of potential prognosis because cases which show less than 2% mutation from germline sequences have poorer prognosis (so-called unmutated CLL, UM-CLL) whilst those that show greater than 2% mutation from germline sequences (so-called mutated CLL, M-CLL) have better prognosis [40, 41]. ZAP70 and CD38 are as well considered to be part of the diagnostic outcome prediction [42-46]. Despite evidence that these prognostic markers identify patients with progressive disease, initial diagnosis results in a “watch and wait” strategy where decision to treat is based on lymphocyte doubling time [47].

The first evidence that distinguished between indolent and progressive disease was that mutation of the IGHV genes were linked to prognosis; M-CLL good prognosis (indolent disease), UM-CLL poor prognosis (progressive disease) [40, 41]. Further study revealed that unrelated CLL patients could share the stereotyped BCR structure in terms of IGHV genes in their respective affected cells [48], and the recognition that only certain IGHV genes were used, and that certain genes, such as IGHV3-21, were associated with particularly aggressive disease[49]. Finally, work from Nicholas Chiorazzi's group showed that BCR expressed on UM-CLL cells was polyreactive to self-antigens whereas that on M-CLL cells was more specific [50]. Together, this work demonstrated a clear role for BCR in the pathogenesis of CLL, and that it plays a major role in driving progression of the disease. There are other contributing factors to the pathobiology of CLL, such as interaction with the tissue microenvironment to receive signals that help with survival and proliferation [36], chromosomal aberration which marks disease as being more resistant to chemotherapies [51], and certain gene mutations (NOTCH1, NFKBIE and SF3B1) which contribute to increased proliferation of the malignant clone [49]. However, among all these contributing factors, BCR is the most important and therapies targeting the signaling pathway emanating from this receptor are now being introduced into the clinic with relative success.

### 1.3.2 B-Cell Receptor Signaling

#### 1.3.2.1 B Cell Receptor signaling (BCR) in normal B cells

In CLL, BCR is one of the main contributors to disease progression. To understand how signals from this receptor contribute to disease progression, I will first review our current understanding of BCR signaling in normal B cells.

On normal B cells, surface immunoglobulin (Ig) can take the immunoglobulin class of either IgM, IgD, IgG, IgA, or IgE. In CLL, the malignant cells express mainly surface IgM and IgD, but some clones can express IgA and IgG. For the purposes of this section, I will only deal with what is known about surface IgM signaling.

Figure 1.4 illustrates the proximal and distal elements of the BCR signaling pathway. Surface IgM that forms the antigen recognition part of the BCR is in association with the disulphide-linked heterodimer proteins Igα/Igβ (CD79A/ CD79B)[52]. These proteins are also transmembrane and contain immune-receptor tyrosine-based activation motifs (ITAMs) which is where the signaling starts. When BCR is engaged and cross-linked by antigen, the ITAMs in Igα/Igβ become phosphorylated by Lyn, a tyrosine kinase[53, 54]. This creates a binding site for SYK (spleen tyrosine kinase), which binds phosphorylated Igα/Igβ through its SH2 domains and then, in turn, becomes activated. Active SYK then phosphorylates the scaffold protein B cell-linker (BLNK), which then serves to recruit Bruton's tyrosine kinase (BTK) and phospholipase Cγ2 (PLCγ2) to the developing signalosome. Concomitantly, activated Lyn also phosphorylates CD19 to create binding sites for the p85α subunit of Phosphoinositide 3-kinase δ (PI3K δ) and the RhoGTPase VAV[55]. The binding of the p85α subunit to phospho-tyrosine residues activates the associated catalytic p110δ subunit of PI3K to convert phosphatidylinositol 4,5 bisphosphate (PIP2) to phosphatidylinositol 3,4,5 trisphosphate (PIP3) in the membrane[56]. PIP3 acts to recruit other signaling proteins to the membrane through interaction with the pleckstrin homology (PH) domain within each one. These proteins include BTK, PLCγ2, VAV, PDK1 and AKT among others[57]. The close association of BTK and PLCγ2 through their interaction with BLNK and PIP3 activates BTK to phosphorylate PLCγ2 and

stimulate its enzymatic function to convert PIP2 to inositol trisphosphate (IP3) and diacylglycerol (DAG)[58]. These latter signaling molecules function to induce calcium release from intracellular stores and activation of protein kinase C, which is ultimately involved in activation of the NFkappaB, and JNK pathways through its ability to phosphorylate the CARD11/BCL10/MALT1 complex and stimulate the activity of TAK1 [59]. The released DAG also interacts with a RasGTPase (RasGRP1) to generate GTP-loaded Ras, which then acts to activate the Raf-MEK-ERK (MAPK) pathway[60]. Recruitment of AKT and PDK1 to the membrane by PIP3 results in the activation of AKT which is responsible for mediating growth (through activation of mTOR), pro-survival (through phosphorylation of GSK3beta) and anti-apoptotic through phosphorylation of BCL2 associated agonist of cell death (BAD) processes within cells [61].

Importantly, much of what we know about signaling in cells has been determined through the use of antibodies recognising phosphorylated motifs on proteins. Thus, antibodies recognising phospho-ERK and phospho-AKT are commonly used to determine activation of the MAPK and AKT pathways, respectively. Most of these phospho-specific antibodies have been used in Western blot applications, but there are some that can be used in flow cytometry.

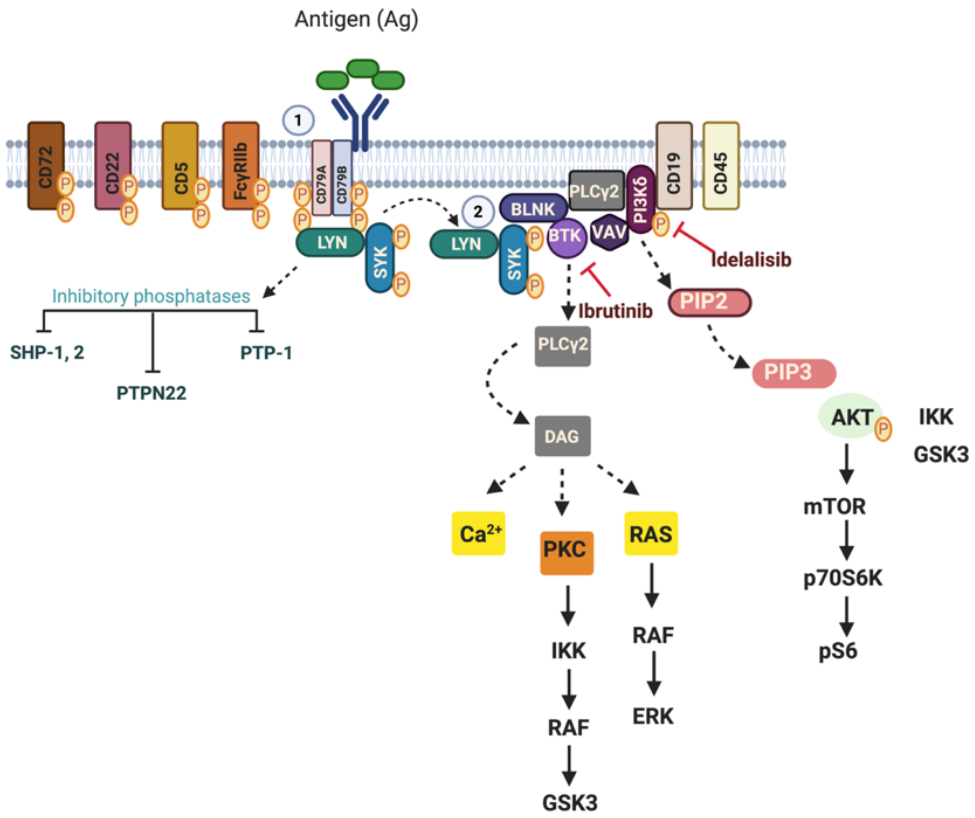


**Figure 1. 4 BCR signaling in CLL with downstream pathways.** After antigen binding, BCR signaling pathway starts to activate a group of kinases and proteins at the sIg composed of SYK, LYN, BLNK, BTK and PLCγ2 and PI3Kδ signaling pathways begins further phosphorylation. BCR signals further downstream components for further distal signaling to be activated. CD22, CD5, CD72 and FcγRIIb are negative regulators that are responsible to manage the BCR signaling intensity after LYN phosphorylation that leads to recruitment of inhibitory phosphatases tyrosine phosphatase-1 (PTP-1), SH2 domain-containing phosphatidyl 5-phosphatase-1 and -2 (SHP-1,2), and protein tyrosine phosphatase nonreceptor type 22 (PTPN22).This figure was created using Biorender.com and inspired from Wiestner *et al* [62] and G.Packham *et al* [58]**.**

#### 1.3.2.2 CLL BCR signaling

The model of BCR signaling described above is largely applicable CLL cells, however, the response of CLL cells to BCR engagement is heterogeneous in magnitude and sustainability. It is well known that the malignant cells from some patients respond very well to BCR engagement, whereas others do not respond at all. Whilst it is known that the strength of BCR-induced signaling correlates with surface expression of IgM, and this, in turn, is related to disease outcome, studies investigating BCR signaling in CLL cells have used techniques which derive information on entire populations of cells which are assumed to be homogeneous in terms of surface expression of IgM. This point is important because much of what we know about BCR signaling is derived from cell lines where surface expression of BCR is high and constant, so it is not clear how surface expression of BCR affects the different pathways described above. This point is also important to CLL because of the introduction of BCR pathway inhibitors targeting BTK and PI3K$\delta$. These inhibitors have largely effective in the treatment of CLL, but development of disease resistance to these therapies is still a problem. One described mechanism of resistance to BTK inhibition is mutation of BTK (C418S) and of PLC$\gamma$2 (R665W, L845F and S707Y)[63], but resistance to ibrutinib can occur independently of these mutations. A potential hint of this independent mechanism is illustrated in the work of Hernandez *et al*. [64] where incubation of CLL cells with IL4 stimulates expression of surface IgM and results in maintenance of BCR-induced calcium flux in the presence of ibrutinib or idelalisib. If CLL cell populations are phenotypically heterogeneous in patients (as indeed they are on a genetic basis), this work of Hernandez *et al*. [64] suggests that clones could be present within patient samples that are already resistant to ibrutinib prior to the beginning of therapy.

Identification of such clones would require methods that would identify individual single cells for study.

#### 1.3.2.3 CLL B cells life cycle

CLL cells live in microenvironment that supports survival by mesenchymal stromal cells, monocyte-derived nurse-like facilitating pro-survival signal, proliferation and growth lymphoid organs and bone marrow [38, 65, 66]. In addition to the BCR signaling that occurs mainly within tissue sites (LN, BM). This can lead to an outgrowth of aggressive resistant subclones that can have different phenotype and characteristics with genomic abnormalities [67] and CLL intraclonal complexity that can be highlighted by the variable expression of CXCR4 and CD5 [68]. The CLL B cells can be divided into $CXCR4^{bright}$ and $CD5d^{im}$ older quiescent cells (OQ), which are located in the lymphoid organs. Newly emerged cells (NE) $CXCR4^{dim}$ and $CD5^{bright}$ found in the peripheral blood. The CLL lifecycle was investigated by Callisano *et al*, studied by separating the subclones using an isotope labelling approach [38]. This approach is a model to study CLL biology in cells in peripheral blood and lymphoid tissue. $CXCR4^{bright}$ CLL cells enter tissue sites where they receive proliferative stimulation from microenvironment. The activation downregulates the CXCR4 expression and upregulates the CD5 expression on the cells allowing egress from tissue site into peripheral blood. This process is associated with BCR signaling, toll-like receptor (TLR), cytokines and chemokines [69, 70]. The phenotype of cells leaving the mesenchymal stromal cells have changes into $CXCR4^{dim}$ and $CD5^{bright}$. Once the cells are circulating in the peripheral blood, the phenotype change with time to prevent cells to undergo apoptosis and have continuous survival support, some cells return to express $CXCR4^{bright}$ and $CD5^{dim}$ allowing re-entering the lymphoid tissues**.**

## 1.4 High-Dimensional Single-Cell Flow and Mass Cytometry Data

### 1.4.1 Flow cytometry

Ability to study single cells within heterogeneous populations has brought great advantage to our understanding of immunology and cancer biology. Possibly the first method able to perform such analysis is flow cytometry where lasers, light scattering properties and fluorescence are used to define properties of individual cells within populations. Figure 1.5 shows a representation of how such “conventional” flow cytometry is configured within a typical instrument. Thus, cells are organised into a stream of single cells that are passed through laser light. The interruption of light as the cell passes through the laser beam is recorded by a photomultiplier detector, and the size of the cell is determined by the length of time this interruption takes place. This is so-called forward scatter in the language of flow cytometry. Light is also potentially scattered to the sides as the cell passes through the laser stream by intracellular granules and/or organelles to give information on the complexity of the cell. This is so-called side scatter. The power of just these parameters to distinguish different cell populations is demonstrated by an ability to discriminate between lymphocytes and monocytes within suspension of peripheral blood mononuclear cells (Figure 1.5).

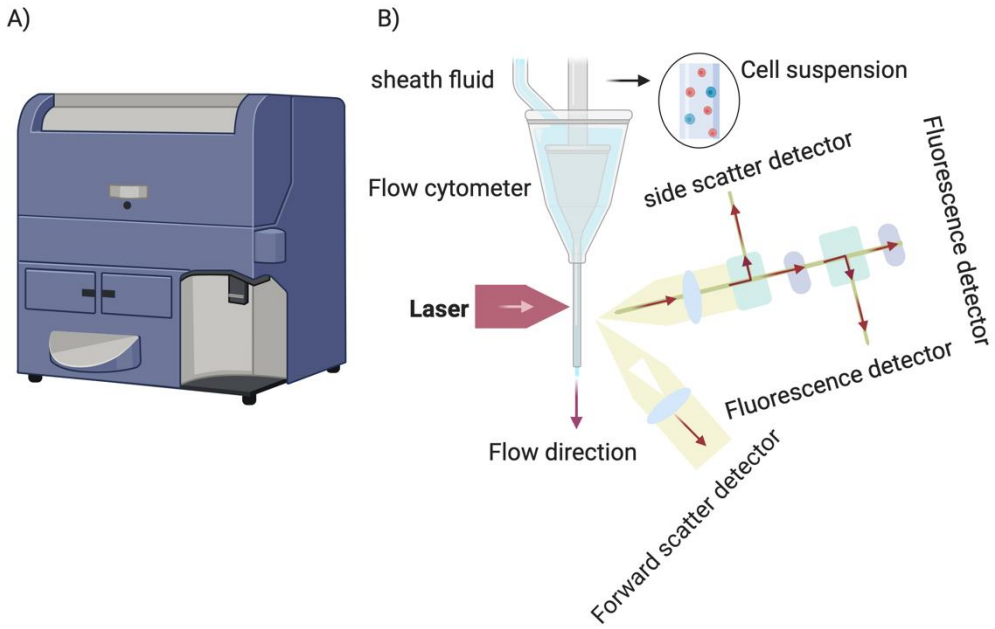


**Figure 1. 5 Schematic diagram of a flow cytometer. A.)** Flow cytometry machine. **B.)** the sample cell suspension is introduced into the flow cytometer the laser beam is reflected on the forward scatter detector for cell size measurement and side scatter detector for integrity, size and density content characteristics. The fluorescence detectors are responsible to detect light signals that is emitted from each labelled antibody by specific fluorophore [71]. This Figure was created using Biorender.com.

To exploit fluorescence properties, antibodies recognising surface and internal antigens on cells have been developed which are labelled with a fluorophore. When cells bearing such antibodies pass through the laser stream, fluorescence is activated and emits light of specific wavelength which is detected by photomultiplier detectors which see the fluorescent light through filters that only allow certain wavelengths of light to pass (Figure 1.6A). The first fluorophore used for this purpose was fluorescein isothiocyanate (FITC) which is stimulated to fluoresce using an argon laser with emits light at a wavelength of 488nm. Subsequent to this, other fluorophores have been developed which have different fluorescent properties to allow more dimensions to be

measured simultaneously. At the time when this thesis was conceived the most advanced flow cytometer was the BD LSR-Fortessa™ equipped with 5 lasers and ability to measure 18 different colours. Such multidimensional flow cytometry is now used to distinguish and describe various subsets of lymphocytes and monocytic cell types. This is a tool that not only serves basic research but is now commonly used also in pathology laboratories for the diagnosis of disease world-wide.

However, the sensitivity of conventional flow cytometry is found to be limited. The fluorophores that are used can emit a broad spectrum of light that potentially spans two or more measurement wavelengths. This phenomenon is called emission spectral overlap, and compensation to reduce this overlap is required so that false positive expression is not interpreted. An example of such spectral overlap is demonstrated by the emission spectra of FITC where primary fluorescence measurement is performed at 530nm, but fluorescence associated with this fluorophore extends also into the range where the fluorescence of another fluorophore, phycoerythrin (PE), is also measured (585nm) (Figure 1.6B). Thus, when antibodies coupled to FITC or PE are used together, there is potential to interpret PE reactivity when there is none. Another problem is that not all fluorophores are alike in terms of brightness, FITC is much dimmer than PE with respect to the fluorescent light it generates when excited at 488nm by the argon laser. In practical terms this means that consideration must be made with respect to antigen expression levels, it is better to investigate high-expressed antigens with dimmer fluorophores and low-expressed antigens with bright fluorophores. Finally, there is also intrinsic fluorescence associated with cells, and this competition with fluorophores requires inclusion of labelled non-specific control antibodies to be able to subtract any detected auto-fluorescence from specific fluorescence.

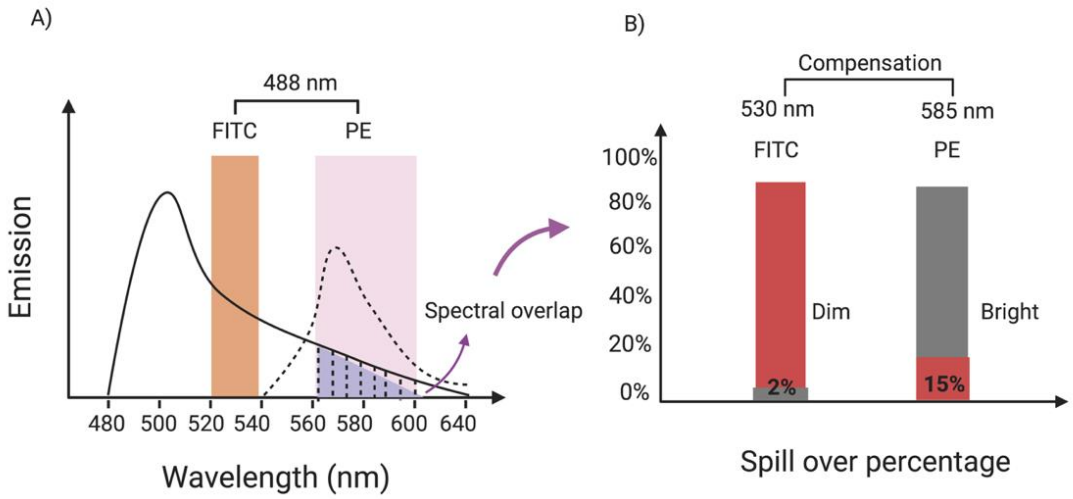


**Figure 1. 6 Demonstration of spectral overlap of fluorescence. A.)** Emission spectra of FITC and of PE when each fluorophore is excited at 488nm. The respective reading windows are shown to illustrate spectral overlap of FITC fluorescence on to the PE channel **B.)** Shows the percentages of spill over from FITC on to PE where 15 % of the perceived PE fluorescence is due to FITC fluorescence. The contribution of PE fluorescence on to FITC is much smaller (2%). Both require compensation for accurate measurement FITC and PE-associated fluorescence [72]. This Figure was created by Biorender.com.

Taken together, the above limitations effectively allow studies of up to 13 different colour parameters associated with cells to be taken into consideration with the most advanced technology that was available at the time. Therefore, careful consideration would have to be made with respect to investigation of cell signaling within particular populations of cells; for instance, comparison between T and B cells might not be possible because of the necessity to define one or the other population before intracellular signaling parameters could be assessed. Alternatively, specific cell signaling pathways might be compared between different lymphocyte subtypes where the bulk of the antibodies used differentiate between these different subtypes. Such

multi-dimensional analysis could be achieved using multiple tubes where different panels of staining antibodies are used, but this could be limiting when the source material is also limited. Ideally, a tool that increases the dimensionality of analysis without the problems of conventional flow cytometry would be very useful for the study of signal transduction in heterogeneous populations of cells, such as CLL cell populations within patients.

### 1.4.2 Mass cytometry:

A tool that increases both resolution and parameterization is attractive for researchers because it would give greater resolution and clarity in multiplexed single-cell measurements [73]. One of these tools is mass cytometry which has been developed to offer opportunity of investigation using multi-dimensional immunophenotyping for the understanding of disease biology. Mass cytometry, known as **Cy**tometry by **T**ime **O**f **F**light (CyTOF), couples flow cytometry with Time Of Flight (TOF) mass spectrometry to detect heavy metals that label reagents, such as antibodies, to determine phenotypic properties of cells. The heavy metals that are exploited for CyTOF are generally from the lanthanide series of elements within the periodic table, chosen because of their ease of detection by TOF mass spectrometry and because this series of elements have multiple stable isotopes which can be purified for labelling purposes. This purity then allows increased dimensionality because measurement on one channel is not likely to contribute to another. Thus, machines have been developed that are capable of measuring up to 135 different channels. In practice however, these machines can effectively measure between 40 and 50 different parameters because of limitations in the preparation of purified isotopes and of the chemistry involved in labelling the reagents for describing cell phenotype.

Surface / internal antigens, and, more recently, mRNA species, can be detected by CyTOF using labelled reagents. DVS Sciences, which developed the CyTOF technology, also developed the technology for heavy metal labelling. In principle this technology relies on reagents that are metal chelators that bind lanthanide metals with high affinity that can then be coupled to proteins, such as an antibody, via modification of an internal cysteine or lysine residue within the peptide chain [74]. This heavy metal labelling process is not unlike that which is involved in fluorophore labelling of antibodies.

Figure 1.7 shows a schematic of a mass cytometer: suspended cells that have been labelled with heavy metal isotopes are passed through a nebuliser to create droplets containing a single cell, these droplets are then passed to an inductively coupled plasma (ICP) were the metal isotopes are ionized before passing through a quadrupole magnetic field that filters light from heavy ions before entry of the latter into the Time of Flight chamber (TOF). Detected metal ions then undergo quantification and are processed into an FCS file that is not unlike the FCS files generated for conventional flow cytometry. This FCS file can be uploaded to Cytobank, which is a cloud-based software platform, for further analysis and interpretation.

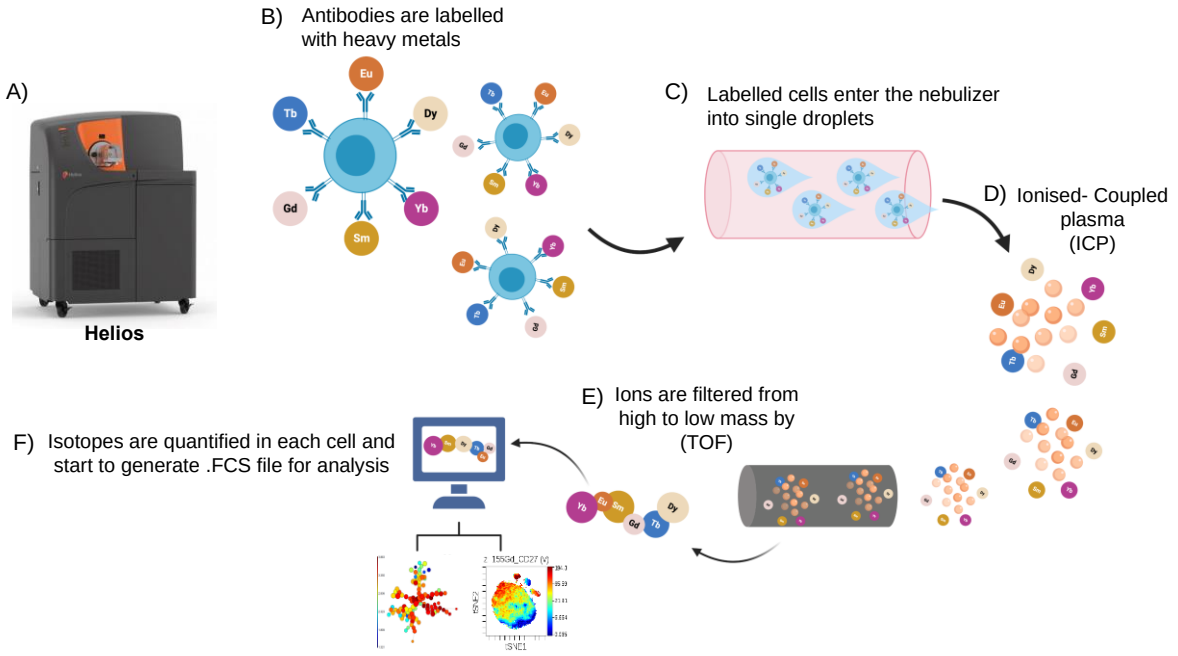


**Figure 1. 7 Demonstration of single-cell suspension in a mass cytometer A.)** Helios third generation of mass cytometer. **B.)** All cells are stained with antibodies that are labelled with heavy metals. **C.)** A nebulizer is used to create droplets, each containing a single cell. Single cells are ionised within an inductively coupled plasma (ICP)**. D.)** The cell-associated ion cloud is passed through a quadrupole to remove light ions. The remaining heavy ions are subjected to time-of–flight (TOF) mass spectrometry. **E.)** Data is generated as an .FCS file ready for upload. **F.) .**FCS files are uploaded in Cytobank™ for analysis. Created with BioRender.com

A major sacrifice with use of CyTOF is the loss of optical information (ie cell size (FSC) and complexity (SSC) to determine single cell events. CyTOF compensates for this by using a DNA intercalator that is labelled to iridium isotopes ($^{191}$Ir and $^{193}$Ir) and detecting a set length as a “single cell event”. Other physical parameters can then be determined; live cells can be distinguished from dead cells using cisplatin where detection of the most common platinum isotope ($^{195}$Pt) is a determinant of dead cells.

#### 1.4.2.1 Antibody conjugation to metal containing polymer tags

Mass cytometry has focused on using lanthanide (Ln) elemental mass tags (EMT). These elements are useful because many of them have multiple isotopes that are stable, and these elements have a similar chemistry that allows chelation using compounds that can be attached to IgG monoclonal antibodies and other reagents [75]. In addition to Ln elements other EMT have been introduced; 15 rare earth elements, 4 noble metals, 2 post-transition metals and 1 halogen. Thus, the diversity of EMT available for mass cytometry has expanded channel usage to 56, making this technique useful for measurement of multiple parameters including surface and internal antigen expression on cells using tagged antibodies, detection of DNA using tagged intercalating agents, determination of cell viability using cisplatin and barcoding with palladium isotopes so that multiple samples can be measured simultaneously [76]. Crosstalk between these channels is affected the purity of the isotopes, and by their state of oxidation which can affect how they are detected by the TOF mass spectrometer [75]. Figure 1.8 is an illustration of the types of crosstalk that can be expected. Known as spillover, the crosstalk from isotope impurity is demonstrated is best illustrated by the effect $^{152}$Sm feeding on to $^{154}$Sm and vice versa, and the effect element oxidation which makes one element appear similar to another is illustrated by $^{170}$Er feeding on to $^{154}$Sm. Generally, however, the influence of such crosstalk is small and can be compensated for. Thus, EMT can replace fluorescent tags, having been found to show high sensitivity and better resolution.

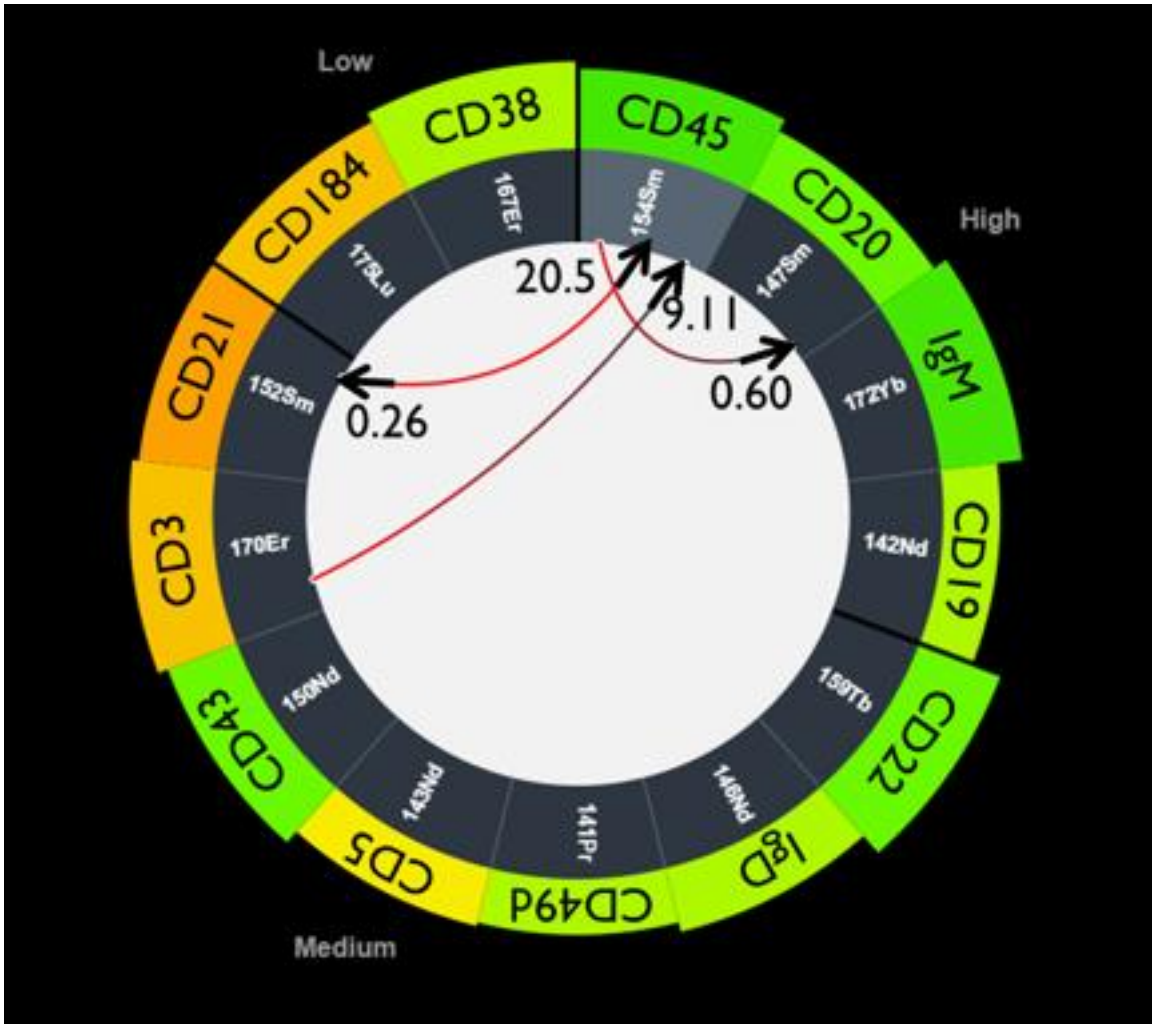


**Figure 1. 8 Illustration of spill over in Fluidigm™ panel designer wheel.** The figure shows MaxPar® panel designer (www.dvssciences.com) to choose antibody conjugates compatible with my experiments. The figure shows two channels with the greatest overlap CD3 ($^{170}$Er) on to CD45 ($^{154}$Sm) and CD21 ($^{152}$Sm) on to CD45. The degree of signal overlap is significant. However, CD45 is such a strongly expressed antigen, it is likely that the signal overlap imposed will not lead to artefact and require further titrating to get an optimal concentration for staining.

Fluidigm™ manufactures the metal chelating compounds that can be attached to IgG antibodies. The compounds are polyaminocarboxlyate polymers where attached 1,4,7,10-tetraazacyclododecane-1,4,7,10-tetraacetic acid (DTPA) polymers function as a bi-functional chelating agent (BFCA) to trap Ln elements with high affinity (Figure 1.9) [75, 77] Named MaxPar® polymer X8, these compounds have the ability to trap up to 8 atoms of a given Ln element. The MaxPar® reagent uses 2 maleimide groups (Bismaleimides) as a linker to the Fc region of an IgG antibody, exploiting reduced thiol groups within the labelling procedure [78] . Figure 1.9 illustrates the antibody labelling procedure. Reduction of thiol groups in antibodies, or other proteins, is achieved using Tris-(2-carboxyethyl)phosphine hydrochloride (TCEP) which converts disulfide bonds of adjacent cystine groups into free thiols (now cysteine residues) to allow interaction with the maleimide groups of the MaxPar® polymer [77]. MaxPar® polymer is incubated with the Ln element of choice, and both reduced antibody and labelled polymer are purified by centrifugation dialysis using 50kDa and 3kDa filters, respectively. Once pure, both can be then mixed and then repurified once conjugation is complete. The labelled antibody is now ready for use. A detailed protocol used for this thesis conjugated SH2 domains with Ln-polymer labelling kit from Fluidigm™ is described in chapter 2, material and methods, section 2.2.7.

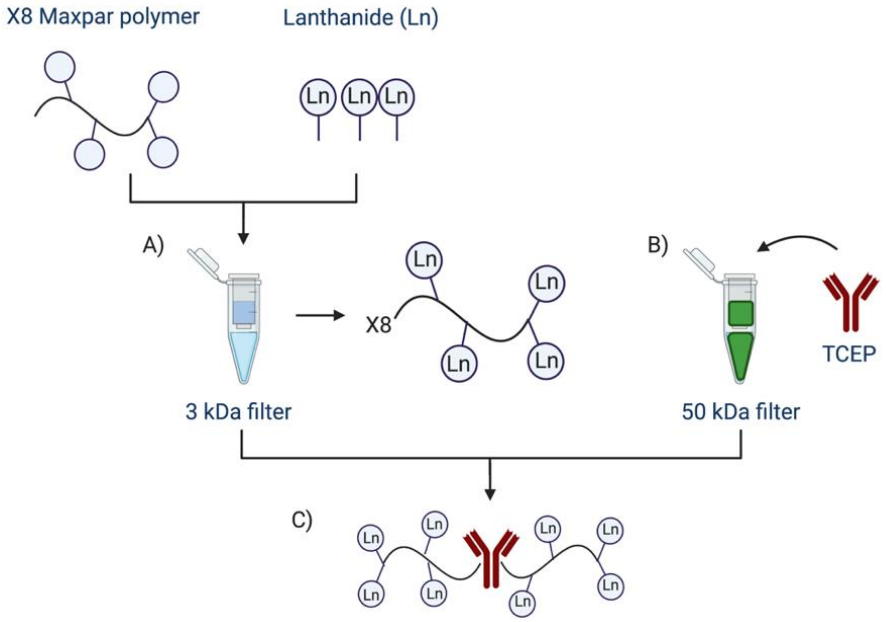


**Figure 1. 9 Overview of MaxPar® Metal conjugation labelling diagram. A.)** workflow of Lanthanide conjugated to the X8 polymer is by loading first the Lanthanide (Ln) into the 3kDa filter and **B.)** a preparation of the antibody is added into 50 kDa filter that undergoes loading, purification, retrieval of a partially reduced used TCEP to serve a stronger binding after both concentrates are mixed together into 50 kDa filter to form **C.)** a stabilized lanthanide polymer. Created with BioRender.com

### 1.4.2.2 Palladium-based Mass Tag cell Barcoding

Barcoding (BC) allows differentiation between either single or subpopulations of cells. In terms of flow cytometry [called fluorescent cell barcoding (FCB)], such barcoding uses different reactive fluorophores that can tag an antibody that reacts in a similar fashion with the different populations of cells of interest [79]. With haemic cells, such an antibody would target CD45 because of its high expression on most haemic cells. An alternative epitope is beta-2 microglobulin [80]. FCB is useful to pool samples together so that expression of particular epitopes can be directly compared between samples. An example of such a comparison would be measuring CD154 expression on resting and TCR-activated CD4+ cells where the latter express this epitope and the former do not. Thus, this methodology was developed for reduce artefacts in staining by reducing antibody concentration and improving measurement reproducibility between samples. The same can be done in mass cytometry where antibodies are labelled in heavy metals. FCB has improved efficiency of antibody staining and has led to a reduction in inter sample variability.

With the advent of mass cytometry, a second method of barcoding is possible. Called mass tag cell barcoding (MCB), this method uses palladium (Pd) isotopes as tags to label each sample to provide unique barcodes that allow easier pooling of multiple samples in one tube. MCB exploits six different palladium isotopes (Pd) with masses of $^{102}$Pd, $^{103}$Pd, $^{104}$Pd, $^{105}$Pd, $^{106}$Pd, $^{108}$Pd, and $^{110}$Pd [75, 81]. This allows up to 20 different barcodes through rearrangement of three Pd isotopes for each barcode that labels each sample (Figure 1.10). These Pd isotopes are considered to be low-sensitivity isotopes because they are weakly detected by TOF mass spectrometry. Pd also has ligand properties that are more compatible to BFCAs such as ethylenediaminete-traacetic acid disodium salt dihydrate (EDTA) chelators and

dodecane tetraacetic acid (DOTA) than diethyl-enetriaminepentaacetic acid (DTPA) [76, 82]. These compounds have a weaker affinity for other lanthanides isotopes that are used to detect primary antibodies and so allows easy use without interference. For this thesis I have used MCB approach, the details of MCB protocol is written in details in chapter 2 material and methods section 2.2.4.

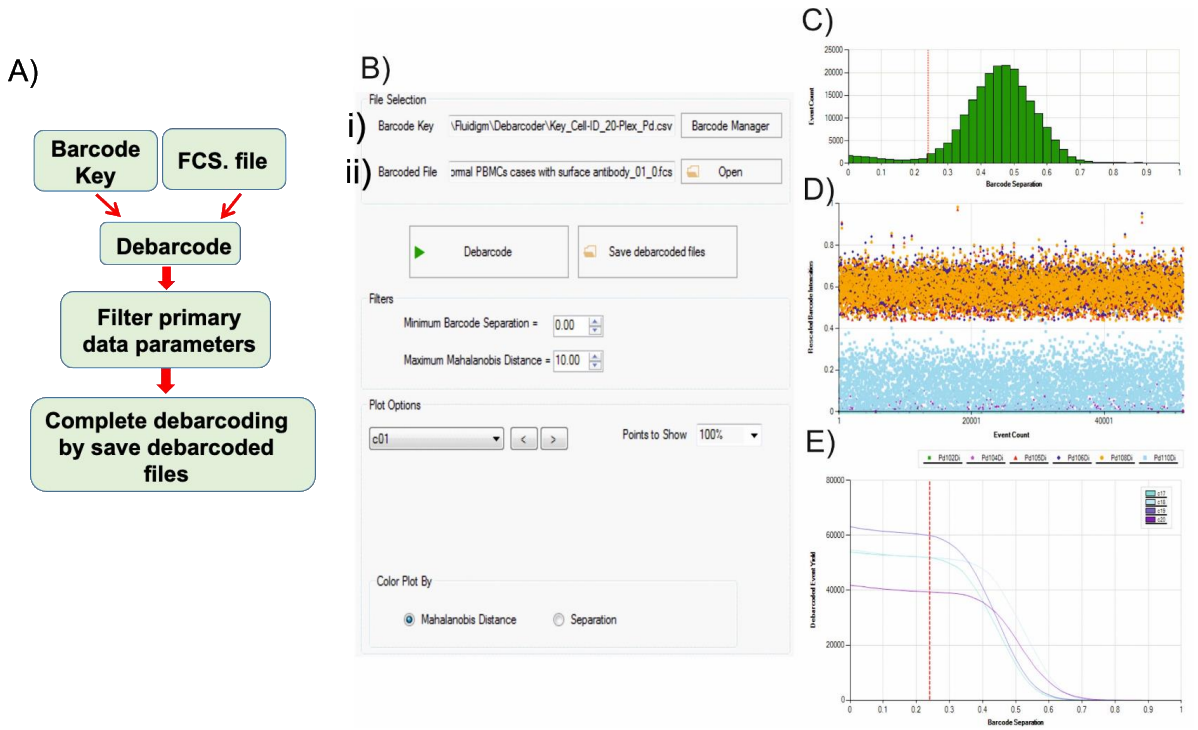


**Figure 1. 10 Barcodes and how they are analysed A.)** Schematic of palladium mass-tag arrangements according to the 20 barcodes included in the MaxPar® barcoding kit. **B.)** Illustrated algorithm of how the Debarcoder software (file version 1.4.0.0, Fluidigm) works. **i)** Algorithm of how FCS files are filtered according to barcode. **ii)** Front page of where the operator is requested to input barcode key and FCS file information. **C.)** Histogram showing total event count of the combined samples prior to decoding. The red line indicates a filter for analysis of the data. Only those events to the right of the line are analysed because those represent the majority of the sample being measured. **D.)** This example contains four barcodes combined; the illustration shows how these barcodes are separated and the less than 0.2 are eliminated from the filter. The distribution of measured events (orange and blue) are well separated, indicating that the barcoding was successful, and the samples may be further analysed. **E.)** Graph showing four different samples that were separated after being filtered and each barcoded sample represents a sample, meaning that the barcoded samples are now separated into four different FCS files and are ready to be analysed by Cytobank software (file version 6.7, Fluidigm™) [81].

### 1.4.3 Computational methods used in mass cytometry data:

The most advanced flow cytometers at that time could simultaneously measure a maximum of 20 parameters and analysis was restricted to manual gating in order to understand expression single antigens on cells. Such analysis had the distinct disadvantage of not being able to simultaneously appreciate how these 20 parameters applied to a single cell or population of cells. The number of parameters conventional flow cytometry can measure has since increased to 30 parameters [83], and a recent flow cytometer, called OMIP-069, was developed to achieve 40 colour parameters [84]. With this increase in dimensionality comes also the need to understand the relationship between each other with respect to single cells in order to bring insight into the biology of these cells. Such a need also applies to data generated using mass cytometry, and has resulted in the generation of analytical tools that reduce dimensionality and allow simultaneous appreciation of measured parameters to bring identification, characterisation and insight into unknown or unexpected cell populations and phenotypes where analysis is performed in an unsupervised manner [85].

Convention and mass flow cytometry data is encoded in .fcs files that can be analysed with a host of propriety and free software programs. Typical examples of such propriety programs include Flowjo™ and FACSDiva, and these programs are used for manual gating of cell populations. However, Cytobank software (**www.cytobank.org**) is an online web-based tool that also be used for manual gating of cell populations, but also comes equipped for analysis of larger datasets where the multidimensional properties of these datasets allow for a detailed phenotypic examination for each cell population [86]. This allows researchers to answer many questions by, for example, identification of rare cell populations and quantification of cell population diversity.

Cytobank allows such analysis through the use of two algorithms: dimensionality reduction and clustering.

#### 1.4.3.1 Dimensionality reduction algorithms:

The two most common algorithms used in flow cytometry data analysis for dimensionality reduction are principle components analysis (PCA) and stochastic neighbor embedding (SNE). In simple terms, the difference between these two algorithms is that PCA maps data based on the variance of each point to each other, whereas SNE maps data based on the similarity of each point to another. In terms of visualization both PCA and SNE are presented as 2D plots where actual data proximity is recorded by the creation of a linear relationship that can be viewed as data points within vertical and perpendicular axes. This approach to dimensionality reduction is potentially limited by the masking of other dimensions that give important relational information, ultimately causing inaccurate interpretation of the data set [87]. To overcome these potential limitations of PCA and SNE, a modification of SNE was developed by Amir *et al*, known as t-distributed stochastic neighbor embedding (tSNE) which eliminates potential crowding of data points when only SNE is used. In Cytobank, tSNE is further modified to visualization stochastic neighbor embedding (viSNE) so that newly uncharacterized cell populations can be identified with greater ease by creating [88] a cloud structure in 2D that shows where rare or unique populations that can be allocated anatomically within the larger population of cells being analysed [89]. An additional advantage to using viSNE is that it gives quantitative proportional information (eg the percentage of a particular subpopulation of cells within the whole population) without losing single cell resolution.

Additional tools have also been developed for visualization of multidimensional data. [90, 91]. A similar to t-SNE is **A**utomatic **C**lassification of **C**ellular **E**xpression by **N**onlinear **S**tochastic **E**mbedding (ACCENSE, developed and used by Python software), where the algorithm is designed to differentiate clusters of cells within the multidimensional data without any single cell resolution loss to present data similar to that in 2D viSNE plots. Shekhar *et al*, have applied this tool along with 35 different parameters using mass cytometry to explore CD8+ T cells derived from specific pathogen-free and germ-free mice and was able to distinguish subpopulations of naïve and memory T cells using this method of data analysis [92]. Another tool that is used to Analyse mass cytometry data is Wanderlust, a algorithm that uses both linear and non-linear processes such as k-nearest neighbor graphing (KNN) to view data. Bendall *et al*, have used the Wanderlust tool in combination with mass cytometry data to investigate human B cell development during lymphopoiesis [93]. Wanderlust is ideal for exploring differentiation of cells that are undergoing any continuous developmental process, presenting this information as trajectory graphs within a one dimensional linear process [87]. The ACCENSE and Wanderlust computational methods, and additionally PCA, can all be performed outside of the Cytobank platform. As part of my thesis, I used the different algorithmic methods that are part of the Cytobank software to do analysis on my data.

### 1.4.3.2 Clustering algorithms:

The other algorithm of mass cytometry data analysis used in this thesis is the clustering algorithm SPADE (**S**panning-tree **P**rogression **A**nalysis of **D**ensity-normalised **E**vents). This method of analysis uses down sampling of data as a mechanism to detect rare populations during dimensional reduction [94]. It works by hierarchical clustering all the relevant markers which are phenotypically similar on cells, converting them into nodes to form a tree presentation known as a SPADE tree. As an example, Bendall *et al* [95] applied SPADE to study the immune system, characterising both cellular phenotype and functional properties of cells responding to specific stimuli to demonstrate the utility of CyTOF [96]. Similar to SPADE is FlowSOM, that uses a new **S**elf-**O**rganizing **M**ap (SOM) clustering algorithm to create an artificial neural network (ANN). This method of analysis has an advantage over SPADE because data is not down sampled, and information is not lost [97]. FlowSOM is demonstrated able to cluster unsupervised large datasets faster than SPADE, and present the data in the form of a minimal spanning tree (MST) where rare populations of cells are identified without the requirement of down sampling that can contribute their loss [90].

A clustering tool that similar to SPADE is called CITRUS, which consists of **C**luster Identification, characterization, and regression [90]. This tool is designed for the analysis of groups of samples to understand how they compare, and is, for example, useful for clinical studies where the reasons for poor and good patient outcomes to a particular therapy can be Analysed. CITRUS allows study of the relationship between surface markers to identify cell populations and intracellular signaling within those populations in groups of up to 10 user-defined inputs by identifying the clusters that are similar cells in all samples in an unbiased approach. The cells are clustered

according to the parameters chosen by a minimum cluster size threshold (MCST) that is set by default to 5% for analysis [90]. This shows the cluster abundance within each group patients and presents them as scatter plots of expression levels of each parameter [98]. Gaudillière *et al*, have used Citrus to measure 32 patients that have undergone hip replacement surgery and have divided them into groups with different recovery responses and has found patients suffering from functional impairment and pain had a strong correlation in STAT3, CREB, NF-kB and $CD14^{+}$ monocytes which were markers that have guided for post-surgical recovery [99].

### 1.5 Use of mass cytometry in CLL cells.

At the beginning of this thesis, there was no study of either CD5+ B cells or CLL cells using mass cytometry. There were many studies that had used conventional flow cytometry to immunophenotype these cells, but none that specifically addressed BCR signaling within identifiable subpopulations, particularly with respect to the effects of new therapies targeting BCR signaling and how they might target such signaling in CLL cell subpopulations and healthy B cells.

During the course of my study there were 2 reports published where CLL cells were studied with mass cytometry [100, 101]; the former study investigated complications associated with idelalisib treatment of CLL patients, focussing on the effect of this inhibitor on T cells, and the latter study used mass cytometry to investigate phenotypes cells in splenic tissue from CLL patients. Neither of these studies investigated CLL or healthy B cell subpopulations, and how they respond to BCR crosslinking. Although one report used conventional flow cytometry to investigate and compare BCR signaling in indolent B cell lymphomas, including small cell lymphoma (SLL) and CLL, because this study could not combine phenotypic and phospho specific antibodies,

they could not address subpopulation response [102]. At this point it is important to note that CLL cells in tissues or in circulation have different phenotypes depending on the stimulation by BCR or Toll-like receptors (TLRs) [69, 70]. This allows CLL cells to migrate into the periphery to further activate and divide for clonal expansion in the germinal centre's with $CXCR4^{dim}/CD5^{bright}$ phenotype and when CLL cells expanded in the periphery, with time gradually cells start to express $CXCR4^{bright}$ and $CD5^{dim}$ cells and return into the tissues and lymphoid organs or undergo apoptosis. Calissano *et al,* described life cycle of CLL cells bearing newly emerged and older quiescent phenotypes based on differential expression of CXCR4 and CD5 [38, 103]. Until now, how CLL cells bearing these phenotypes respond to BCR crosslinking was unknown. Furthermore, Aguilar-Hernandez et al showed that IL4 can stimulate BCR expression on the surface of CLL cells, leading to restoration of signaling despite inhibition of PI3K$\delta$ and BTK with idelalisib and ibrutinib respectively [58, 64, 104]. This implies that CLL cells bearing different levels of surface immunoglobulin may respond differently to these BCR inhibitors, and that studying whether such cells exist within whole populations of CLL cells may give clues to mechanisms involved in the development of clonal resistance to these inhibitors. Mass cytometry provides a tool with which to identify and study individual clones of CLL cells and their response to BCR crosslinking when they are exposed to idelalisib and ibrutinib. To increase my ability to detect signaling in CLL cells, I also investigate the use of tools additional to phospho-specific antibodies, this involved using Src homology 2 (SH2) domains to detect signaling in cells [105, 106]. Thus, in this thesis, I use mass cytometry to investigate BCR signaling in CLL and healthy B cells presenting the high dimensionality data generated to understand CLL and potentially answer the therapeutic challenges associated with the treatment of this disease.

## 1.6 Hypothesis and Aims:

Mass cytometry can be used as a novel approach to characterise different B cell subsets of normal B and CLL cells, to identify the CLL subclones that respond differently to BCR signaling and show heterogeneity in the responsiveness to the BCR inhibitors. Using a multidimensional algorithmic approach allows to identify resistant subclones addressing them phenotypically in a single-cell resolution.

Aims:

1) Identify normal B and CLL subsets using mass cytometry.

2) Understand the reproducibility of mass cytometry in producing useable data.

3) Measure B cell receptor signaling in normal B subsets and in CLL total clones using combinations of phosphoproteins and surface antigens.

4) Measure the effects of idelalisib and ibrutinib on BCR signaling in CLL cell subclones.

# Chapter 2: Materials and Methods

## 2.1Tissue Culturing Techniques

### 2.1.1 Isolation and storage of normal blood from buffy coats

Buffy coats from healthy blood donors were purchased from the NHS Blood and Transplant Service (Liverpool, UK) and used with the approval of the Liverpool East Research Ethics Committee (16/NW/0810). All samples were processed according to a standard operating procedure provided by the Liverpool Leukaemia Biobank, University of Liverpool. Buffy coats were diluted 1:1 with RPMI-1640 media (Sigma Aldrich, Gillingham, UK), and 30 ml was carefully layered over 12.5 ml lymphoprep (Alis-Shield PoC AS, Oslo,Norway) in a 50 ml Falcon tube. Samples were then centrifuged at 800xg for 30 min at room temperature (RT), using 0 deceleration brake at termination. The peripheral blood mononuclear cells (PBMCs) were collected from the plasma/lymphoprep interface using a sterile plastic Pasteur pipette and placed into a new 50 ml Falcon tube. PBMCs were then washed once with RPMI-1640 media using the following centrifuge settings: 550xg for 10 mins, RT, and normal braking. To prepare the cells for cryogenic storage, the cell pellet was resuspended in 50 ml of cold 100% foetal calf serum (FCS), followed by the addition of an equal volume of cooled 80% FCS + 20% DMSO in a dropwise fashion while swirling over a period of approximately 25 min, keeping the entire suspension on ice. One millilitre of the final cell suspension was placed into cryovials (cell concentration approximately $2x10^7$/ml) and then placed in Styrofoam for controlled freezing in a -80$^o$C freezer. Following the completion of this first freezing stage, the cryovials were then moved to -150$^o$C freezers for long-term storage.

### 2.1.2 Thawing of cryopreserved cells

Cryopreserved cell samples were removed from -150°C and placed in a 37°C water bath until all traces of ice crystals were gone. Thawed samples were placed on ice until further manipulation was required. When ready, thawed cell samples were transferred into a cooled sterile 20 ml universal centrifuge tube using a sterile plastic Pasteur pipette. Ice-cold full RPMI1640 media (Table 2.1) was added drop-by-drop while gently shaking the ice box containing the universal tube after each drop. A total volume of 10 ml of media was added before further manipulation was undertaken. This step typically takes approximately 30 min.

Table 2. 1 Media preparations used in this thesis for tissue culture.

| Media | Contents | Amount |
|---|---|---|
| Full RPMI 1640 media | Media | 500 ml |
| | 10% HI FBS | 50 ml |
| | 100 U penicillin | 5 ml |
| | 0.1mg/ml streptomycin | 5 ml |
| Full RPMI 1640 media+2mM $MgSO_4$ mix | Media | 500 ml |
| | 10% HI FBS | 50 ml |
| | 100 U penicillin | 5 ml |
| | 0.1mg/ml streptomycin | 5 ml |
| | Magnesium sulphate | 95 mg in 500 ml |

Once the thawing procedure was completed, the samples were centrifuged for 5 min at 550xg, maintaining a temperature of 4°C. The supernatant was removed using pipetting, and the cell pellet gently resuspended with 10 ml of fresh full RPMI1640 media. For CLL, Maver1, and Jeko1 cells, a similar further centrifugation step was performed, leaving the cells ready for assessment of viability, counting, and further use. For PBMC samples, the cells were centrifuged for 10 min at 150xg, maintaining a temperature of 4°C. This step is performed to separate loose debris and platelets from heavier intact cells. The resulting cell pellet is flocculent, and removal of the supernatant had to be done carefully to avoid white cell loss. The cell pellet was then resuspended in 10 ml of fresh full RPMI1640 media, and a further centrifugation at 550xg followed, maintaining a temperature of 4°C. The cell pellet was then resuspended with 3 ml of fresh full RPMI1640 media, which contains 2mM $MgSO_4$ and benzonase endonuclease (5KU). The cells were then incubated at 37°C in an incubator (5% $CO_2$) for 1 h, after which cell viability and numbers were determined. This step was followed by centrifugation at 550xg at RT. Thereafter, the cell pellet was resuspended in fresh full RPMI1640 media using a volume in which the end cell concentration was 1 x $10^7$ cells/ml.

### 2.1.3 Assessment of cell viability and count

Cell concentrations were initially assessed using a Nexcelom cell counter machine. In principle, 20 μl of cell suspension was mixed with 20 μl of Trypan Blue solution and loaded on to the cell counter slide. The machine was set to automatically count the live and dead cells, based on brightness and size, and presents the results as a live cell concentration with a viability percentage. This method worked very well for cell lines where the size of the cells was uniform. However, for primary cell suspensions,

especially PBMCs from normal subjects, manual haemocytometer counts were performed because of non-uniform cell sizes that could not be distinguished by an automatic cell counter. The haemocytometer consisted of chambers that is equally covered with the cover glass. The sample is aliquoted into the chamber of 20 μl and covered with cover glass that helps to load the cells equally. The haemocytometer is placed under the microscope to count each cell within the all the four squares are divided by four. The total cell number is calculated after adding 20 μl of trypan blue mixed with 20 μl of cells and under the microscope where only the dead cells are stained by trypan blue and the live cells that are unstained. The total cell number is calculated: total cell/ml= ($n^0$ of cells X dilution) X 10000 ($10^4$) / number of squares counted.

### 2.1.4 in-vitro stimulation of CLL and normal B cells through the BCR

BCR engagement was studied in this thesis using anti-IgM as a stimulus. B cells were stimulated with either unlabelled goat anti-IgM F(ab`)$_2$ used at a concentration of 20 μg/ml, or with FITC-labelled goat anti-IgM F(ab`)$_2$ (both from Cambridge Bioscience, UK), used at a concentration of 20 μg/ml. F(ab')2 are fragment antibodies that are used in my experiments to prevent any non-specific binding antibodies that are located at the Fc portions of the antibodies I am using and the Fc receptors that are present on B cells. The labelled IgM-FITC was used after filtering the sodium azide, and was measure using a nanodrop to identify the concentration by measuring of the absorbance at 280 nM. Pipette 1μl into the nanodrop pedestal to read the absorbance and calculate the concentration. This follows with adding the appropriate amount of sterile PBS and the proper concentration should be used to stimulate the cells. Prior to incubation with anti-IgM, cells were maintained at 37°C in a $CO_2$ cell incubator.

Following stimulation, 1 ml of ice-cold PBS was added to the cell suspension to stop stimulation, and the cells were centrifuged at 600xg for 3 min, maintaining a temperature of 4$^{o}$C. The cell pellet was resuspended in ice-cold PBS, ready for mass cytometry staining.

### 2.1.5 Pervanadate treatment

Maver-1 and Jeko-1cell lines were treated with Pervanadate solution prepared by adding 200 mM of $H_2O_2$ and 200 mM Orthovanadate, which provided a final concentration of 100 mM Pervanadate. Pervanadate is a form of a peroxidised vanadate, and it acts as an irreversible inhibitor that reverses the protein tyrosine phosphatases (PTPs). Pervanadate should be used at 100 µM 1:1,000 dilution with properly mixed cells. To treat, maintain for 30 min at 37$^{o}$C in an incubator with 5% $CO^2$.

### 2.1.6 Inhibitor treatments of cells

Ibrutinib (BTK inhibitor) and Idelalisib (PI3K$\delta$ inhibitor) were both purchased from Selleckchem (Absource Diagnostics GmbH, Munich, Germany). These compounds were dissolved in DMSO to stock concentrations of 10 mM, respectively. The optimal dose concentration was selected after western blot analysis to comprehend the effect of the up and down stream signaling in the BCR pathway in Maver-1 and CLL subclones. The optimisation of the optimal dose concentrations consisted of 100 nM, 200 nM, 500 nM, and 1 µM in both BCRI, that were added to cells, which were then kept for one hour in an incubator (5% CO2) at 37$^{o}$ C.

## 2.2 Mass Cytometry

List of antibodies used: Table 2.2 lists all the antibodies used for mass cytometry within this thesis. Selection criteria are fully discussed in Chapter 3.

### 2.2.1 Viability staining of cells for mass cytometry

The viability of healthy PBMCs and CLL cells was determined by staining with Cell-ID Cisplatin reagent of 5 μM final concentration (Fluidigm, UK). This reagent works by binding covalently to proteins where access is permitted. With viable cells, access of cisplatin is limited to proteins located on the surface of cells because of a natural barrier provided by the plasma membrane. With dead cells, cisplatin can also label internal proteins due to a lack of membrane integrity. Thus, in terms of results, dead cells stain more strongly with cisplatin than do live cells.

With respect to this procedure, $1x10^7$ cells were suspended in 300 μl of PBS in a 1.5 ml microcentrifuge tube. One microliter of Cell-IDTM Cisplatin reagent was added, and the cells were incubated for 5 min at RT. The cells were then centrifuged at 550xg for 5 min and washed once with PBS. Important: This step requires the use of a centrifuge equipped with a swing-out rotor to allow all cells to pellet properly in the tip of the microcentrifuge tube without attaching to the sides of the tube.

### 2.2.2 Human B phenotyping antibody surface and intracellular list

Table 2. 2 Fluidigm panel antibodies used for primary and CLL cells

| Fluidigm Intracellular panel antibodies | Heavy Metal | Clone |
|---|---|---|
| Anti-p38 [T180/Y182] | 156Gd | D3F9 |
| Anti-pERK1/2 | 167Er | D13.14.43 |
| Anti-pTyrosine | 144Nd | p-Tyr100 |
| Anti-Human Lck | 153Eu | LCK-01 |
| Anti-pAkt | 152Sm | D9E |
| Anti-pPLCg2 | 162Dy | [K89-689][PY759] |
| Anti-pZAP70 | 171Yb | 17a |
| Anti-pS6 | 172Yb | N7-548 |
| Anti-NF-kB | 166Er | K10-895.12.50 |
| **Biolegend Intracellular** | **Flouresecent** | **Clone** |
| PE-Anti BTK phospho [TYR223/TYR180] | PE | A16128C |
| **Fluidigm Surface Human B cell panel antibodies** | **Heavy Metal** | **Clone** |
| Anti-Human CD45 | 154Sm | H130 |
| Anti-Human CD49d | 141Pr | 9F10 |
| Anti-Human IgD | 146Nd | IA6-2 |
| Anti-Human CD5 | 143Nd | UCHT2 |
| Anti-Human CD20 | 147Sm | H1 |
| Anti-Human CD19 | 142Nd | H1B19 |
| IgM UNLB goat anti-human | 148Nd | polyclonal |
| Anti-Human IgM | 172Yb | MHM-88 |
| Anti-Human CD43 | 150Nd | 84-3C1 |
| Anti-Human CD21 | 152Sm | B1B |
| Anti-Human CD27 | 155Gd | L128 |
| Anti-Human CD22 | 159Tb | H1B22 |
| Anti-Human CD3 | 170Er | UCHT1 |
| Anti-Human CD38 | 167Er | H1T2 |
| Anti-Human CD184 [CXCR4] | 175Lu | 12G5 |
| Anti-Human IgG FC FITC | FITC | M1310G05 |
| Anti-Human IgG kappa | 160Gd | MHK-49 |
| Goat Anti-Human IgA | 148Nd | polyclonal |
| **Fluidigm Secondaries** | | |
| Anti-FITC | 160Gd | FIT-22 |
| Anti-PE | 165Ho | PE001 |

### 2.2.3 Maxpar panel design for surface and intracellular antibodies

The antibodies used for mass cytometry in this thesis are listed in Table 2.2.

The choice of antibody label (the metal tag) for each antibody was made with the use of webtool provided by DVS sciences added. (**http://www.dvssciences.com/paneldesigner/experiment/8688**).

This tool was specifically designed to calculate and quantify signal overlap and channel spill-over for the metal isotopes used in this study. Where channel spill-over is apparent, it is important to choose antigens with expression levels that will not influence interpretation of the data. For example, an optimal configuration would be to choose a weakly expressed antigen (for example FoxP3) to be probed by a metal-labelled antibody that had spill-over on to a channel used to detect a highly expressed antigen (for example CD45) so that the contribution due to spill-over to measurement of CD45 expression is negligible. Figure 3.2A demonstrates the algorithm of antibody selection using this tool, and Figure 3.2B shows an example of the result where the colour wheel indicates where spill-over is low (green shading) and where it is higher (orange). A red colour on the wheel indicates the same metal. Therefore, the panel shown in Table 2.2 lists the surface and intercellular antibodies and their heavy metal conjugates that were used in this thesis. This panel was selected for close examination of B cell subsets, for differentiation of B cells from T cells, and for examination of intracellular signaling in stimulated B cells.

### 2.2.4 Palladium Mass-Tag cell barcode multiplexing in primary cells

Palladium Mass-Tag barcoding was used to pre-label cell populations within samples prior to antibody staining. This procedure uses the isotopes of Palladium ($^{102}$Pd, $^{103}$Pd, $^{104}$Pd, $^{105}$Pd, $^{106}$Pd, $^{108}$Pd, and $^{110}$Pd) organised in 20 different arrangements to act as barcode labels for cells (Figure 1.9). The addition of a barcode to cells provides an approach to avoid cross-channel contamination effects to interfere with isotopic impurities, leading to the reduction of antibody measurement parameters and standardised antibody staining between samples. Once samples have been analysed, the barcoding acts as a sample identifier for the decoding software downloaded from **http://www.dvssciences.com** that was supplied by Fluidigm™.

The barcoding procedure used to label CLL cells and normal PBMCs is as described by the manufacturers of the kit used. Briefly, 1x$10^7$ cells stained for viability using Cell ID Cisplatin, as described above, were suspended in 300 μl of Fix I Buffer or prepared fresh 1.6% PFA solution. The cells were incubated for 10 min at RT and then centrifuged at 800xg for 3 min. The supernatant from this step was discarded, and the cell pellet was washed twice with 1 ml of barcode perm buffer (prepared from 10X barcode buffer). The washed cell pellet was resuspended with either 200 μl barcode perm buffer or 200 μl RT PBS + 0.1% tween, to which 2 μl of Palladium barcode was added. The cell suspension was incubated for 30 min at RT, and the now barcoded cells washed twice with 300 μl of Maxpar Cell Staining Buffer. Samples, now individually barcoded, were then combined together for antibody staining.

### 2.2.5 Cell surface staining in primary cells

MaxPar® Cell Staining Buffer, 45 μl, was used to resuspend 5x$10^6$ cells. Thereafter, 5 μl of Human TruStain FcX™ (Fc Receptor Blocking Solution) (Biolegend, London) was added to the tube and allowed to for 10 min at room temperature. Surface antibody was then added without washing. Surface antibodies for staining are made up as a cocktail, adding 1μl of each antibody/sample, so that the total volume added to stain cells is 50 μl according to the fluidigm antibody cocktail preparation guide protocol. The tube containing the antibody/cell mixture was gently vortexed and then incubated for 30 min at room temperature. This was followed by washing twice with Maxpar Cell Staining Buffer. After the final wash, 1 ml of the cell intercalation solution containing MaxPar® Intercalator-Ir was added. At this point cells can be analysed following 1 h incubation at room temperature or stored overnight at 4°C. Prior to analysis, the cells were washed twice with MaxPar® Cell Staining Buffer and once with MaxPar® Water. Finally, the cells were resuspended to a concentration of 2.5–5.0 x$10^5$ cells/ml in MaxPar® Water containing to EQ™ Four Element Calibration Beads at the dilution recommended by the manufacturer. The cells were then ready for analysis by mass cytometry, performed by using a Fluidigm CyTOF-3 machine. In this study, 1–2 million events were normally acquired for subsequent analysis.

### 2.2.6 Detection of intracellular signaling in K562 cell lines using SH2 domains

Dasatinib treatment:

Dasatinib was used in my experiments and it is used to treat CML to inhibit all tyrosine kinase pathway and mainly target BCR-ABL.

K562 cell lines were treated with Dasatinib at a concentration of 150 nM and incubated for 24 hours at 37ºC in a 24-well plate.

K562 cell line permeabilise the cells for intracellular staining either with Methanol on ice or Triton x-100 0.1% at RT.

After treating the cell line with Dasatinib, the cells were fixed with Maxpar® Fix I Buffer for 10 min at RT. In this study, two permeabilising reagents were used to ascertain which has superior permeabilising for SH2 signaling within K562 cells. Thereafter, the cells were centrifuged at 800xg for 5 min at RT once and 1 ml of ice-cold methanol was added for 10–15 min on ice. The methanol should initially be kept at -20 $^{o}$C before mixing gently and incubated for 15 min on ice or kept at -80$^{o}$C till the next day. The samples were washed twice with Maxpar® Cell Staining Buffer.

Triton x-100 0.1% was used as a second permeabilising reagent, and 2 ml was added at RT for 10 min, followed by four washes with 1 ml Maxpar® Cell Staining Buffer cells. SH2 domains/Streptavidin different concentrations antibodies are mentioned in Table 4.1 are added were incubated for 30 min at RT with a final volume of 100 µl. Lastly, 1 ml of the Cell-ID™ Intercalator-Ir was added to each tube, which was then incubated for 1 h at room temperature or overnight at 4$^{o}$C. Cells were then washed with Maxpar® Cell Staining Buffer twice and once with 1 ml of Maxpar® Water. The sample was adjusted to cell concentration to 2.5-5 x $10^{5}$/ml with Maxpar® Water mixed with EQ™ Four Element Calibration Beads and ready to run for CyTOF-3.

### 2.2.7 Heavy metal conjugated to SH2 domains purified proteins.

In determining whether the Maxpar® Antibody Labeling Kit can be used to tag the SH2 domains with heavy metal isotopes, lanthanides, four SH2 domains were used to test for intracellular signaling in cell lines and each domain labelled for a specified metal

(Table 4.1). Each SH2 domain was provided by Professor Peter Nollau Laboratory and has different concentrations.

Initially, the SH2 domain's molecular weight is about 15–20 kDa in size, the filters required for use in the metal labelling protocol are 50 kDa and 3 kDa filters, and the time of the centrifugation is increased to 25 instead of 10 min each time.

The first steps are to preload the polymer with the lanthanide for each SH2 domain by adding 95 µl of L-buffer (Maxpar Antibody Labeling Kit, Fluidigm) into the polymer provided by the kit.

Mix both solutions adequately, then add 5 µl (2.5 mM) of the final concentration of the lanthanide metal solution to the Eppendorf 1.5 ml, mixing the solutions thoroughly and adequately. Then, each lanthanide mixture is placed into the heat block at 37$^{o}$C to incubate for 35 min.

During the incubation period, to prepare the buffers exchange and partially reduce the antibody, add 300 µl R-buffer to a 3 kDa filter and add the volume needed of each SH2 domain that will be used for a correct final concentration of 100 µg, adding it to 200 µl of the R-Buffer in the 3 kDa filter for 12,000 x g, 25 min at RT. Then, the 0.5M Tris(2-carboxyethyl)phosphine hydrochloride (TCEP) stock by diluting 8ul of 0.5M TCEP into 992µl of R-Buffer to have TCEP-R buffer solution and aliquot 100 µl into each antibody and mix it adequately after centrifugation is finished and discarding the column.

After the mixing, incubation is required at 37$^{0}$C for 30 min. The next step is to purify the lanthanide-loaded polymer after the preloading and incubation period are done by adding 200 µl of L-buffer to a 3kDa filter first and then adding the metal-loaded polymer mixture into the L-buffer followed by centrifugation at 12,000xg for 25 min at RT. After centrifugation, add 300 µl of C-buffer into the metal-loaded polymer and follow with the same centrifugation. The next step is to retrieve the purified, partially reduced,

antibody (SH2 Domain) after the incubation period and add the 300 µl of C-buffer into the filter containing SH2 domain and centrifuge. After centrifugation, discard the supernatant, add 400 µl of C-Buffer to the filter, and centrifuge again for 10 min at 12,000xg at RT.

At this stage, there should be two 3 kDa filters, one containing the lanthanide-loaded polymer and the SH2 domain partially reduced antibody. At this stage is when the conjugate the SH2 domain with the lanthanide loaded polymer.

Using a pipette, resuspend the lanthanide-loaded polymer in 60 µl of C-buffer and transfer the resuspended content to the partially reduced antibody in a 3 kDa filter, mix the contents adequately by pipetting, and allow the mixture to incubate at $37^0$C in the heat block for 60 min.

After the 60 min incubation, add 300 µl of W-buffer to the conjugated antibody mixture. Centrifuge for 10 min and discard the supernatant. This step is followed by four washes.

The final step is to recover the conjugated antibody by adding 50 µl W-buffer and pipette to mix and to rinse the wall of the filter twice to obtain all the antibodies. Then, the filter is inverted over a new collection tube, and the collection in the tube is centrifuged for 1,000xg for two min. A meniscus seen in the collection tube suggests that protein is present due to hydrostatic attraction with the plastic walls of the tube.

Check that the amount of SH2 domain collected in each tube is 120 µl of conjugated SH2 domain and add 40 µl of 40% glycerol to the 120 µl of protein to a total volume of 160 µl to have a final concentration of 10% glycerol.

Test the conjugated SH2 domains using CyTOF-3 by taking 10 µl of SH2 domain-heavy metal and diluting it to 400 ul with deionised water. Assuming 90% recovery of

SH2 domains (90% of 100 µg = 90 µg), the final volume is 160ul, 90 ug in 160 µl the final SH2 concentration.

Results of the mass spectrograph show successful antibody labelling with SH2 domains by indicating the black bar presence in the rain plot individually, as shown in Chapter Four, Figure 4.2.

These SH2 domains were kindly provided by Professor Peter Nollau (Forschungsinstitut Kinderkrebs-Zentrum, Hamburg, Germany).

### 2.2.8 Combination of surface and intercellular signaling proteins in primary cells

When the cells were thawed and prepared with stimulation or treatment was added following viability staining, as mentioned above, the cell count was adjusted to a cell concentration of 5 x $10^6$ cells/ml. Centrifuge cells 300 µl ic-PBS, remove supernatant and resuspend in 300uL of ice cold 1.6% PFA OR 1X Fix I buffer (e.g. resuspend cells in 240uL ic-PBS and add 60 µl of either ice cold 8% PFA or ice cold 5X Fix I buffer). The solution should be mixed immediately and left on ice for 10 min; then, wash cells in 500 µl ic-CSB, removing as much supernatant as possible from the pellet. Resuspend the sample in 45 µl of ic-CSB, add 5 µl of Human TruStain FcX™ (Fc Receptor Blocking Solution) (Biolegend, London), and leave on ice for 10 min. It prevents non-specific staining on cells by blocking Fc receptors. Add 50 µl of a 2X antibody solution made in ic-CSB (antibodies concentration should be optimised) and leave on ice for 30 min. For example, add 1.1 µl of each 1 ug/µl antibody and make up to 55 µl with ic-CSB for a double antibody solution with 10% extra for pipetting errors, providing a final concentration of 1:100 (10 µg/ml); two samples require 2.2 µl of each antibody and then topped up to 110 µl with CSB, and so on. Leave the surface antibodies on ice for 30 min and then wash with Maxpar® Cell Staining Buffer twice

600 x 3 min at 4°C. Weigh out BS3(bis(sulfosuccinimidyl)suberate) powder, allowing time for BS3 to reach room temperature before weighing an appropriate amount in an Eppendorf (see below for the approximate quantity) and then centrifuge it to the bottom at 6,000rcf for 10 sec. Dissolve the BS3 powder in ic-PBS just prior to adding to the cells below; BS3 is required to be at 5 mM final.

Calculation:

Mass (g)/MW = Volume (l) x Concentration(M)

Mass (g)/572.43 = Volume (l) x 0.005

Volume (l) = (mass (g)/572.43)/0.005

Example:

Weigh out 0.00,456 g of BS3 powder

Volume = (0.00,456 g/572.43)/0.005

Volume = 0.00,159 L = dissolve BS3 in 1.59 ml of ic-PBS

Once this has been done, centrifuge the solution to the bottom for 1 min. Dissolve the BS3 powder in ic-PBS just prior to adding to the cells the BS3 at 5mM final concentration. Centrifuge, remove the supernatant, break the pellets up by flicking the tube, and then resuspend the cells in 300 µl ice cold methanol. Leave cells on ice for 10 min, or, alternatively, cells can be stored in methanol at -80°C for several weeks to months. Centrifuge cells, remove methanol, and wash cells in 500 µl ic-CSB.

If it is required to add pallidium barcodes, centrifuge the cells, remove the methanol, and wash the cells with 200 µl cold PBS +0.1% tween for the first wash, and the second wash should be warm PBS +0.1% tween pellet. The first wash should be cold, and the second wash should be done with warm PBS. Prepare 10% tween-aliqout, 10 µl into 1ml of PBS. Resuspend the pellet with room temperature PBS +0.1% tween, then add

2 µl of barcode pallidium isotopes and incubate for 10 min at RT. Centrifuge twice with CSB at RT and combine the samples. Resuspend the cells in 100 µl of room temperature internal antibody cocktail (antibody concentration needs to be optimised) and leave at room temperature for 30 mins. Thereafter, incubate the cells at 37°C in a heat block with a mild vortex for 30 min. Wash the cells twice in ic-CSB and resuspend the cells in 1.6% PFA in PBS (or 1X fix I buffer) with 500 uM intercalator-Ir at 1:8,000.Cells can be stored for up to 2 weeks at 4$^{o}$C and then prepared and run on CyTOF. Add the fix andperm bufferon the day of the run, add Ir 1 hour RT and prepare for CyTOF.

### 2.3 Western Blotting

#### 2.3.1 Protein Extraction and Quantification

The first process to prepare samples I used for western blot, to use clear lysis buffer that isolates all the proteins from other parts of cell by breaking the cell membranes. In addition to the sonication that is required as second step to completely reach full protein extraction and cell structure is denatured. Sonication was set for five cycles using a Biorupter Water Cooler. Quantification of proteins was prepared according to Bradford Protein Assay Bio-Rad on 96 well plate. The first two columns were for the standards and the next columns for the Maver-1 and Jeko-1cell lines, with different IgM time point stimulation and the same IgM 20 µg/ml concentration. The result was read using a spectrophotometer (Bio-Tek uQuant Universal Microplate Spectrophotometer) to measure the proteins absorbance of light at specific wavelength to measure sample protein concentration and graph analysis that followed the standard criteria.

### 2.3.2 Western Blot

For this study, the aim is to confirm whether IgM stimulation on Maver-1 and Jeko-1cell lines shows expression when probed with the primary phospho- protein antibodies worked in different time points, 0.5 and 15 min. Ten percent acrylamide gel for a Bio-Rad mini gel apparatus (Bio-Rad laboratories Ltd, UK) and 5 ml resolving gel buffer (Geneflow, UK) were mixed with 6.7 ml acrylamide solution (19:1 Acrylamide/Bisacrylamide, Geneflow, UK) and 8.3 $H_2O$. Polymerisation of the gel was initiated with the addition of 250 µl 10% Ammonium persulphate (APS) and 25 µl tetramethylethylenediamine (TEMED). The amount of resolving gel solution created is ideal for casting two 1.5 mm PAGE gels, which were left to polymerize at RT for 1 h. A 5% polyacrylamide stacking gel was prepared by mixing 1.25 ml stacking gel buffer (Geneflow, UK) with 0.85 ml acrylamide solution and 2.9 ml $H_2O$ and then adding 10% APS 25 µl and 5 µl TEMED. Insert the 10- or 15-well combs that were used to create sample chambers for cell lysates in the stacking gel.

Western blotting technique was used to specify the molecular weight proteins and understand the level of expression of both total plcy2 and phosphorylated PLC$\gamma$2, ERK ½, p-BTK, and p-AKT through sodium dodecyl sulphate polyacrylamide gel electrophoresis (SDS-PAGE). The kilodaltons targeted were 150, 60, 75, 44, 42 to understand and evaluate cell lines and expression in each intercellular antibody by first running the samples into 10% SDS-gel electrophoresis, using a 10–15 well comb that takes a maximum of 20–30 µl and transferred onto immobilon-P polyvinilidene difluoride membranes (Millipore Corporation; USA). The primary antibody used, phospho antibody, is rabbit polyclonal antibody in 5% BSA for total caspase-8 and in

5% BSA for treated cell lines by IgM $(Fab)_2$ to confirm the expression between cell lines proteins and IgM expression. Incubation was overnight on a rocker in the cold room. Afterwards, it was incubated by a secondary antibody (goat anti-rabbit/mouse IgG-HRP conjugated) for 2 h at room temperature on a rocker and 200 µl of sodium azide. Following the incubation, ECL substrate was added to view the protein band by capturing through the chemiluminescent reaction using an image reader, LAS-1000 (Fujifilm,Tokyo,Japan), which uses an enhanced chemiluminescence kit (GE Healthcare Life Sciences, Buckinghamshire, UK).There are a few shortcomings in the western blot techniques which have to be considered. First, classical western blots are non-quantitative, whereas they can determine whether a particular protein is present. They do not make it possible to quantify the amount of a protein present. Second, western blot can only be performed if the primary antibody against the protein of interest is available. These primary antibodies are expensive. Third, western blot is challenging to perform properly to obtain consistent excellent results. Fourth, sometimes antibodies exhibit off-target binding which can cause poorer result.

### 2.4 Far western blotting using SH2 domains conjugated to heavy metals

Far western blot is a method similar to the standard Western blot to characterize protein-to-protein interactions, which is a useful technique to detect labelled protein antibody on the membrane blot. In my thesis I used it to measure intracellular signaling, using glutathione-S- transferase purified Src-homology-2 SH2 domains, and were biotin-labelled probe and detected by streptavidin HRP (biotinylated). Src homology region 2 (SH2) domains have specifically bound to phosphorylated tyrosine proteins. In my experiments I used the calculation used to probe the unlabelled and labelled SH2 domains with heavy metals and Streptavidin biotinylated, according to (Table 4.1) with a final concentration of 50ng/ml in 10 ml total end volume for each SH2 domain to incubate them on the membrane blot for one hour RT after the lysates are separated by SDS-PAGE electrophoresis and transferred into the membrane. To prepare the complex formation in 10 ml, each SH2 domain concentration (Table 4.1) is aliquoted in 1.5 ml Eppendorf, and added 1% BSA/1xTBST solution was prepared, and added to the mixture to be diluted in a 10ml to incubate for 30–60 min.

K562 cell lysates were treated with Dasatinib 150 nM for 24 hours and Mec-1 lysates treat with pervanadate 100 μM 15 mins. Each lysate was quantified and ready to run for far western. Initially, the western blot was done and probed anti-phosphotyrosine antibody (PY20) as a confirmation that the cells were responsive for Dasatinib and pervanadate treatment (Figure 4.3).

### 2.5 Cytobank software Analysis

All experiments conducted by CyTOF-3 are analysed by Cytobank software, which features a specific in-depth gating method and detailed phenotypic examination of each cell population and its subsets where data produced by several different parameters are analysed. This provides the answers to many questions by the identification of rare cell populations, quantifying a diversity of cell populations, and the focused phenotypic examination inside rare populations and cell expression.

The Cytobank provides a view of the analysis in different algorithms and computerised skills. It allows to analyse data using unsupervised algorithm using dimensionality reduction algorithm (viSNE) and clustering algorithm (SPADE, FlowSOM), to view the important data information to understand cellular abundance, expression identification.

#### 2.5.1 Visualization stochastic neighbour embedding algorithm (viSNE):

viSNE analysis is an unbiased gating of the cell population. The sample files for each population are selected from a pre-gated live cell singlet that is further subdivided into subsets as shown in (Figure 3.6A). The next step is to select all the different parameters required to visualize the phenotypic markers expression as shown in (Figure 3.6B) CyTOF allows for the addition of more than 30 different parameters to measure every single cell. Each population measures the event sampling proportional or equal to the desired total events versus events per population. This is a principal components analysis where each point is related to others within n dimensions that its end results a cloud formation structure of clusters with all the parameters and provides an in-depth visualization of phenotypic examination. This platform is a tool that uses the tSNE (t-distributed stochastic neighbour embedding algorithm) for interpretation.

### 2.5.2 Spanning-tree Progression Analysis of Density-normalised Events (SPADE)

The SPADE hierarchical algorithm mechanism transforms the data by first down sampling the data to capture different cell populations, including rare subsets that clusters them phenotypically to similar cells into ‘nodes’, into a tree format, a SPADE tree. In order to generate the spanning tree, it is required to set the first number of nodes to allow to cluster to identify the population and to select the number according to less or more clusters to present in the tree as shown in (Figure 3.8A). To gate a rare population, the number of nodes should be reduced to remove unnecessary noise and provide a chance to find the rare population. A high number of nodes can also be used to detect large populations. The next step is down sampling which detects the density dataset according to number of total events per population, helps to filter out the event, and allows the presentation of only one of the desired clusters, especially in rare populations as shown in (Figure 3.8B). If the rare population has 500 events and down sampling is 10%, it will remove 450 events and keep only 50 of the total events after down sampling. Thereafter, the required and desired population is selected, with the phenotypic markers that are required for the clustering analyses that are included within the selected population as shown in (Figure 3.8C).

### 2.5.3 Self-Organizing Map (FlowSOM)

FlowSOM is a new visualization and SOM clustering algorithm that has recently been used to analyse flow and mass cytometry data. The algorithm is able to cluster on larger datasets with or without manual gating, which is a superior way to detect a rare population faster. It is similar to SPADE, but the clustering algorithm is different in that representation of the data figures by star charts and meta clustering of nodes that can be calculated in a new way, visualised in the grid. The principles to start the FlowSOM

algorithm by reading the data that starts to process several FCS files and allows comparisons between them. Thereafter it starts to build the self-organizing map As shown in (Figure 3.17A), according to the grid node, and connects each similar node and neighbouring other nodes as shown in (Figure 3.17B) so that results can be viewed as a minimal spanning tree (MST), and this results in computing a meta-clustering which creates a background colour within the nodes.

# Chapter 3: Characterising B cell subsets in samples of PBMCs derived from healthy individuals and patients with CLL with mass cytometry.

**3.1 Introduction:**

Phenotypic characterization of B cell subsets has typically been performed by fluorescence-based flow cytometry which is used to identify surface expression of proteins that indicate cell differentiation [6, 107]. In this respect antigens such as CD19, CD20 and CD27 are used to classify naïve and memory B cells from the total B cell population. However, there are challenges to this method because there is limitation in the number of markers that can be simultaneously assessed due to spectral overlap of the fluorophores that are used to tag antibodies. Such spectral overlap requires compensation as a required step for interpretation of the data. In addition, background fluorescence can also interfere with detection, and algorithms that correct for this background fluorescence need to be employed. Together, these elements restrict conventional flow cytometry to a limited number of parameters that can be measured simultaneously [108].

The ability to measure multiple surface antigens on B cells has distinct advantage in a clinical setting in terms of distinguishing disease from healthy phenotypes. Typically, the Liverpool Clinical Laboratories (NHS) use a panel of antibodies that recognise 16 different antigens in 3 different measurements (tubes) to determine if malignant B cells are present in samples of whole blood. The process of B cell recognition by flow cytometry technologies could be made more efficient. A new generation technology, mass cytometry, is developed to remove the limitations of conventional flow cytometry

[109]. At the beginning of this thesis mass cytometry had not yet been extensively used to characterise normal and malignant B cells. The aim of this chapter is to investigate the use of a third generation of mass cytometer, Helios (CyTOF3) that is theoretically able to measure up to 135 different parameters associated with a single cell without any compensation [6, 110], in the analysis of B cells within PBMC preparations from healthy individuals and patients with CLL.

## 3.2 Results

### 3.2.1 Design of the antibody panel for use in mass cytometry.

Table 2.2 lists all the antibodies used to analyse normal and malignant B cells in peripheral blood samples. In this section I list the surface markers used to study normal and CLL B cells (Table 3.1).

Table 3. 1 Fluidigm surface human B cell panel antibodies

| Surface Human B cell panel antibodies | Heavy Metal | Clone |
|---|---|---|
| Anti-Human CD45 | 154Sm | H130 |
| Anti-Human CD3 | 170Er | UCHT1 |
| Anti-Human CD5 | 143Nd | UCHT2 |
| Anti-Human CD43 | 150Nd | 84-3C1 |
| Anti-Human CD19 | 142Nd | H1B19 |
| Anti-Human CD20 | 147Sm | H1 |
| Anti-Human CD21 | 152Sm | B1B |
| Anti-Human CD22 | 159Tb | H1B22 |
| Anti-Human CD27 | 155Gd | L128 |
| Anti-Human IgM | 172Nd | MHM-88 |
| Anti-Human IgD | 146Nd | IA6-2 |
| Anti-Human CD184 [CXCR4] | 175Lu | 12G5 |
| Anti-Human CD38 | 167Er | H1T2 |
| Anti-Human CD49d | 141Pr | 9F10 |

The rationale for choosing the above 14 surface antibodies is to be able to identify different B cell subsets within populations of leukocytes and characterise them (Figure

3.4). Starting with CD45, this is a glycoprotein marker that is known as the common leukocyte antigen (LCA) which is present on all haemic cells with the exception of mature erythrocytes[111]. This antigen was used to identify white blood cells within the samples I used, cells bearing this antigen are counted as the total leukocyte population. CD3 is the next important marker. Expressed mainly on T cell lymphocytes use of this marker allows exclusion of T from B cell populations. CD5 is a marker also present mainly on T cells, however, there is a rare population of B cells that express this antigen (so called CD5+ B cells that are equivalent to “B1a” cells in mice) from which CLL cells develop [112]. This particular population of CD5+ B cells also express CD43, differentiating these cells from other B cell populations which are low in expression of this antigen. T cells typically express high levels of CD43 [111]. CD19 is a marker of B cell lineage and is expressed on all B cells from early stages of haematopoiesis[113]. CD20 is similar to CD19 in expression, with the exception that it is not expressed on plasma cells. Both CD19 and CD20 can be used to identify the total B cell population. CD21 is a marker expressed on mature B cells where it functions to assist in antigen complex internalisation. CD22 is also a marker of mature B cells and is a lectin that recognises carbohydrate residues. Together, these 4 B cell antigens play important roles in B cell receptor signaling [114]. CD27 is a marker expressed on both B and T cell populations. On B cells expression of this antigen differentiates between memory $CD27^+$ and naïve $CD27^-$ B cells. On T cells, this expression pattern is reversed and naïve $CD27^+$ and memory $CD27^-$ subpopulations can be identified within total $CD4^+$/$CD8^+$ T cells [115, 116]. Immunoglobulin membrane proteins IgM and IgD form the B cell receptor and their expression can be used to distinguish naïve from memory B cells. IgM is highly expressed on memory B cells, whereas IgD low or absent. In contrast, on naïve B cells IgD surface expression is high

and IgM is somewhat lower than that observed on memory B cells. CD38 is an ectoenzyme marker only present on early and late developing B cell populations [117]. CD38 is also a marker for poor disease prognosis when expressed on the malignant cells of CLL [118]. CD38 is present on activated T cells and on myeloid cells [119]. A second prognostic indicator that is used in CLL and included in the panel is CD49d, or $\alpha$4 integrin. This integrin is normally expressed on B cells where is plays an important role in leukocyte trafficking and activation [120]. In CLL, expression of CD49d correlates with progressive disease, particularly when 30% of cells show positivity [121]. The final antigen within this panel is CXCR4, or CD184, which is a chemokine receptor for CXCL12 and is expressed by all B cell subsets [122]. When used in conjunction with CD5 expression on CLL cells, this marker gives information about newly emerged which is highly expressing CD5+ cells and CXCR4- cells and older quiescent cells expresses CD5- cells and high CXCR4+ within populations derived from PBMCs [38].

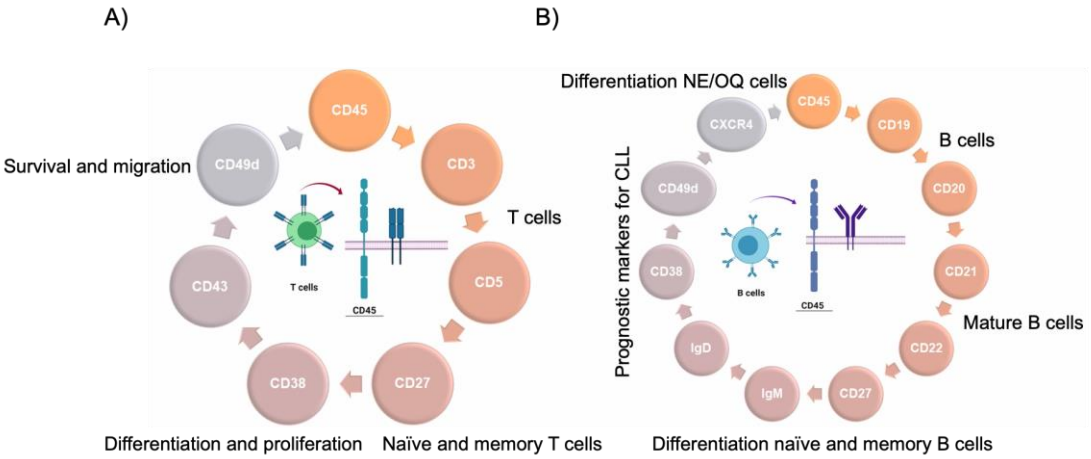


**Figure 3. 1 Differentiation of T and B cell subtypes by antigen expression.** Diagram presentation of B and T cells antigen expression on membrane showing CD45 is present in both T and B cells and CD19/CD20 CD21/CD22 presents in B cells, CD27 naïve and memory B cells and T cells, with IgM/IgD expression present. CD38/CD49d prognostic predictor marker for CLL, CXCR4/CD5 divides the B cell CLL into two subsets newly emerged and older quiescent cells.CD3/CD5/CD43 expressed in T cells. CD5/CD43 are expressed in B cells in low levels.

I next chose heavy metal tags for the antibodies in Table 3.1. Figure 3.2A shows a schematic of the algorithm I used. Antibody targets were entered into the MaxPar Panel Designer webtool (**http://www.dvssciences.com/**) that allows optimised selection of heavy metal conjugates. Here it is important to consider that signal and tolerance value play an important role in preventing spill over from one measurement channel on to another to potentially affect quantification of the analysis. Figure 3.2B shows how this web tool selects heavy metal conjugates to produce a table of how one isotope can spill into the measuring channel of another and is illustrated in a panel wheel (Figure 3.2Bii and iii). The panel wheel is divided into 3 sections describing the tolerance associated with each isotope [high (>40), medium and low (<4)], which is a number associated with the potential for spill over into another channel. The height of the fin indicates the sensitivity with which the mass cytometer detects a given isotope, the larger the fin the more sensitive the detection. Finally, colouring indicates high

(orange), moderate (light green) and low (dark green) potential for spill over based on tolerance so that the user can insure that antibodies to antigens that are highly expressed do not contribute artefacts to channels associated with antibodies to low expressed antigens.

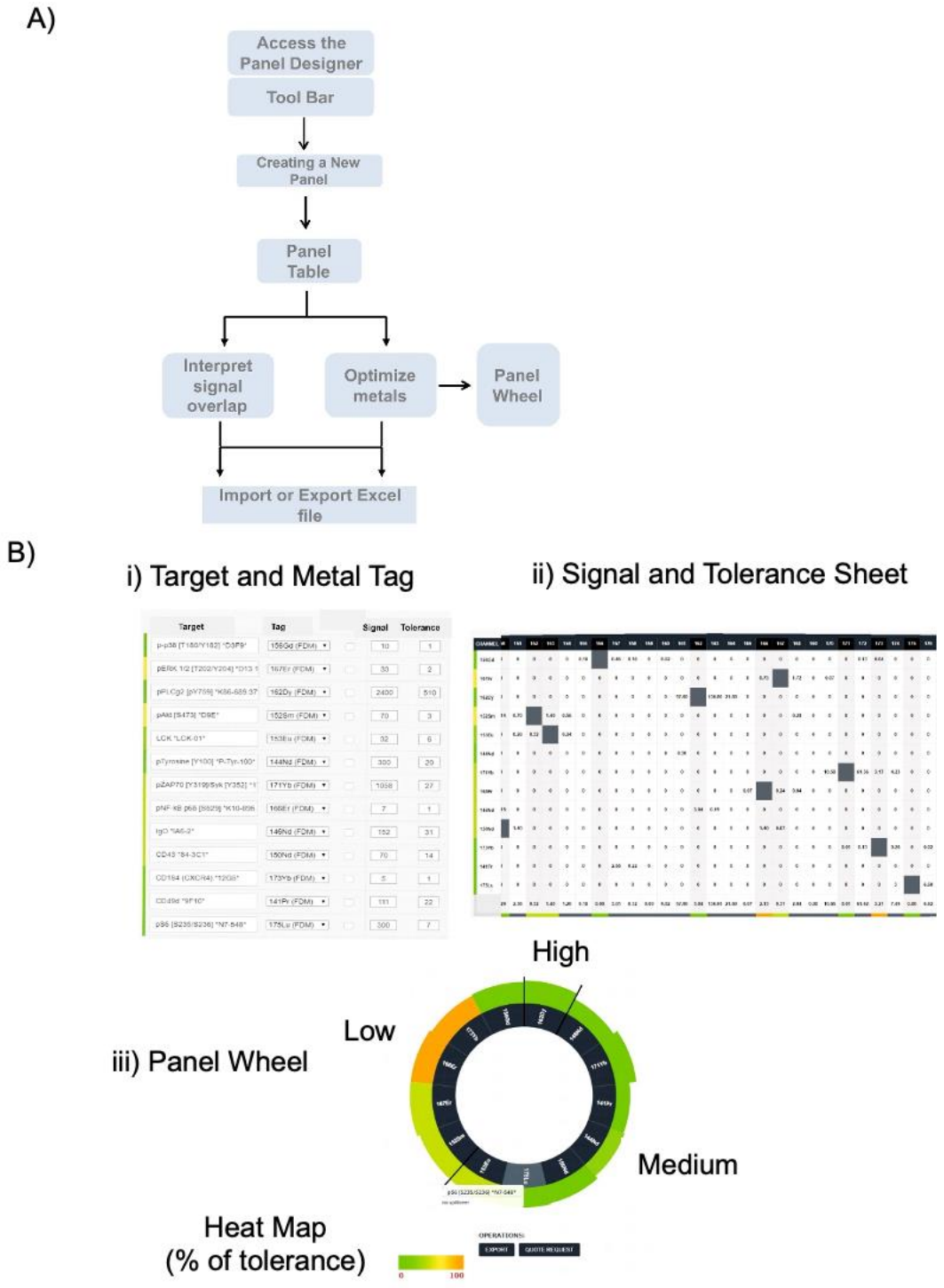


**Figure 3. 2 MaxPar® panel designer webtool demonstration. A.)** A simplified stepwise algorithm showing antibody selection using the MaxPar® panel designer tool. **B.) i)** Target and Metal Tag an illustrated example of how targets (antibody) and tags (metal-tag) are chosen in combination. **ii)** Signal and Tolerance sheet where each channel shows each channel spill over into and out which is then coloured by a panel wheel that indicates high, medium and low signals and tolerance **iii)** Panel wheel presentation of pS6 no spill over to any channel. A red colour on the wheel indicates the same metal.

### 3.2.2 Doublet discrimination by mass cytometry.

Mass cytometry measures events (cells) by detecting intact nuclei within cells, whereas conventional flow cytometry measures events by detecting the optical parameters associated with cells. An important consideration when interpreting data generated by these techniques is the discrimination of events associated with single particles (cells) from those associated with two or more particles. Mass cytometry detects nuclei with a DNA intercalator, Cell-ID™ Intercalator-Ir, that has been coupled with natural abundance iridium where cells are stained and bind to the nucleic acid and is detected by the 191Ir and 193Ir isotopes in the nucleated cells that are present as they are in nature. Figure 3.3 shows the dot plots associated with cells where this compound has been used and iridium detected by mass cytometry. Figure 3.3A shows the relationship between $^{191}$Ir and time, Figure 3.3B shows the relationship between $^{191}$Ir and $^{193}$Ir in the way they stain nuclei and other particles, and Figures 3.3C and D show the relationship between event length (the size of the ion cloud) and $^{191}$Ir and $^{193}$Ir, respectively. In each section the events are coloured according to density where the red-orange-yellow colouring indicates the highest density. The narrow line (in Figure 3. 3A) and discreet dots (in Figures 3.3B-D) associated with the most intense signals indicate events associated with single cells. Figure 3.3A shows the consistency of this concentration of events over the entire course of experimental measurement and is a gauge of quality control. Figure 3.3B shows the linearity of the relationship between $^{191}$Ir- and $^{193}$Ir-intercalator incorporation in differently sized particles, corresponding to DNA content, where the majority of particles are of a single size. Similarly, Figures 3.3C and D shows the relationship between particle size and DNA staining. Drawing a gate around the areas of highest density events in each dot plot yields similar results (89.4%, 88.5%, 88.6% and 86.0%, respectively). This

consistency indicates that each method can be used to discriminate doublets, for the purpose of this thesis I used the relationship between $^{191}$Ir and time.

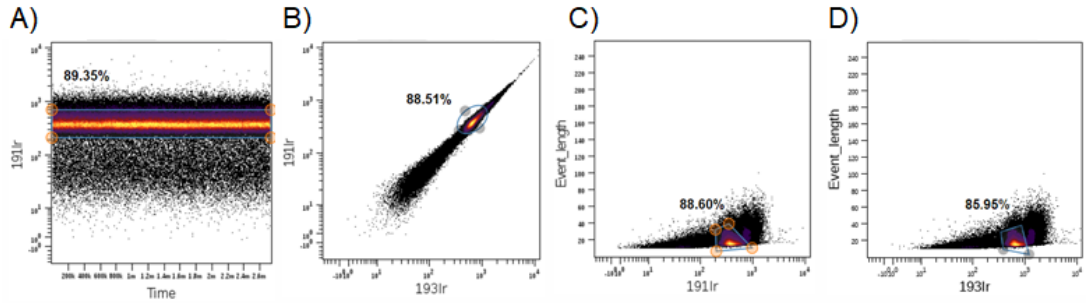


**Figure 3. 3 Gating templates for discrimination of doublet from singlet cell events.** Different variations of doublet discrimination in mass cytometry generated data presented as event density bivariate (dot) plots. The gated singlets represent yellow red colour in each dot plot. **A.)** incorporation of $^{191}$Ir intercalator versus Time of experimental measurement (in minutes). **B.)** $^{191}$Ir versus$^{193}$Ir. **C.)** Event length versus$^{191}$Ir or **D.)** $^{193}$Ir.

### 3.2.3 Identification of B and T cell subsets in PBMC preparations (manual gating).

After determining that my cell population of interest were singlets, the next stage of my analysis was gating for different lymphocyte subsets. Figure 3.4 shows the process I took to perform this function.

Discrimination of live from dead cells was performed using the Cell-ID Cisplatin reagent. Cisplatin, also called cis-diamminedichloroplatinum(II), is considered to be a cytostatic agent [123] and works by covalently binding to exposed sulfhydryl groups on proteins and nitrogen donor atoms on DNA, the latter interaction leading to damage of the DNA and concomitant blockade of replication [124]. With respect to the assay that distinguishes live from dead cells, it is the ability of cisplatin to label proteins that is important. The 5 min incubation of the assay allows interaction of cisplatin to available proteins which is limited on live cells because they require active transport to take this compound up. In contrast, the proteins of dead cells, because of the

permeable nature of their membranes, are easily labelled. Thus, live cells are detected as the population with low amounts of $^{195}$Pt over time, whereas dead cells will have considerably more. In Figure 3.4 the top right hand dot plot shows that a majority of events is associated with a low incorporation of $^{195}$Pt and were taken as the live cell population. The next gate involved selection of CD45+ cells (CD45 is highly expressed on all leukocytes), followed by selection of cells which were positive for CD19 (a specific B cell marker). I found that it was necessary to further gate the CD19+ for CD3 because my doublet discrimination step in normal B cells as to further eliminate any doublets and aggregations that can commonly occur in frozen buffy within the populations. This step was very important because the population of CD5+ B cells I am interested in is rare and I did not want interference from contaminating T cells. Thus, in the end I was left with pure CD19+/CD20+ populations of cells for further gating. Naïve and memory B cell subsets were identified on the basis of CD27 expression, the former being negative whilst the latter being positive. CD5+ B cells were identified from the whole population of B cells based on CD5 and CD43 expression. At each stage the proportion of total, naïve, memory and CD5+ B cells with respect to total leukocytes and was consistent with normal values [125].

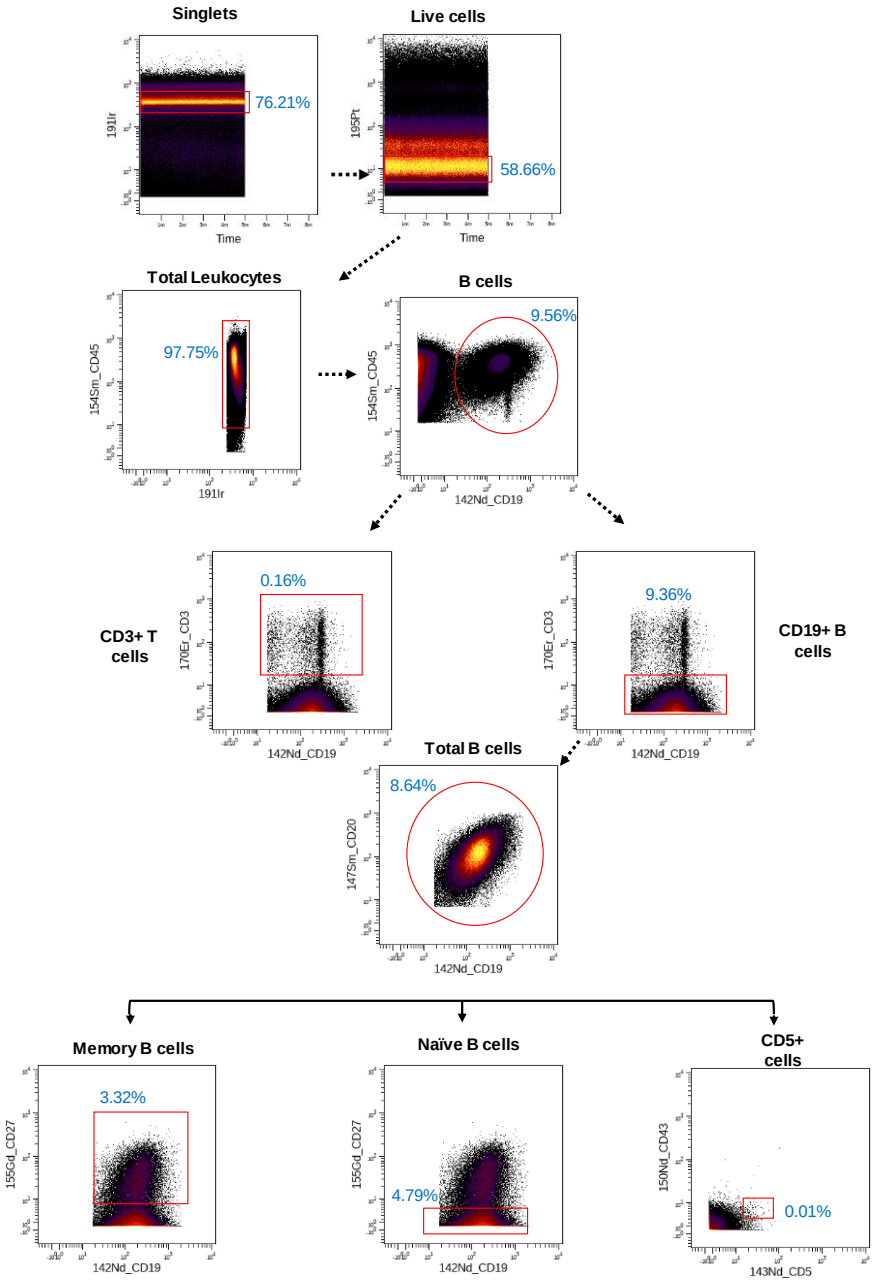


**Figure 3. 4 Manual gating strategy to identify B cell subsets in normal PBMCs by mass cytometry.** Each dot plot connected by arrows represents consecutive gates to identify B cell subsets within populations of PBMCs. Singlet discrimination is performed by plotting $^{191}$Ir/Time. The main population of cells represented by the yellow red line (indicating density) are taken (drawn box) and reanalysed for viability by plotting cisplatin $^{195}$Pt vs time. Those cells with low levels of $^{195}$Pt are taken for identification of total leukocytes by CD45 expression. B cells are then identified by CD19 expression, and then within this population contaminating T cells are removed by CD3 expression. This leaves total B cells as demonstrated by CD20/CD19 positivity. Memory and naïve B cells are identified by CD27 expression, and CD5+ B cells are identified by CD5 and CD43 as is described [24]. Drawn gates represent the proportion of identified cells in the total leukocyte population.

In a similar way to B cells, I next gated for T cell populations as shown in Figure 3.5. Here I start with CD45 expression and then show how serial gating results in identification of some T cell features. For example, CD3 and CD5 are used as identifiers of T cells, CD19 is used to remove B cell contamination, and finally CD27 is used to discriminate naïve (CD27+) and memory (CD27-) T cell populations. Together, the manual gating strategies I employed show that mass cytometry data can be used to identify B and T cell subsets.

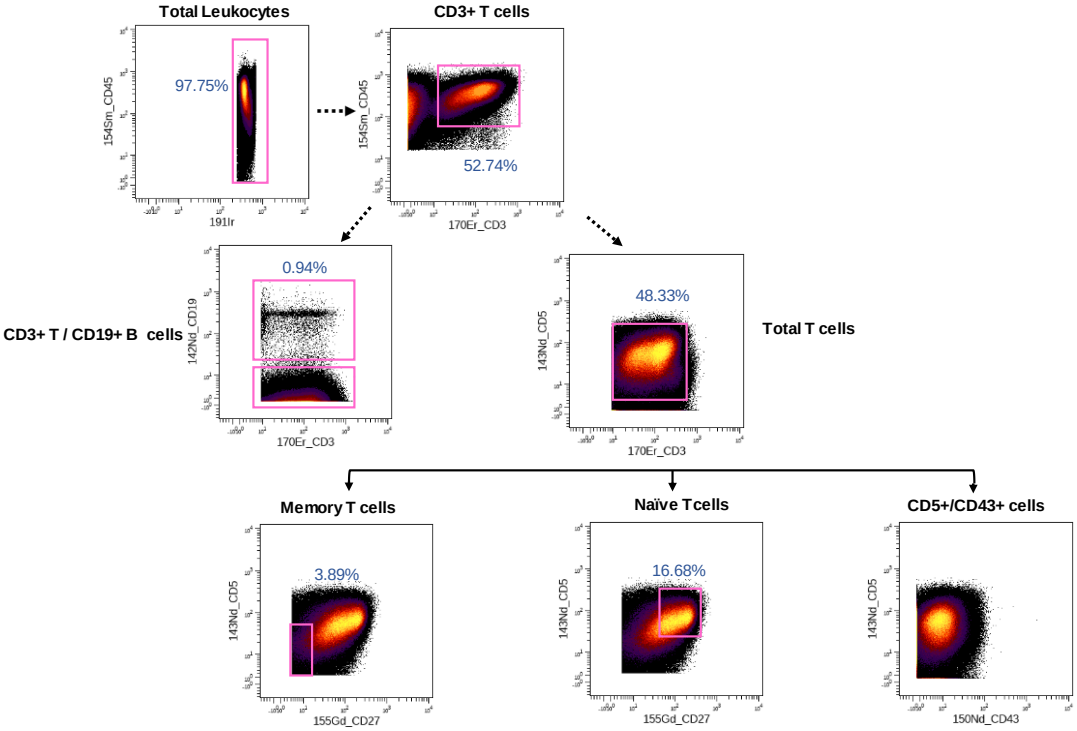


**Figure 3. 5 Manual gating strategy to identify T cell subsets in normal PBMCs by mass cytometry.** Each dot plot connected by arrows represents consecutive gates to identify T cell subsets within populations of PBMCs. Doublet discrimination and cell viability are as described in Figure 3.4. Identification of total leukocytes is made by CD45 expression (*top left panel*). T cells are then identified by CD45/CD3 expression, and then within this population contaminating B cells are removed by CD19 expression. This leaves total T cells as demonstrated by CD5/CD3 positivity. Memory and naïve T cells are identified by CD27 expression. CD43 on T cells is shown in the bottom right panel. Drawn gates represent the proportion of identified cells in the total leukocyte population.

### 3.2.4 Discrimination of cell phenotypes using reduction algorithms for high-dimensional mass cytometry data

#### 3.2.4.1 viSNE

Gold standard analysis of flow cytometry data is achieved through traditional manual gating as I have already demonstrated. A limitation of this approach is the bias towards the cell population of interest (i.e. B cell vs T cell populations) that is taken by manual gating where it becomes increasingly difficult to appreciate expression of a single antigen on all cell types within the whole population of leukocytes. This is particularly important for the high dimensional data that mass cytometry can generate. To resolve this limitation dimensionality reduction algorithms have been developed [88] that allow for simultaneous analysis of antigen expression on all cells. One method is termed "viSNE" and projects mass cytometry data on to a 2-dimensional plot using t-distributed stochastic neighbor embedding algorithms (tSNE). This method reduces dimensionality by positioning data associated with a single cell in relation to its closest neighbor. Such analysis allows the entire population of cells (leukocytes for the purpose of this thesis) to be visualised on the basis of phenotype and give insight into where antigens are expressed and located anatomically within.

Figure 3.6 shows the analysis viSNE will generate from the data produced in a typical experiment. The data used was the same as was used for manual gating in Figures 3.4 and 3.5. Because small populations of CD3/CD19+ doublets were present, it was decided to gate these doublets out so that they would not contribute to the final viSNE analysis. Figure 3.6A shows a dot plot representation and example of the gate used to select data for further analysis.

With the appropriate data selected, a viSNE plot could now be realized (Figure 3.6B). Each of the 14 panels shows reactivity of a single antibody across the entire population

of Analysed live leukocytes. Events corresponding to single cells are arranged in islands of similarity, and these islands can be associated with particular cell types based on presence of a defining antigen. For example, there is a large island of cells that react strongly with the CD3 antibody signifying that these cells are T cells. Immediately to the left of the T cells are 2 islands of CD19+ cells, cells which are B cells. North of the T cell island is an island likely to represent myeloid cells because they are neither CD3 nor CD19 positive, nor do they express other antigens within the panel that are expressed by lymphocytic cells (eg CD20, CD5 and CD22).

With the viSNE projections it is now possible to simultaneously observe variance in expression of different antigens across all cell populations. For example, CD27 expression can be observed in the upper left island of B cells, in the small region of the putative myeloid island likely corresponding to natural killer cells, and across a large swath of the T cell island. In a similar way expression of other antigens can be observed; CXCR4 is largely present on B and T cells, CD38 expression is restricted to subpopulations of B, T and myeloid cells, *et cetera*.

viSNE analysis also reveals cell numbers. The size of each island is representative of the proportion of events that are similar; as expected T cells are the dominant island whereas the islands representing B cells are somewhat smaller. In this way, quantitative data of a similar nature to what can be obtained using manual gating can also be obtained through this automated algorithm.

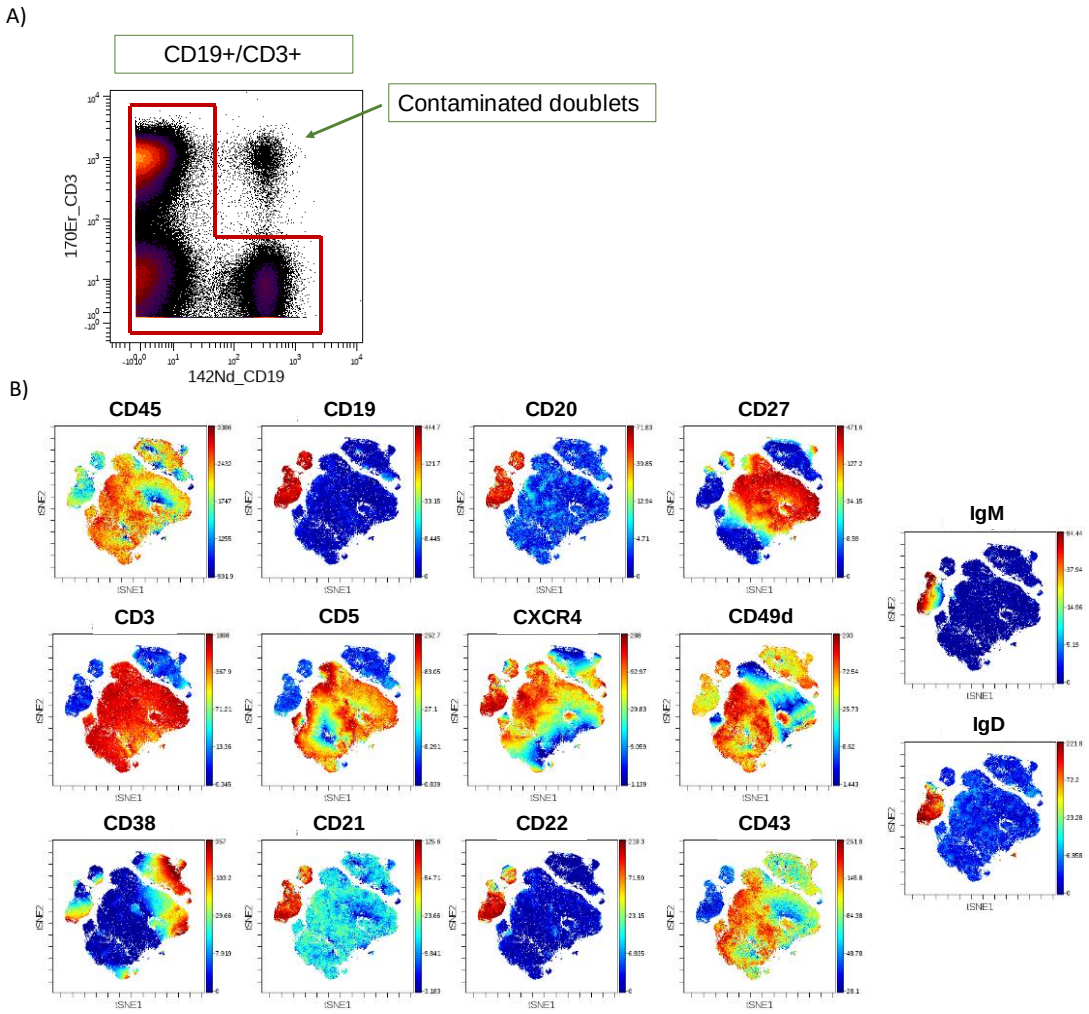


**Figure 3. 6 viSNE analysis of mass cytometry data generated from normal PBMCs stained with surface markers. A.)** Dot plot representation and gate applied to select data for viSNE analysis. **B.)** viSNE plots of mass cytometry data generated by surface staining of PBMC samples from healthy adults using the antibody panel listed in Table 3.1. The rainbow intensity is a measure of indicated antibody reactivity with each island of similar events.

Following analysis of the total leukocyte population, I then focused on the B cell island. Figure 3.7 shows a close phenotypic visualization of this population of cells giving insight into the geography and range of reactivity for each antibody in the panel I used Table 3.1 The total B cell population is uniformly strongly positive for both CD19 and CD20 (99.7%). Such reactivity is shared by CD21 and CD22, but the latter shows variable reactivity with CD27+ memory B cells. Similar variable reactivity with different B cell subsets was also observed with CXCR4 and CD49d. Naïve and memory B cells

can be identified by CD27 expression where the south island of cells are largely negative (comprising 6.40% to total leukocytes) and the north island and a northern segment of the south island show a range of reactivity with CD27 (comprising 3.31% to total leukocytes), respectively. Memory B cells within the north island are negative for both IgD and IgM signifying that they likely to have undergone class switch to either IgG, IgA or IgE positive cells. Memory B cells grouped in the northern part of the southern island, in keeping with the literature [126] are strongly positive for IgM and show a range of reactivity with IgD. Naïve B cells within the southern island are uniformly strongly positive for IgD expression but show a vast range of positivity for surface IgM. CD38 expression also shows wide variation in expression on the north and south B cell islands. On the north island strong CD38 expression likely corresponds to plasmablast cells where sIg and CD27 expression is low [127]. On the south island, strong CD38 expression likely corresponds to B cells that have been activated or are CD5+ [128]. Correspondingly, in my experiments, it is this same CD38+ region of the south B cell island that is weakly positive for CD5. These same cells do not show expression of CD3 and are therefore likely to be a true population of CD5+ cells as is described by[129, 130]. These CD5+ B cells comprise 0.06% of the total leukocyte population, their rarity is consistent with established studies.

Taken together, these data show that B cell subsets can be discriminated and quantitatively assessed using viSNE as an approach to the analysis of mass cytometry data.

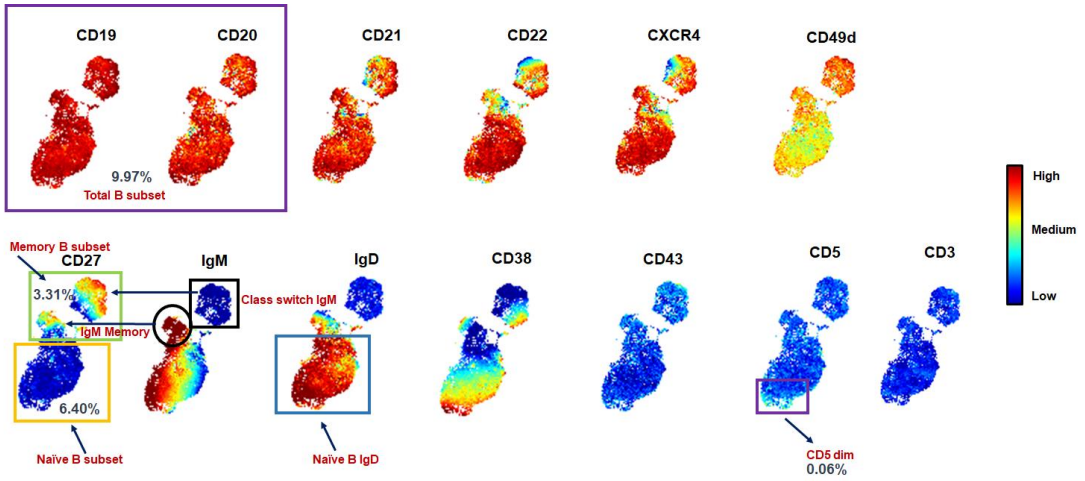


**Figure 3. 7 phenotypic examinations within each subset.** In-depth phenotypic examination of the total B cells $CD19^{+}$ population from the Total Leukocytes. See $CD27^{+}$ memory B cells $CD27^{-}$ naïve B cells expression within the B cell. IgM and IgD are expressed in the lower part of B cells. CD5 /CD43 cells are dim within the B cell population. CD43 & CD5 cells more over expressed widely in the T cell compartment.

### 3.2.4.2 SPADE

A second method I used for analysis of high dimensional data is Spanning-tree Progression Analysis of Density-normalised Events (SPADE). This is a computerized gating approach that works by assigning hierarchical clusters to groups of cells based upon their abundance as defined by similarity of each marker expression within the population as a whole [131]. The resultant SPADE tree is a reduction of dimension where each cluster is connected to another by a minimum spanning tree (MST) which is constructed through density down sampling the data so that rare populations of cells are not lost from the total population. Defining the number of nodes is important in the construction of a meaningful SPADE tree and takes into consideration the selection of markers that will be used and the desired cell population (Figure 3.8A). Too many nodes, such as the 200 used to generate the SPADE tree illustrated in Figure 3.8B (left panel) creates nodes without any meaningful data that leads to disintegration of results. For example, in order to accommodate the 200 nodes the algorithm down

samples a restricted number of events (in this case 3,797 cells) in order to preserve the overall analysis structure. In contrast, the use of 45 nodes leads to the down sampling and analysis of a data set which is 4X larger (14,726 cells), thereby using the generated data more efficiently without affecting or losing a rare population that could be shadowed or hidden within a large cluster if too few nodes were chosen [Figure 3.8B (upper right panel)]. This optimised representation shows B, T and Myeloid cells as a sequence of connected nodes where different sizes and colour indicate cell numbers within each. This gives quantitative data regarding proportion of cells within each defined population and can now be better represent as a series of equally sized nodes so that colour information can be better viewed [Figure 3.8B (lower right panel)].

Figure 3.8C shows SPADE trees now organised into myeloid, and T and B cells where the colouring within each of the 45 nodes represents the medians associated with antigen expression. The colour scale ranges from blue (negative) to red (strongly positive), clearly showing that the B subsets are discriminated from T cells and myeloid cells by strong co-expression of CD19, CD20, CD21 and CD22. Similar to viSNE, simultaneous expression of the antigens used in my panel can be observed on myeloid, T and B cells giving appreciation of comparative antigen expression on these haemic cell subtypes where potential new and interesting features can be found. For example, IgD positive nodes are identified within the T and myeloid cell bubbles, [132, 133] nodes that do not show any other B cell marker. These cells are also identified within the viSNE plots (Figure 3.6B) and are rare within the entire population of leukocytes. Finally, the rare population of CD5+ B cells are indicated and comprise 0.15% of total leukocytes.

Taken together, these data show that peripheral blood cell subsets can be discriminated and quantitatively assessed using SPADE as an approach to the analysis of mass cytometry data.

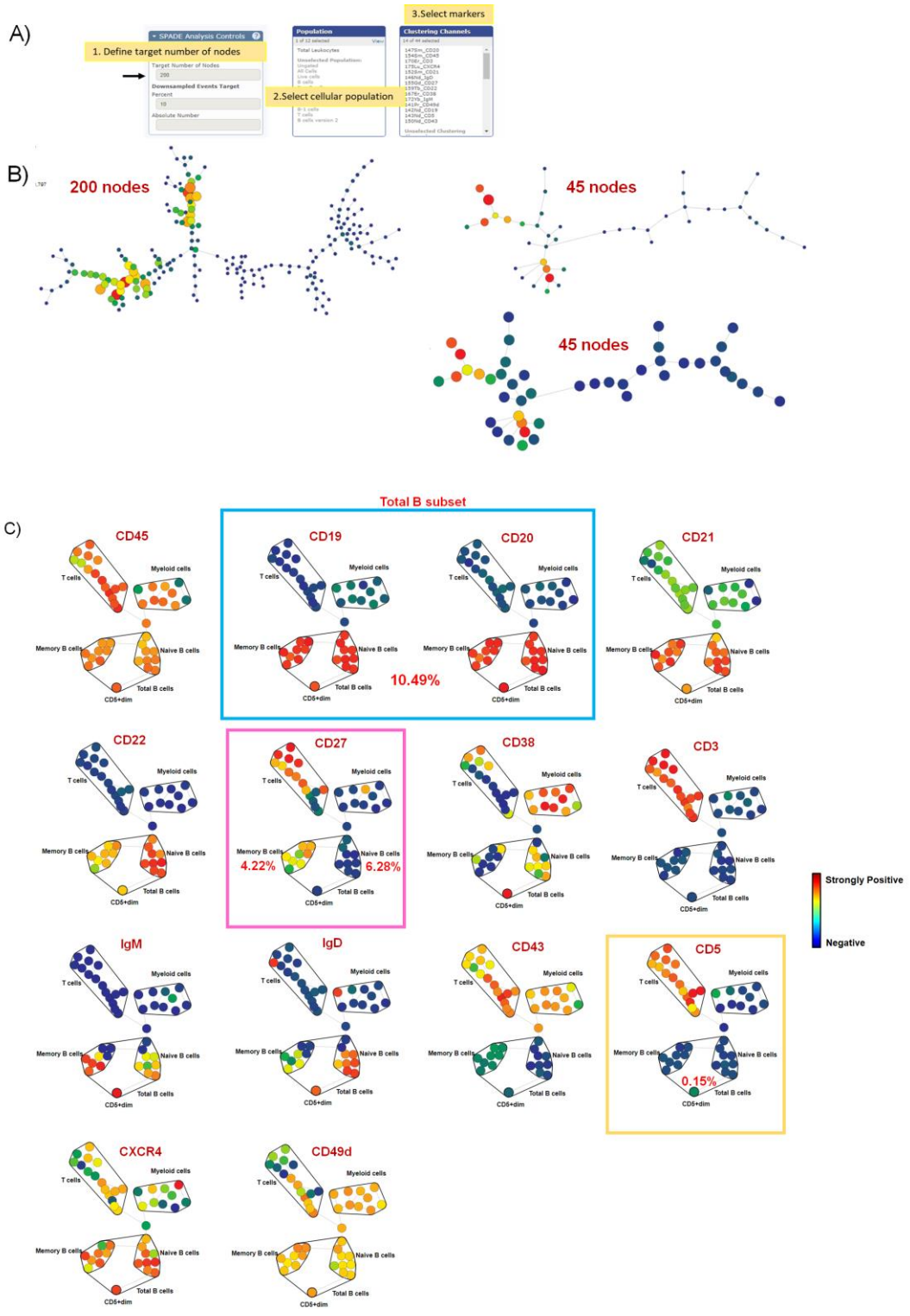
A)
1. Define target number of nodes
2.Select cellular population
3.Select markers
B)
200 nodes
45 nodes
45 nodes
C)
Total B subset
CD45
CD19
CD20
CD21
CD22
CD27
CD38
CD3
IgM
IgD
CD43
CD5
CXCR4
CD49d
10.49%
4.22%
6.28%
0.15%
Myeloid cells
T cells
Memory B cells
Naive B cells
Total B cells
CD5+dim
Strongly Positive
Negative

**Figure 3. 8 SPADE analysis of mass cytometry data generated from PBMCs.** Normal PBMCs were stained with the antibody panel listed in Table 3.1. **A.)** Input settings to create a SPADE tree. **B.)** Comparison of SPADE trees generated using the default setting of 200 nodes (*left hand tree*) and optimised setting of 45 nodes (*right hand tree*). Automated downsampling within each setting analysed 3,797 cells in the former setting and 14,726 cells in the latter. **C.)** Bubble cluster representation of myeloid, T and B cell-associated nodes for comparison of expression for each listed antigen. The nodes in this part were made equal size to enhance appreciation of colour within each. The colour scale indicates negative (blue) to strongly positive (red) expression. The blue, pink and yellow boxes are to show the B cells subsets and SPADE percentage.

### 3.2.5 Comparing reproducibility of high dimensional dataset analysis.

It is clear from my use of manual gating, or of unsupervised approaches, to the analysis of mass cytometry data that information regarding cell numbers within common and rare/new cell populations and antigen expression of those cells can be gained. An important aspect to consider now is the quality of the data that is generated where variations can be introduced by how the user is preparing the experiments. Such preparation needs a demonstration of reproducibility which then supports any generated conclusions. Furthermore, validity of the unsupervised approaches to data analysis should be consistent with results generated using conventional manual gating, this then allows in-depth and clearer visualisation of the data where large numbers of parameters are investigated per cell to enhance the value of any conclusions made. This section will demonstrate reproducibility of mass cytometry analysis, and show consistency between analytical methods of data analysis to determine if any significant differences in identifying B cell subsets are apparent.

#### 3.2.5.1 Reproducibility of antigen staining.

To make sure that sample handling was consistent for staining preparation I measured antigen expression on a single sample multiple time. Figure 3.9 shows the results of this experiment where a normal PBMC sample was surface stained separately on

three different days and run on three different days. The antigens displayed in the figure are representative of all the antigens measured within the panel of antibodies I used, demonstrating a high precision with respect to marker intensity and expression within Total, Memory and Naïve B cell subsets. This data indicates that the procedure I used for surface staining generates reproducible results and gives confidence for the application of unsupervised algorithms.

#### 3.2.5.2 Comparison of viSNE and SPADE in detecting B cell subsets and CD5+ B cells.

I next compared viSNE and SPADE to the conventional manual gating of one normal PBMC case with the purpose of determining whether each approach generated a similar result. Figure 3.10A-C shows this comparison and demonstrates that each approach reproducibly generates similar results, accurately identifying the proportion of each B cell subset present in the total leukocyte population, including the rare population of CD5+ B cells. With respect to the SPADE analysis, there was a small difference in the recorded percentages, but the values generated are within the normal ranges of B cell population percentages [125]. This variation could be the result of how the SPADE analysis works, viSNE and manual gating observe the whole data while SPADE down samples a part of the dataset and such partial observation may lead to differences in accuracy. Precision measurement of B cell subset proportions extended to 8 further PBMC samples analysed where viSNE, SPADE and conventional manual gating all yielded similar results (Figure 3.11A-C). Each sample showed a different percentage of the B cell subsets, but these percentages remained within the normal reference percentage and so were unremarkable.

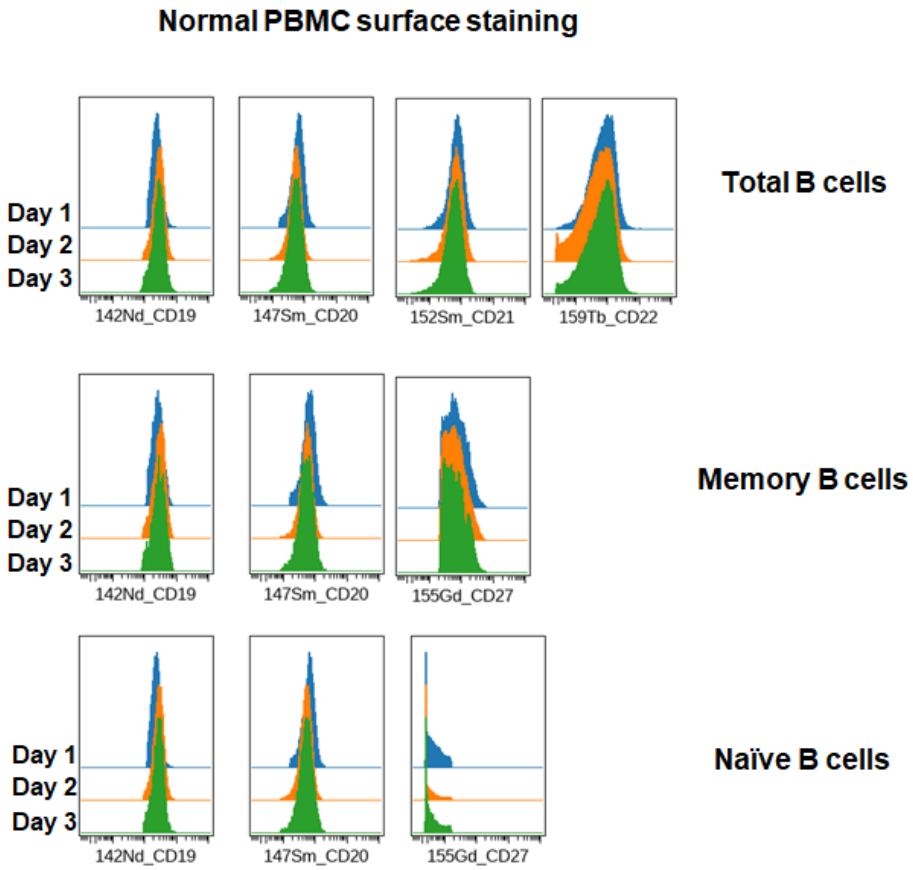


**Figure 3. 9 Standardization and quality control of surface staining from healthy donors.** Histogram demonstration of the indicated antigen expression on B cells from a single healthy donor measured on different occasions (Day 1, 2, 3). Antigen expression on different B cell subsets is indicated. This is a representative example of the 8 patient samples measured in this Chapter.

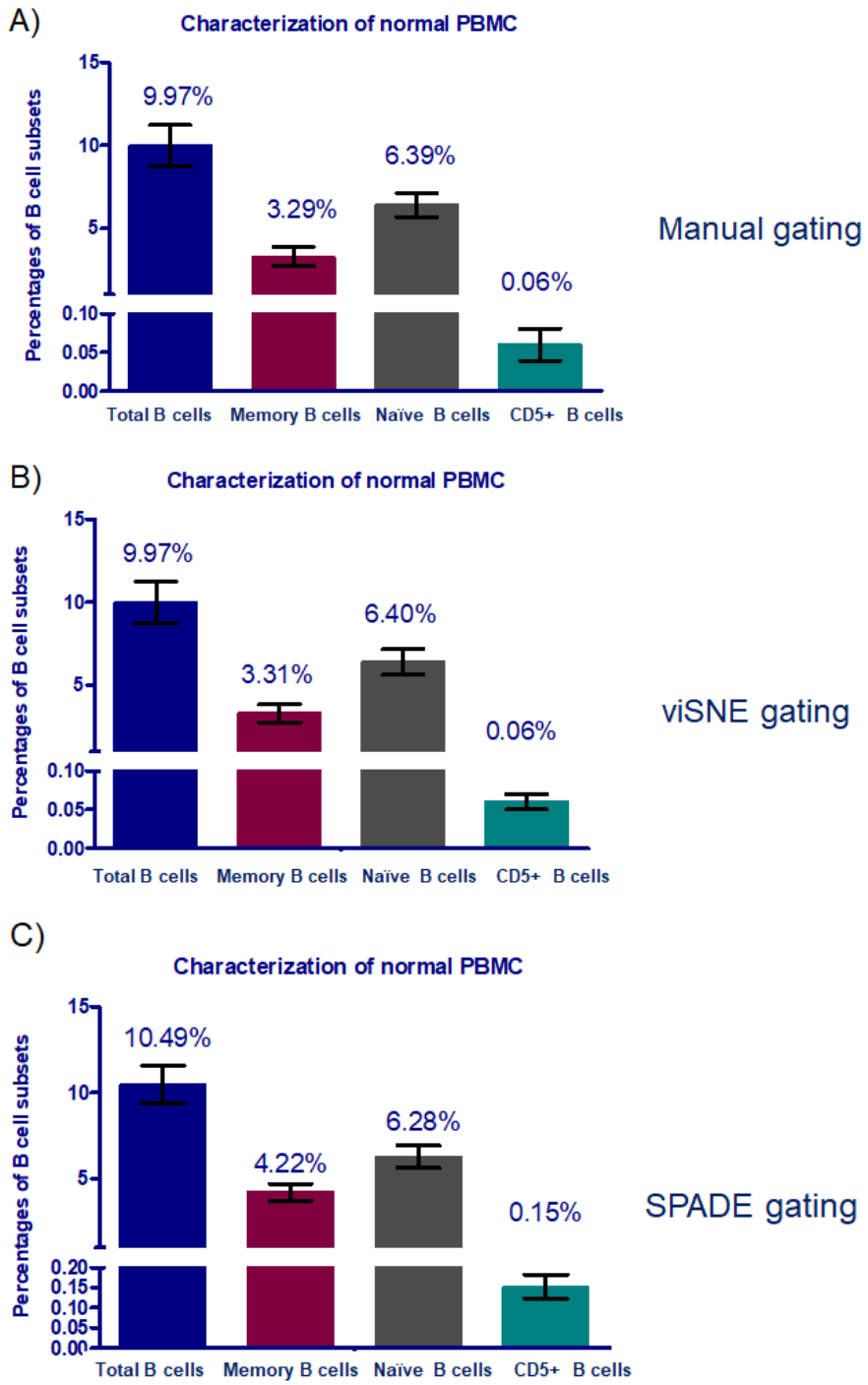


**Figure 3. 10 Comparison of automated algorithms versus manual gating for identification of B cell subsets.** PBMCs from a single patient sample were stained and analysed 3 independent times using **A.)** Manual gating **B.)** viSNE and **C.)** SPADE analysis. The bar graphs represent mean ± SEM and numbers above indicate the percentage of the indicated B cell subset within the total leukocyte population.

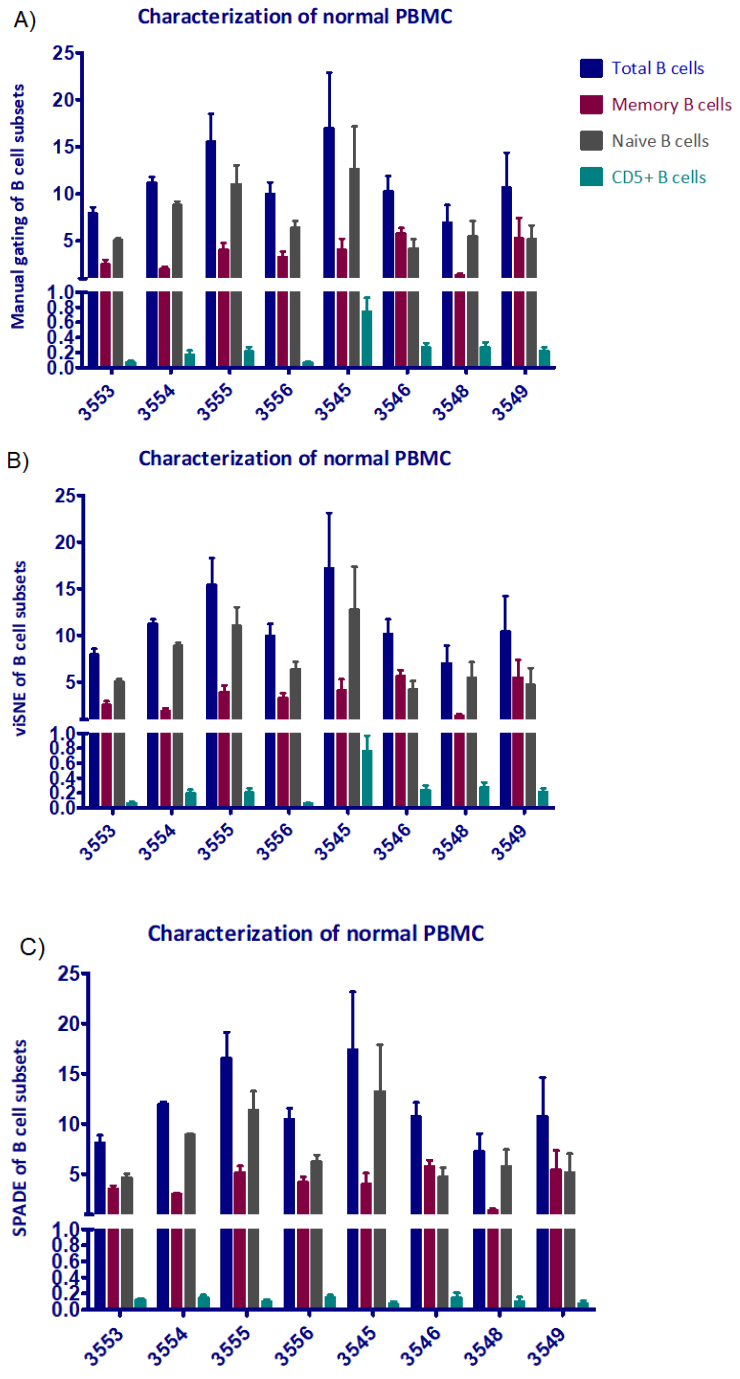


**Figure 3. 11 Assessment of manual and unsupervised gating using normal PBMCs to identify B cell subsets. A.)** shows the manual gating of different healthy individuals (n=8) and how each individual shows variations of Total B subsets, Memory and Naïve B cells. **B.)** illustrating the same cases and are gating by viSNE gating to identify B cell subsets. **C.)** SPADE analysis was performed on the same normal individuals show reproducible in large B cell population than $CD5^{+}$ rare population. Each staining and gating were performed in three repeats (n=3).

Figure 3.12 demonstrates further investigation on the comparability of manual gating, viSNE and SPADE in determining B cell subset percentages. Percentages of Total B cells, Memory B cells, Naïve B cells and CD5+B cells were subjected to one-way Anova confirming there is no significant difference in the way that each method measures these subsets. These observations are further validated in Figure 3.13 which shows a correlation analysis between manual gating, viSNE and SPADE where each individual case is represented. Thus, manual gating highly correlated with viSNE and SPADE, and viSNE showed high correlation with SPADE, in determining percentages of the total, naïve and memory B cell subsets. However, this relationship did not hold true for CD5+ cells, particularly with respect to the correlation of SPADE with either manual gating or with viSNE. This could be due to the limited data that SPADE analyses, through down sampling, in comparison to manual gating and viSNE. Nevertheless, the data presented in this section show that mass cytometry is highly reproducible with respect to surface antigen expression and determination of B cell subset percentages.

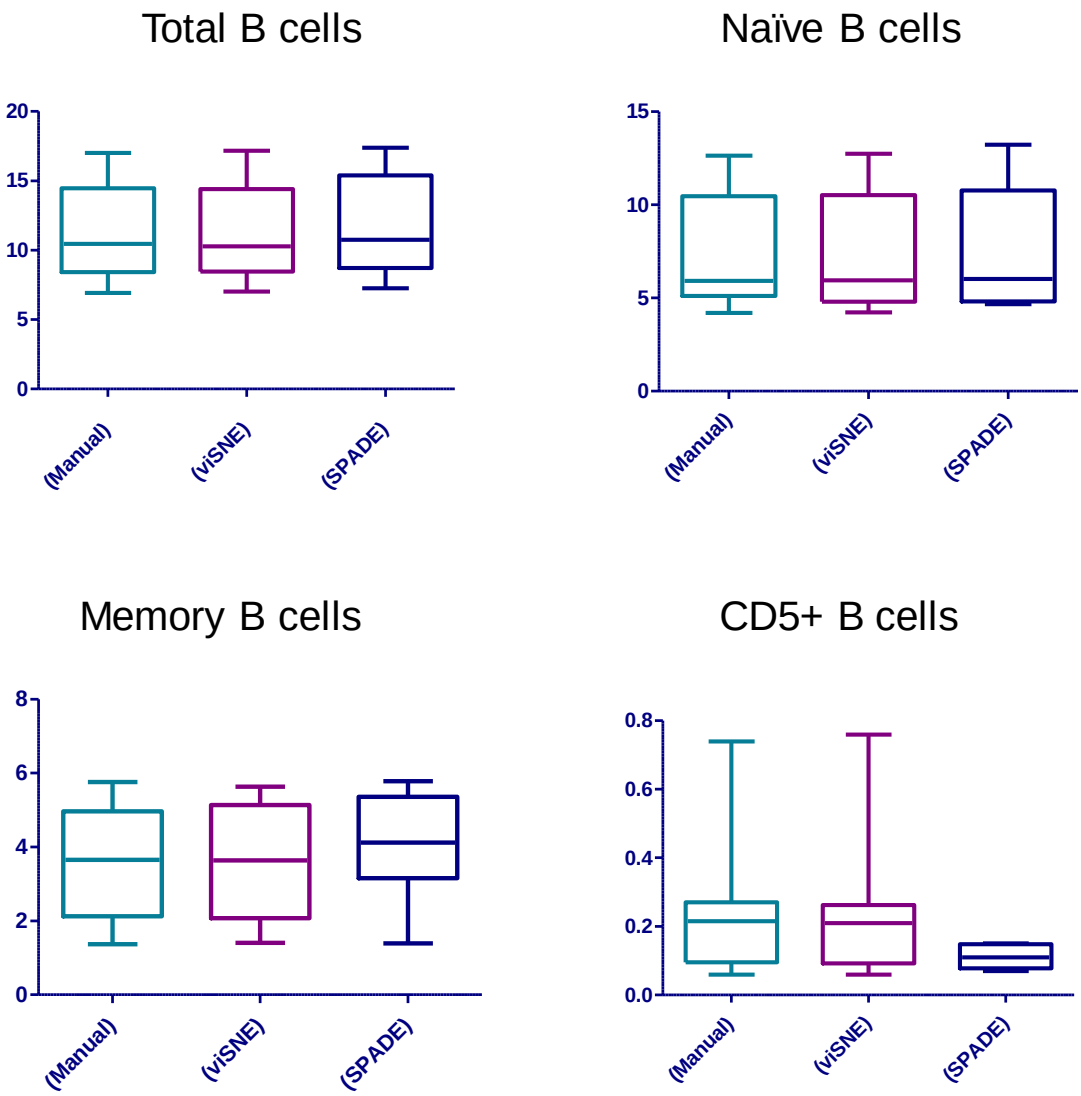


**Figure 3. 12 B cell subsets assessment in manual and automated gating in normal PBMCs** in different normal PBMCs (n=8) and comparing each B subsets to one another and see the difference of average in three gating settings, manual gating, and visualisation clustering algorithms viSNE and SPADE (n=3). One-way Anova statistical analysis was done by GraphPrism™. Each Population compared to different gating algorithms states no significance.

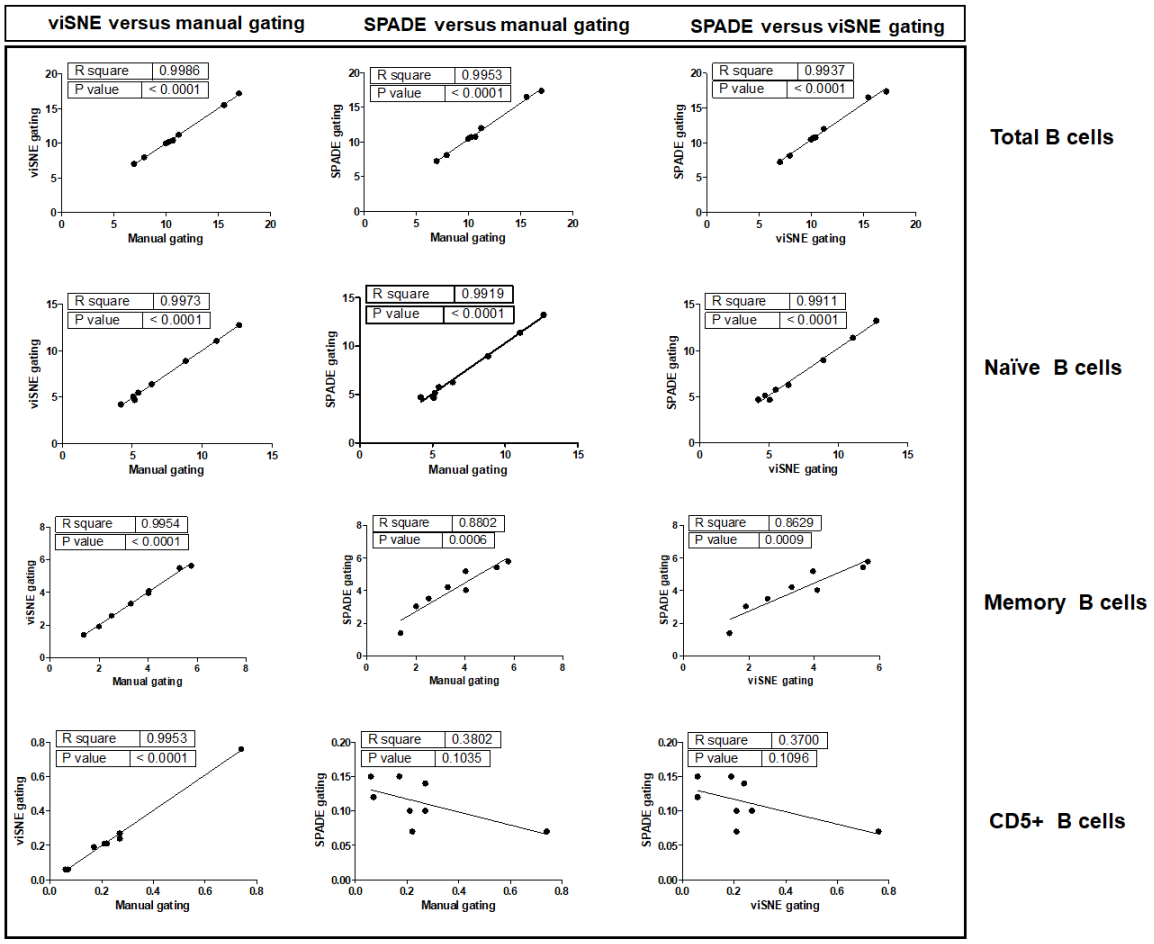


**Figure 3. 13 Correlation analysis of B cell subsets in normal PBMCs between different gating settings.** The table exemplifies different gating settings in correlation with all B cell subsets. The variables are the manual, viSNE and SPADE gating within the identification of the following Total B, Memory B, Naïve and $CD5^+$ B cells. The B cell subsets are strongly correlated than $CD5^+$ B cell subset when correlated to SPADE gating. The normal individuals (n=8) are surface stained and replicated three times (n=3). Linear regression analysis was done for this statistical analysis by Graphprism™.

### 3.2.6 Intra-clonal variability of surface antigen expression in CLL cells.

CLL is a clonal expansion of $CD5^{+}$ malignant B cells that accumulate in peripheral blood and lymph nodes. Despite this monoclonal nature, CLL is also considered a heterogeneous disease due to different genetic features that then determine progressive or indolent behaviour. Another source of intra-clonal heterogeneity of CLL cells, particularly those in peripheral blood, is defined by phenotype where those cells emerging from proliferation centres have been characterised as $CXCR4^{dim}/CD5^{bright}$, and those cells which have been longer in circulation and are senescent being $CXCR4^{bright}/CD5^{dim}$ [38]. Respectively, these cells have been referred to as newly emerged (NE) and older quiescent (OQ) CLL cells.

In this section I apply mass cytometry to CLL with the purpose of characterising intraclonal heterogeneity. I used cells from 12 patients, and study 2 patients at 2 time points in their disease, these cases and clinical history are listed in Table 3.2. Figure 3.14 shows the gating strategy I used to identify CLL cells within these samples. The percentage of B cells within each sample was calculated in relation to total leukocytes, and corresponded with data collected from each sample about the malignant cell count and patient history from the clinic (Table 3.3). This data set associated with CLL cells was then taken for further analysis.

Table 3. 2 CLL clinical history

| No. | Date of sample | Sample | WBC, Lymph | Age | Sex | Stage | IGHV status | Karyotype | P53 mutation | Therapy |
|---|---|---|---|---|---|---|---|---|---|---|
| **1** | 29/06/2017 | 3566 | - | 66y | M | C | M | 13q-(biallelic) | no | untreated |
| **2** | 30/06/2017 | 3568 | 86.0, 76.3 | 76y | M | A | UM | Normal(2014) | no | untreated |
| **3** | 28/07/2017 | 3577 | 85.7, 75.8 | 50y | M | A | - | 17p-(2017) | - | 4xFCR 2013;Ofat+Chl 2013/14;Ibru April 2017 |
| **4** | 16/08/2017 | 3585 | 136.8, 128.1 | 68y | M | A | UM | 11q-, 13q- | no | untreated |
| **5** | 16/08/2017 | 3589 | 107.6, 104.9 | 76y | F | C | M | normal | no | untreated |
| **6** | 04/05/2016 | 3527 | 98.0, 95.0 | 75y | F | C | M | normal | no | untreated |
| **7** | 20/09/2017 | 3601 | 87.2, 85.6 | 57y | M | B | - | normal | - | 4XFCR 2016 |
| **8** | 13/07/2016 | 3530 | - | 56y | M | B | - | normal | - | 4XFCR 2017 |
| **9** | 21/09/2017 | 3602 | 50.8, 49.9 | 61y | M | C | UM | 11q- | no | Ibrut+veneto started at 2017 |
| **10** | 11/02/2015 | 3450 | 85.6, 80.8 | 71y | M | - | - | 13q- | no | In progression, R-lenalidamide started 2/2015 |
| **11** | 18/06/2015 | 3472 | 104.6, 96.1 | 77y | F | B | - | 13q- | - | In progression, Enrolled to RIALTO trial 06/2015 |
| **12** | 23/09/2013 | 3367 | 444, 439.6 | 76y | M | - | - | 17p- | - | Probably in progression, enrolled into CLL210 |
| **13** | 01/02/2016 | 3511 | 226, 221.9 | 80y | M | C | - | 13q-, trisomy 12 | - | untreated |
| **14** | 09/06/2014 | 3413 | 124.2, 118.4 | 86y | F | A | - | 13q- | - | Previous chlorambucil, started ibrutinib 6/2014 |
| **15** | 16/01/2018 | 3634 | 23.8, 11.3 | 83y | M | - | M | 17p-, 13q- | yes | Previous Rituximab + pred |
| **16** | 26/11/2018 | 3711 | 173.3, 161.5 | 64y | M | - | M | normal | no | untreated, started FCR 11/2018 |
| **17** | 06/12/2018 | 3712 | 79.7, 75.8 | 62y | M | B | M | - | no | untreated, in progression, start ibrutinib, |

| | | | | | | | | | | |
|---|---|---|---|---|---|---|---|---|---|---|
| | | | | | | | | | | venetoclax 1/2019 |
| **18** | 16/08/2017 | 3587 | 257, 216.1 | 55y | M | - | M | 13q- | no | Untreated, in progression, started Ibrut+ rituzimab on flair trial 10/2017 |
| **19** | 07/01/2014 | 3380 | 88.2, 83.7 | 75y | M | - | - | 17p-, 13q- | - | |
| **20** | 25/07/2018 | 3691 | 213.3, 196.7 | 69y | F | - | M | 13q-, trisomy 12 | no | Untreated, in progression ,started R-ibrutinib 8/2018 |
| **21** | 24/01/2018 | 3637 | 144.6, 134.9 | 69y | M | A | UM | 11q-, 13q- | no | Untreated |
| **22** | 15/03/2018 | 3647 | 145.9, 138.2 | 67y | F | - | M | normal | no | Untreated, in progression, started FCR 03/2018 |
| **23** | 31/01/2018 | 3640 | 177.5, 163.4 | 82y | M | A | UM | 13q- | no | Untreated |

Table 3. 3 Total B percentages from total leukocytes

| no. | CLL samples | Total B percentages |
|---|---|---|
| 1 | 3601 | 77.70% |
| 2 | 3602 | 90.70% |
| 3 | 3589 | 94.13% |
| 4 | 3450 | 98.01% |
| 5 | 3472 | 97.24% |
| 6 | 3527 | 98.26% |
| 7 | 3530 | 92.88% |
| 8 | 3511 | 86.90% |
| 9 | 3367 | 95.20% |
| 10 | 3413 | 80.77% |
| 11 | 3566 | 96.42% |
| 12 | 3568 | 98.33% |
| 13 | 3577 | 91.70% |
| 14 | 3585 | 97.00% |

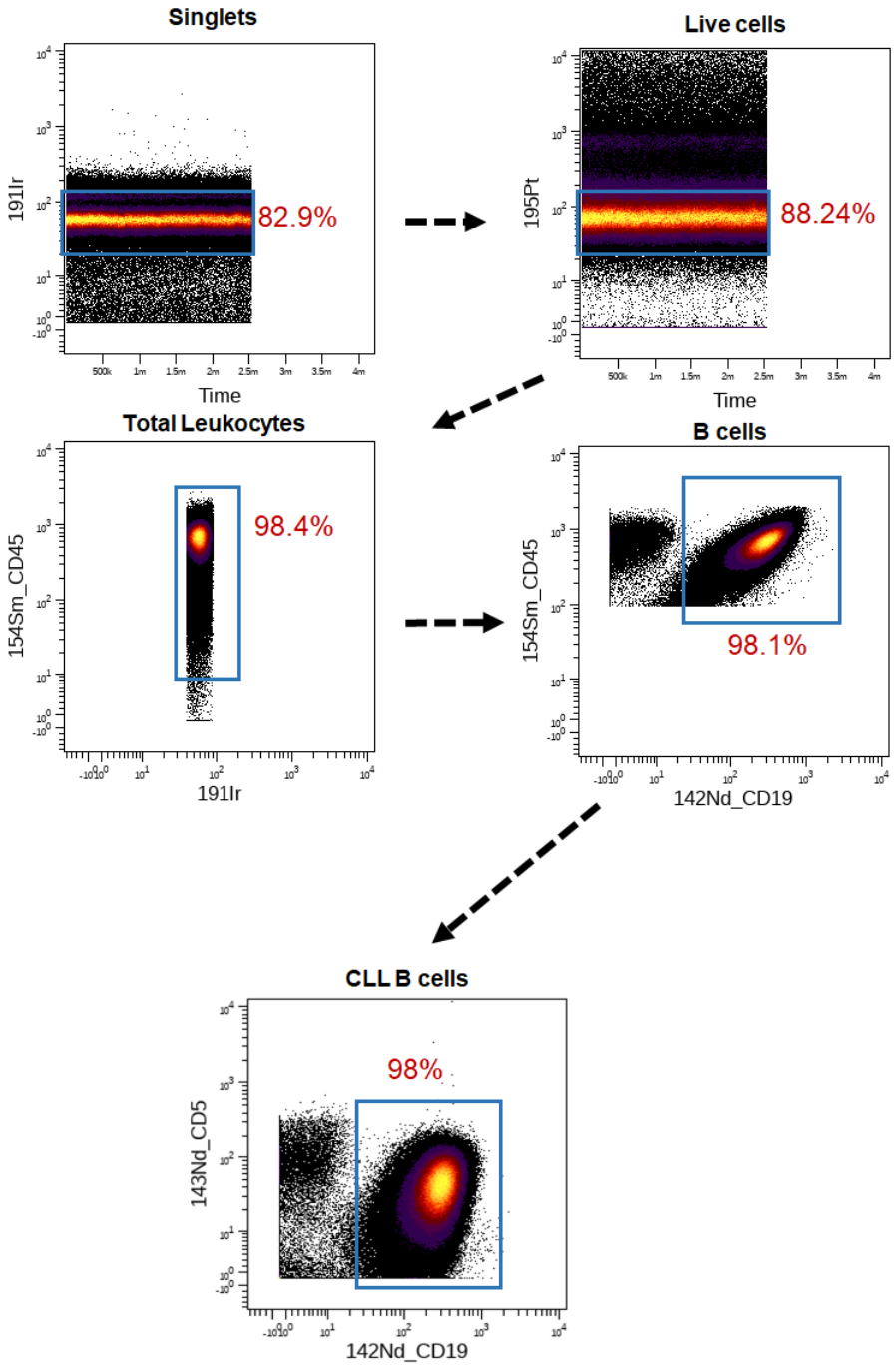


**Figure 3. 14 Identification of Chronic Lymphocytic Leukaemia B cell subsets.** The gating strategy of CLL CD19 positive cells and CD5 positive cells. Looking within the active population of CLL B cells they are further divided into CLL B cell subsets by CXCR4/CD5 markers. The older quiescent (OQ) and newly emerged cells (NE).

### 3.2.7 Characterisation of intraclonal heterogeneity within samples of CLL cells.

After identifying CLL B cells within patient samples it was next necessary to understand any differences between individual cases. To do this I organised heat maps of antigen expression associated with each of the seven CLL cases I analysed using raw mean surface expression (Figure 3.15A). CLL cells from each case showed slight differences between each other, possibly indicating specific disease characteristics. The CLL samples I analysed included repeat analysis from the same patient at two different time points (Figures 3.15B and C). Samples 3530 and 3601 were drawn nearly 1 year apart and show slight differences in surface antigen expression. These differences could be associated with emergence of a distinctive clone at the second time point because case 3530 was $\alpha$4- and case 3601 transformed into integrin $\alpha$4+ case (data not shown). Cases these cells 3589 and 3527 were also drawn one year apart but showed less drift of surface antigen expression (Figure 3.15C). Nevertheless, this repeat does show that my staining technique remained consistent as reflected by the heatmap Figure 3.15B and C and surface antigen expression markers showing same expression and no difference in staining or sample preparation. I then generated a heat map for raw mean surface antigen expression of the events I analysed (Figure 3.15D). Unsupervised clustering of these results showed that CLL cases #3577 and 3602 were the most similar in surface marker expression, and #3568 the least similar from the cases I analysed. This explains that variations in surface marker expression are common when compared to other cases. Thus, the analysis so far failed to yield evidence of any functional significance associated with the samples analysed. I next used viSNE and FlowSOM to cluster different sub-populations of CLL cells from a single patient sample based on surface antigen expression. FlowSOM is similar to SPADE analysis in its reliance on stochastic

minimum spanning trees (MST), but it self-organises data into defined 2D maps, and/or grids, and eliminates the need to down sample data. Figure 3.16A shows the viSNE projection of the total B cell population and illustrates the diversity of surface antigen expression across this population. A striking feature of this projection is that although CLL cells are clonal, there are still clusters of cells that define intra-clonal subpopulations that FlowSOM then visualises by layering metaclusters on to the viSNE plot (Figure 3.16B). The default setting of FlowSOM is 10 metaclusters, and 9 of these 10 can be clearly identified with the missing cluster not having enough events to be observed within the projection. Nevertheless, some populations are distinctive, such as the subpopulation of cells expressing relatively high levels of CD38.

An interesting feature of the projection was the appearance of 2 distinct islands, one of which was much smaller than the other (Figure 3.16). This smaller island had distinct high levels of IgD expression that FlowSOM then further subdivided into the 3 metaclusters that are recognisable within this island.

I then applied viSNE and FlowSOM to all 7 CLL cases to investigate any relationship between the samples (Figure 3.17). The viSNE projection again resulted in 2 islands, the smaller of which seeming to have similar properties to the island recognised in Figure 3.16). 10 metaclusters were identified, but the division between the metaclusters seemed associated with individual cases and so I used FlowSOM to project each case with a tree to show how each related to the other. Figure 3.17B shows the results of this analysis. Remarkably, each CLL case analysed seemed to be unique with respect to expression of the surface antigens in my panel. The 7 CLL cases shown each FlowSOM tree generated shows each case is heterogenous and each tree is showing high intensity of CD19 expression located in different branches

of the FlowSOM tree. This distinctiveness associated with each individual case is not likely associated with variation in staining because a similar experiment carried in this lab with barcoded CLL cells from different patient samples showed similar results (data not shown)[1].

So far, the techniques I used did not allow characterisation of particular clones common to all CLL cells from all patients. It was therefore decided to reframe my analysis into an existing paradigm of CLL where newly emerged (NE) and older quiescent (OQ) CLL cells can be distinguished from each other on the basis of CXCR4 and CD5 expression[134]. In this experiment, all CLL cell samples were recovered for 1 hour incubation with full media at 37$^{o}$C in the incubator. Potentially, the introductory of the recovery period could have changed the expression level as its described by Coelho et al, however, since all CLL cell sample were subjected to the same procedure any change that occurred would be common to all cases and justify the creation bivariate dot plots. I therefore created bivariate dot plots of CXCR4 and CD5 expression on CLL cells from different CLL patients (Figure 3.18). In total I could now analyse the cells from 14 different cases, where the topography of cells expressing differing levels of CXCR4 and CD5 could be displayed. As in [38], this topography was slightly different for each case of CLL, but overall there was a gross similarity regardless of CD49d expression.

[1] Information provided with the permission of Mohammed Jawad and Andrew Duckworth (supplemental material).

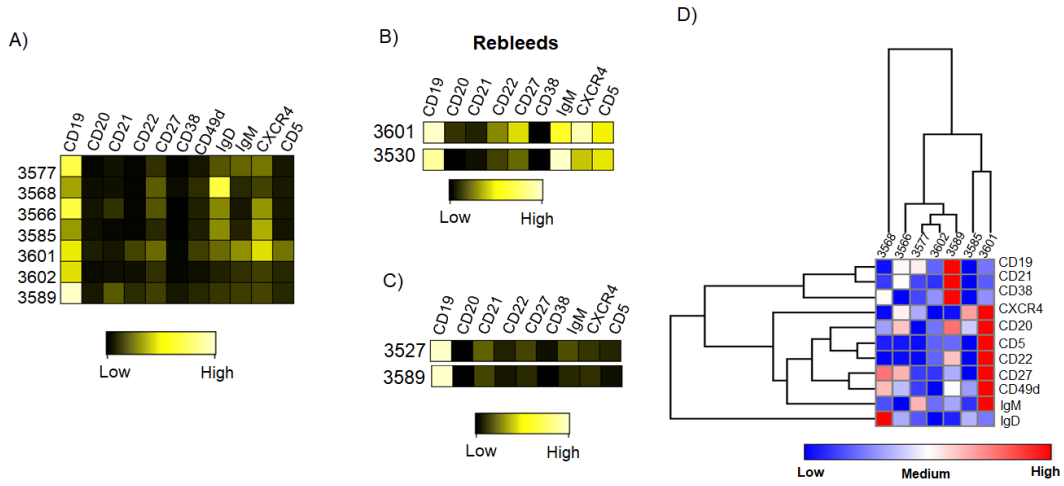


**Figure 3. 15 Analysis of antigen expression on CLL cells from different patients. A.)** Heat map mean expression generated showing raw surface antigen expression in total B cells across 7 CLL cases. **B-C.)** Two cases of rebleeds from same patients comparing surface antigen expression between them. **D.)** Heat map of total B cell population mean expression creating a hierarchy clustering paradigm Pearson correlation relative to surface antigen expression in each parameter. This was generated by GENE-E 3.0.215 software.

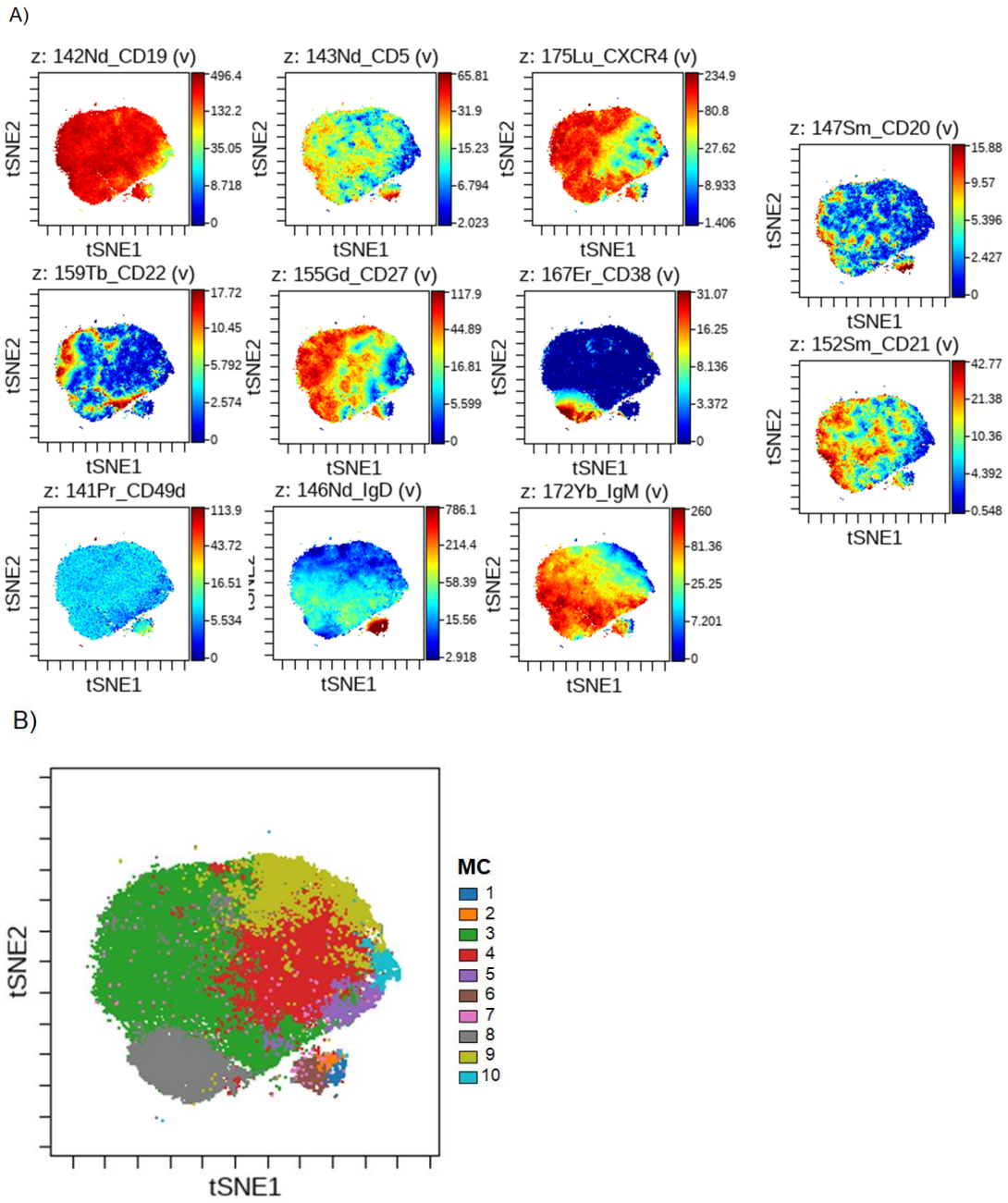


**Figure 3. 16 Differentiation of surface antigen expression in CLL total B cells of surface using unsupervised algorithms. A.)** The 2D viSNE plots show CLL surface antigen expression located within the total B cells and is located is every segment of the B Island. **B.)** FlowSOM on t-SNE data, showing identical viSNE cloud population in metaclusters were generated displaying majority of clusters within the B cell population to look for individual CLL clones.

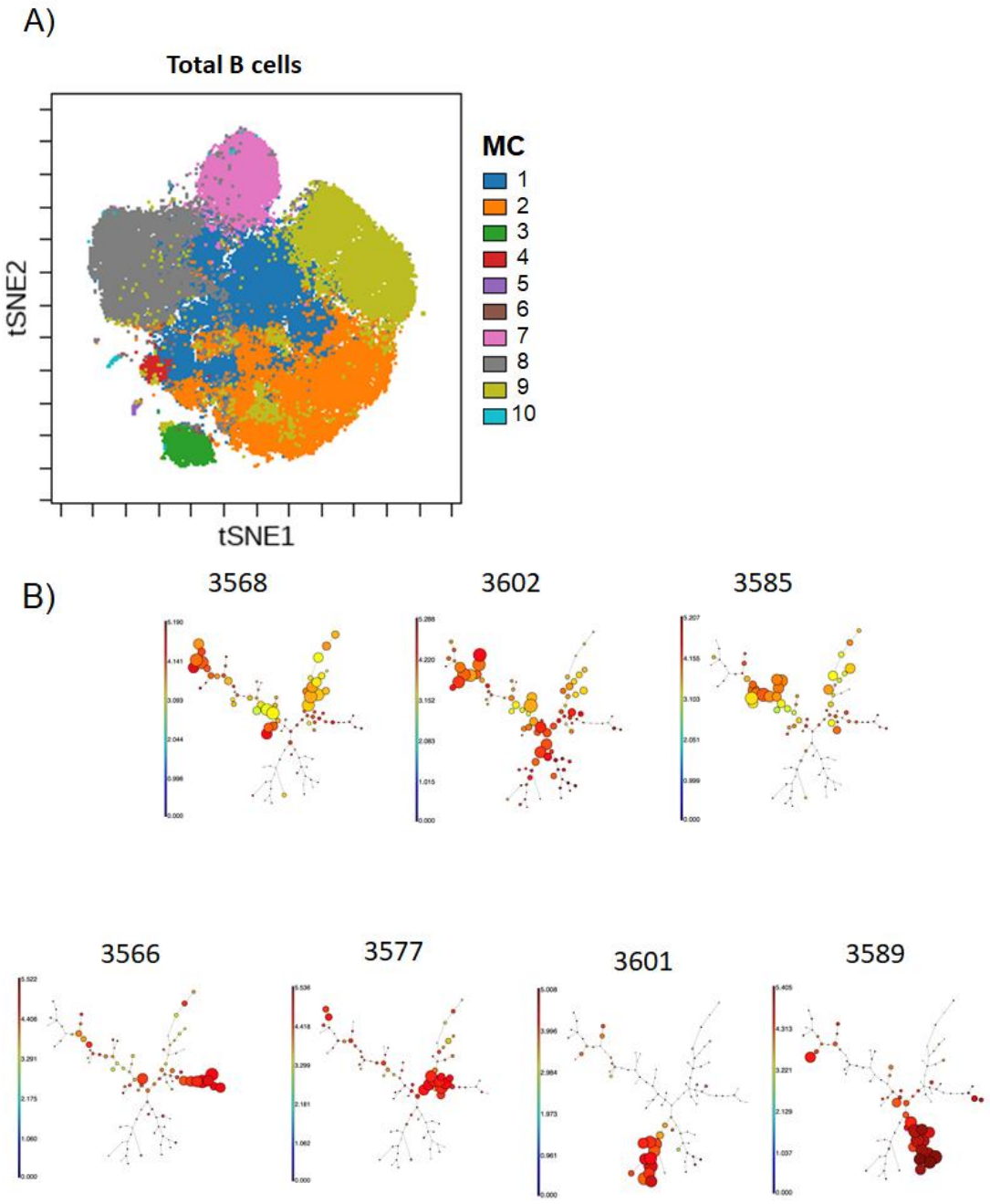


**Figure 3. 17 Differentiation of surface antigen distribution in different CLL patients in total B cells. A.)** shows Combined CLL total B cells in FlowSOM illustration. **B.)** FlowSOM tree showing single cell clustering of surface antigen CD19 distribution in each patient.

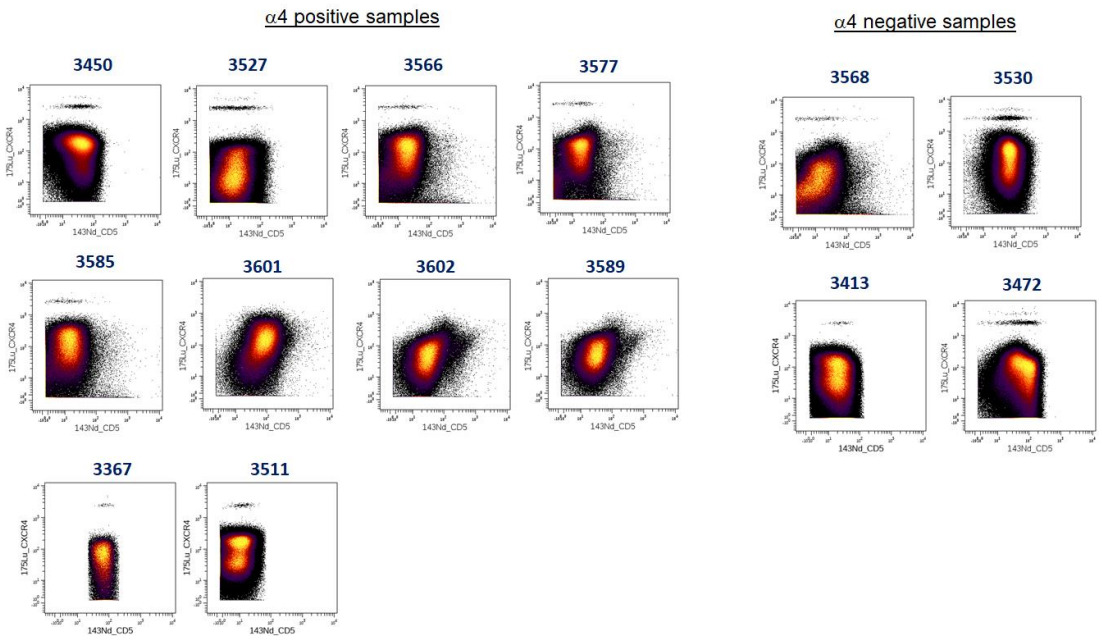


**Figure 3. 18 CLL subsets of different patients.** Colour density bivariate plots of different CLL (n=14) each showing different appearances of CXCR4/CD5 expression within individual CLL clone between older quiescent (OQ) and newly emerged cells (NE). CLL cases are separated in two groups by α4+/- integrin antigen expression.

I next analysed individual expression of the other antigens included in my panel on OQ and NE CLL cells. Figure 3.19 shows CXCR4/CD5 bivariate plots of CLL cells from a single case where the indicated colour shows expression of the different surface antigens. A striking feature is the diversity of staining for certain antigens suggesting intraclonal variability. To study this phenomenon across all the CLL cases I analysed, I created 9 tailored gates where each sample 5% of the total population and are arranged at the receding (CD5 dim, gates 1 – 4) and leading (CD5 bright, gates 5 – 8) edges. The 9$^{th}$ gate samples the CLL cell population with the mean values of CXCR4 and CD5 expression and is taken as the bulk control (Figure 3.19A). To measure variance of antigen expression, the mean surface expression for each gate for a given antigen was calculated and then plotted as fold difference relative the bulk control (gate 9). Figure 3.19C shows the results of this analysis and is presented according to CD5 and CXCR4 expression. Some antigens, such as CD19, CD21, IgM,

and IgD, showed significantly higher expression on CD5 cells. Other antigens, such as CD27, showed high expression on CXCR4 bright cells that then decreases on cells as CXCR4 expression decreases. CD38 showed gates 1 and 2 are low and equal to gates 7 and 8 but some CLL cases show higher in gates 5 and 6. The consistency of the results generated in this analysis lie in contrast to the variability with respect to the FlowSOM analysis. Figure 3.19 shows interpatient similarity of CLL cells where Figure 3.17B suggests interpatient distinctiveness.

This means that CLL cells when investigated the total clone of CD19+ CD5+ cells do show distinct variations in each case. However, when investigated into the subclones of CXCR4 and CD5 they share consistent pattern in all surface antigen expression that suggest that each subclonal gates creates a more understanding of the intraclonal variability in CLL subclones to guide the behaviour of aggressive subclones than others that give a definitive guide to target these subclones at a single cell resolution than total clones.

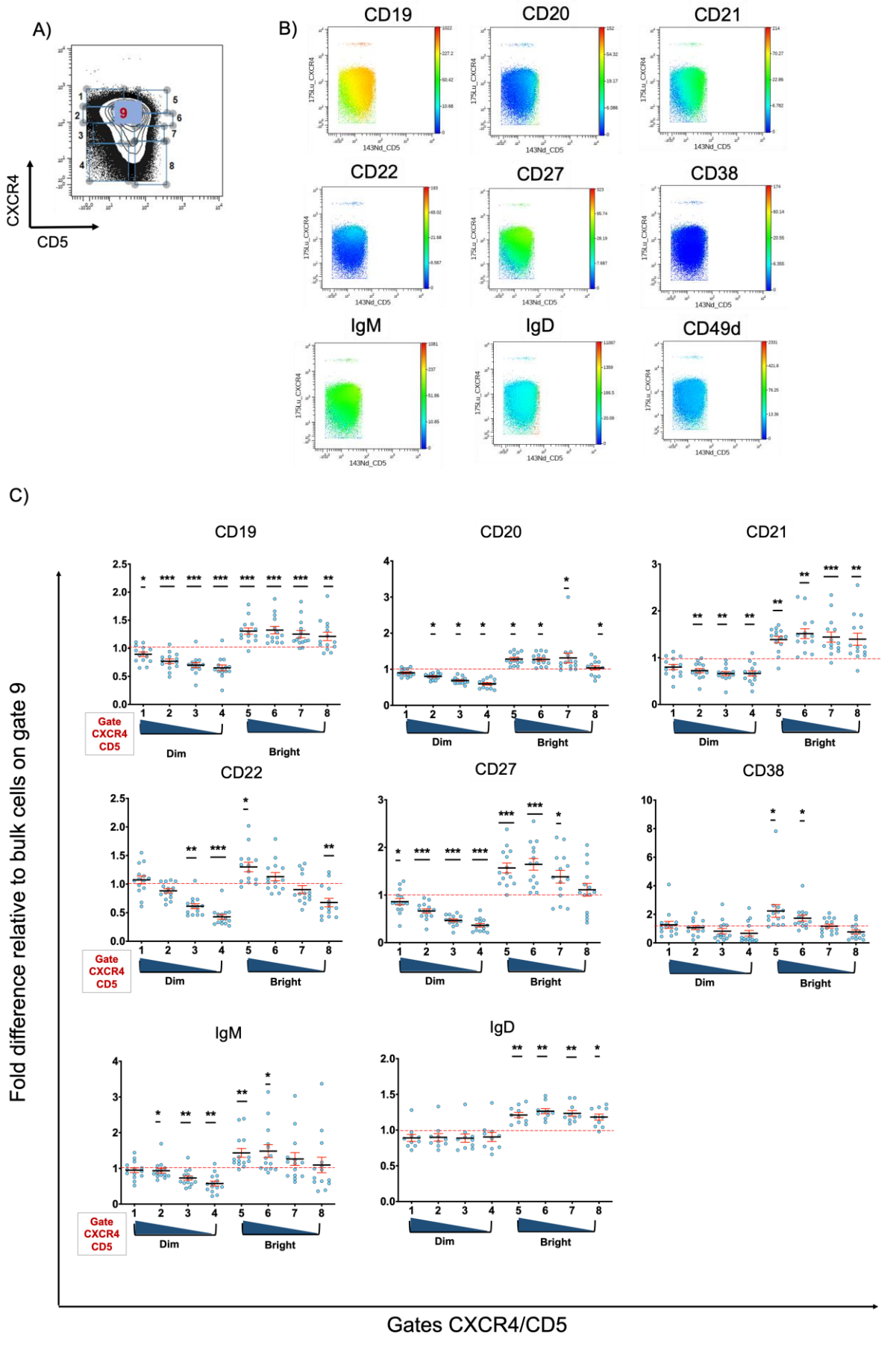
A)
CXCR4
CD5
9
B)
CD19
CD20
CD21
CD22
CD27
CD38
IgM
IgD
CD49d
C)
Fold difference relative to bulk cells on gate 9
Gates CXCR4/CD5
Gate CXCR4 CD5
Dim
Bright

**Figure 3. 19 Fold difference of surface antigen expression within CLL subsets. A.)** Gating of Total B cells each gate 1-8 was dividing the following within CXCR4/CD5 population. In the contour dot plot gates ~5% each gate 1-4 represents the cells from lymph node OQ cells (Dim) and showing all surface markers are lower and gates from 5-8 represents cells from peripheral blood NE cells are higher (bright). **B.)** All surface markers from gate 1-8 showing in dot colour plot of each surface marker expression within the 8 gates in 14 CLL cases. **C.)** Fold difference of each surface antigen expression within the 8 gates that are relative to gate 9 (bulk) of the total B cell population. Case 3589 and case 3527 rebleeds of same patient (one year apart), case 3530 and case 3601 are rebleeds of the same patient (one year apart). IgD have 10 cases only the rest are 14 cases, as 4 cases had no surface antigen stained. Paired t-test was done for statistical analysis in Graphprism™ shows significant difference when compared each gate to gate 9.

### 3.3 Discussion

The main aim of this chapter is to apply mass cytometry as a multiparametric approach to identify B cell subsets in PBMC preparations from healthy donors and CLL patients. The optimised panel was created and designed to show more and overcome the limitation of conventional flow cytometry with respect to the selection of antigens that are common B cell markers, and can be used to distinguish CLL cell clones [135].

The antibody panel was designed to distinguish B from T cells, and further distinguish naïve, memory and CD5+ B cells. Thus, as reported [127, 136], CD19, CD27, IgM, IgD, and CD5 have been used to differentiate between these B cell subsets using conventional flow cytometry. The work of this chapter shows that this differentiation can also be achieved by mass cytometry where additional markers, such as CD38 and CD24, could also be included without the need for compensation. Moreover, I was able to distinguish the proportional representation of naïve, memory and CD5+ B cells using supervised (manual gating) and unsupervised (viSNE and SPADE) approaches. Importantly, I can show that these three methods have high precision in determining these subsets, and the results I achieved are consistent with values reported in the literature [137].

In terms of surface antigen staining, the method I used was reproducible. To demonstrate this, I stained a single patient sample multiple times and observed that each histogram associated with a given antigen was consistent within each replicate (Figure 3.9). I developed an SOP for my staining procedure where total cell numbers within any given experiment were similar, allowing for saturation staining with a given antibody. I used the recommended dilution of antibody (1:100), revealing a potential limitation within my experiments where antibody titration would have potentially generated more efficient use of the antibody. To ensure that my antibody cocktail was

specific, I included a Fc-blocking solution where the effectiveness is demonstrated in the dot plots of CD3 vs CD19 expression on B and T cells. With the exception of a small population of cell doublets, the respective populations of CD19+ and CD3+ cells were negative for CD3 and CD19. This adherence to an SOP, and this demonstration of reproducible staining was important for later experiments using CLL cells which were only analysed once.

One of the aims of this chapter was the identification CD5+ B cells, the normal counterpart of CLL cells [138], in buffy coats from healthy individuals that have been processed and cryopreserved. I could identify these cells, in the proper proportion (less than 1% from total B cell population[24]) using mass cytometry and both supervised and unsupervised data analysis. The rarity of CD5+ B cells puts a limitation on this thesis. I used barcoding as a method of understanding differences in antigen staining between patients, and to make my experiments more efficient. Because I used whole PBMC populations this made observation of rare cell subsets difficult, and I was not able to fully characterise surface antigen expression on the CD5+ B cells I identified. Therefore, no strong conclusion can be made regarding the similarity of CD5+ B cells to CLL cells from the data presented in this thesis. This limitation could have been remedied by B cell purification from PBMC preparations, and by limiting the number of barcodes I used. A further limitation is the preparation for and cryopreservation of PBMC samples, this is reported to affect ability to detect CD5+ B cells [139]. Nevertheless, my experiments show detection of CD5+ B cells within the accepted proportion, indicating that this limitation is likely not important to this thesis.
The accuracy and precision of my measurements with respect to healthy normal B cells gave me confidence to measure CLL cell phenotypes only once. This is important

because of the precious nature of patient-derived samples, particularly if those samples come from clinical studies although this aspect is not relevant to this thesis.

My characterisation of CLL cell phenotype followed two different courses. In the first instance I investigated overall similarity of phenotype between patients. Unsupervised hierarchical clustering did not reveal groupings of patient cells with similar phenotypes shown in Figure 3.15D. In fact, subsequent FlowSOM analysis demonstrated that CLL patient cells appeared to have a unique phenotype, where generated metacluster trees were different for each patient sample as shown in Figure 3.17B. This is a novel finding; other studies have used large panels of antibodies to detect antigen determine phenotype of on CLL cells the purpose of reliable disease diagnosis where the whole population of cells is taken into account. In this context, variable antigen expression on CLL cells is used for the purpose of finding biomarking for potential disease outcome (eg the relationship of CD38 expression with disease prognosis in CLL [140]. Because barcoding allows staining of multiple samples in the same tube, my studies of CLL cells are the first to directly compare surface antigen expression between different patient samples. When coupled with my use of analysis algorithms, I was able to identify potential sub-clones of CLL cells defined by cells having similar characteristics of antigen expression. Whether this represents true sub-clonality remains to be determined, but could correlate with known genetic heterogeneity in CLL [141, 142].

The second course of characterisation involved investigating the elements of similarity between patient CLL cells. A recent paradigm in the biological understanding of CLL is the phenotype of cells as they recycle between the blood and tissues. This phenotype is defined by expression of CXCR4 and CD5, where OQ cells are

$CXCR4^{Bright}/CD5^{Dim}$ and NE cells are $CXCR4^{Dim}/CD5^{Bright}$. Greater phenotypic characterisation of NE and OQ cells has not been easily possible until now, a previous abstract reports an attempt at characterising antigenic differences using conventional flow cytometry is known to be uniquely distinct and recent studies have shown variability within the clonal subpopulations in CXCR4/CD5, OQ and NE cells[38]. My work provides greater characterisation of division of the total population of CXCR4/CD5-stained CLL cells into by dividing this population into 8 equal-sized "gates" that then allowed for the comparison of how individual antigens varied in expression within this total population across all patient samples as shown in Figure 3.19. For example, I found that CD22 stained more strongly within the $CXCR4^{Bright}/CD5^{Bright}$ gate, a finding that concurs with those reported in the abstract [143]. Moreover, in my findings gate 1, CD27 shows to increase in gate 1 and decrease gradually to gate 4. The rest of my surface antigens are lower compared to gates 5,6,7 and 8. In conclusion, I have identified subclone fractions within the total clone of CXCR4/CD5. I show a consistent pattern in different CLL patients, my analysis demonstrates patterns of subclone antigen expression within the OQ subclones from the NE subclones. This builds a foundation for further studies of CLL cell give a clear differential diagnosis of disease criteria to look at targeted subclones within the CXCR4/CD5 population of cells for functional and clinical outcome studies.

This aspect is further investigated with respect to B cell receptor signaling in chapter four where I stimulate CLL cells and B cells within samples of PBMCs with IgM crosslinking antibody. The reason as in literature, CLL main driver to disease progression and heterogeneity in disease prognosis is caused by BCR signaling and the expression of sIgM that drives to contribute to disease pathobiology behaviour. In my next chapter I study the different B cell subsets in normal and CLL subclones to

study BCR signaling response within these cells after anti-IgM and introduction to BCR inhibitors, Ibrutinib and Idelalisib.

# Chapter 4: Investigating BCR signaling in B cell subsets of normal PBMC & Chronic Lymphocytic Leukaemia cells

### 4.1 Introduction

The malignant cells of CLL are driven to survive and proliferate by BCR engagement [37, 51, 53, 144, 145] . Our understanding of the signaling pathway initiated by BCR engagement on these cells has been derived from studies of the entire clone where a limited number of parameters have been investigated. Thus, as is demonstrated in Figure 1.4, BCR crosslinking results in activation of several pathways culminating in the increase in intracellular $Ca^{2+}$ and induction of MAPK and IKK signaling[48]. Importantly, the strength of BCR signaling in CLL cells is related to surface expression of this receptor, and these factors ultimately relate to disease outcome [58]. However, in the previous chapter my data show variable expression of surface IgM on CLL cell clones within patient samples, suggesting that induced signaling will also vary. Previous studies of CLL cell signaling have so far not addressed single cell signaling in CLL with respect to BCR engagement in a multidimensional approach. The aim of this chapter was to investigate this using a highly multidimensional tool called mass cytometry. As a multi-dimensional measurement technique, flow cytometry is optimally suited to the measurement of signal transduction in single cells. Indeed, this method has been used by other groups to investigate this phenomenon in lymphoid cancer cell lines, demonstrating that up to 13 different signaling proteins can be measured at any given time [146]. The limitation here is spectral overlap of the fluorophores available for antibody labelling where there is a trade-off between investigation of signaling versus cell phenotype when

examination of particular subclones within a cell population is necessary. Mass cytometry solves this through its ability to, conventionally, measure more that 40 different parameters and is therefore likely to be an ideal technique to measure BCR signaling in different normal and CLL B cell subpopulations.

In terms of multi-parametric measurement of signaling using flow cytometry, the technique generally employs the use of phospho-specific antibodies. The majority of these antibodies work in Western blot techniques, and this is a way in which the specificity of these antibodies is validated. However, recognition of phosphorylated proteins can be achieved by other means as was demonstrated in a publication by Dierck *et al* [106]. Here SH2 domains recognising phospho-tyrosine motifs within proteins are assembled into an array to detect signaling in cells. Because these SH2 domains are also useful in Far-Western blots for the detection of phospho-tyrosine motifs within proteins, it is a distinct possibility that these domains may be useful within mass cytometry applications. Therefore, the first part of this results chapter focusses on developing SH2 profiling, using cell lines to test and validate this approach. The second half of this chapter then uses phospho-specific antibodies together with antibodies recognising surface phenotypes to investigate normal and CLL B cell response to BCR engagement.

### 4.2 Results

At the beginning of this thesis a major tool to investigate intracellular signaling using flow cytometry was the use of phospho-specific antibodies. While informative, a paper by Nollau *et a*l [106] suggested that the use of peptides containing phospho-tyrosine SH2 domains to recognise phospho-tyrosine residues could also be used to determine signaling in cells. In this paper the authors used these peptides to recognise tyrosine-

phosphorylated proteins where specificity and sensitivity were determined by oligonucleotide tags. On this basis I determined to use such peptides in initial experiments with mass cytometry as a way of enhancing our understanding of global signaling within CLL and normal B cells.

Table 4. 1 SH2 domain profiling assay for far-western

**Far-western SH2/Streptavidin concentration in 10ml**

| Labelled SH2 Domain | Concentration SH2 domain (50ng/ml) | Concentration of Streptavidin (50ng/ml) |
|---|---|---|
| GRB2 | 1.6µl | 3.6µl |
| NCK2 | 1.3µl | 3.6µl |
| PI3KR1 | 1.2µl | 5.4µl |
| SRC | 1.1µl | 3.6µl |

Table 4. 2 SH2 domain concentration conjugated to heavy metal

| SH2 DOMAIN | CONCENTRATION µg/ml | 100µg | ISOTOPIC MASSES |
|---|---|---|---|
| **SRC** | 890µg/ml | 112.36µl | 163Dy |
| **NCK2** | 800µg/ml | 125µl | 176Yb |
| **PI3KR1** | 1250µg/ml | 80µl | 169Tm |
| **GRB2** | 630µg/ml | 159µl | 153Eu |

### 4.2.1 Optimization of SH2 profiling in cell lines.

I began this work by obtaining peptides corresponding to the SH2 binding domains within SRC, NCK2, the p85α subunit of PI3K (PI3KR1) and GRB2 (kindly supplied by Peter Nollau. (*Department of Clinical Chemistry, Center of Clinical Pathology, University Medical Center Hamburg-Eppendorf, Martinistr. 52, 20246 Hamburg, Germany).* These SH2 domains typically recognise specific phosphotyrosine binding motifs sites within proteins and are defined as shown [147].

Table 4. 3 SH2 domains phospho-tyrosine binding motifs for SH2 peptides

Letters indicate corresponding amino acids with the exception of X which indicates any amino acid.

| SH2 domains | Binding Motifs |
|---|---|
| Grb2 | [pY] [Q/Y/V] [N] [Y/Q/F] |
| | [V] [pY] [Q] [N] [W/F] |
| | [pY] [I/V] [N] [I/L/V] |
| | [V/P] [X] [pY] [V/I/M] [N] [M/V] [pY] [V/E] [N] |
| | |
| | |
| PIK3R1 | [pY] [M/I/V/E] [X] [M] |
| | [X] [H/N/M] [pY] [V/E/I/T] [N/M/E] [M/E] |
| | [pY] [V/D] [X] [I/M/V] |
| | |
| Nck2 | [P/D/E/T] [V/I/E] [pY] [E/D/S] [N/E/M/T] [V/P/ A/T] [D] |
| | |
| Src | [pY] [E/D/T] [E/N/Y] [I/M/L] [P/H] [I/P] |
| | [pY] [E/D/V/I] [L/I/E] [I/L/V] [D] |
| | [D/E] [X] [X] [pY] [D] [D/E/φ] [P/I] |

I then tested these peptides in Far-Western blots of whole cell lysates (Figure 4.1). This was an important experiment for validation that the heavy metal labelling procedure to prepare the peptides for mass cytometry did not change their binding characteristics. The cell lines I used in this experiment were K562 and Mec-1; the former cell line is a CML cell line where neoplastic growth is driven by BCR-ABL [148], whilst the latter were derived from a CLL patient undergoing prolymphocytic transformation[149] where the oncogenic driver is less defined. Figure 4.1 shows a schematic of the Far Western experiment where the SH2 domains (in contrast to an antibody) are used to detect phospho-tyrosine motifs within proteins that have been separated by SDS-PAGE (Figure 4.1A). The SH2 domains are biotinylated and can be detected by HRP-conjugated streptavidin (Figure 4B). The SH2 domains can also be tagged by heavy metals. , Streptavidin is used to capture the SH2 domains into a quaternary structure for efficient detection of phospho-tyrosine binding motifs when used in mass cytometry or Western blot in accordance to the procedure described by Nollau *et al* [106].

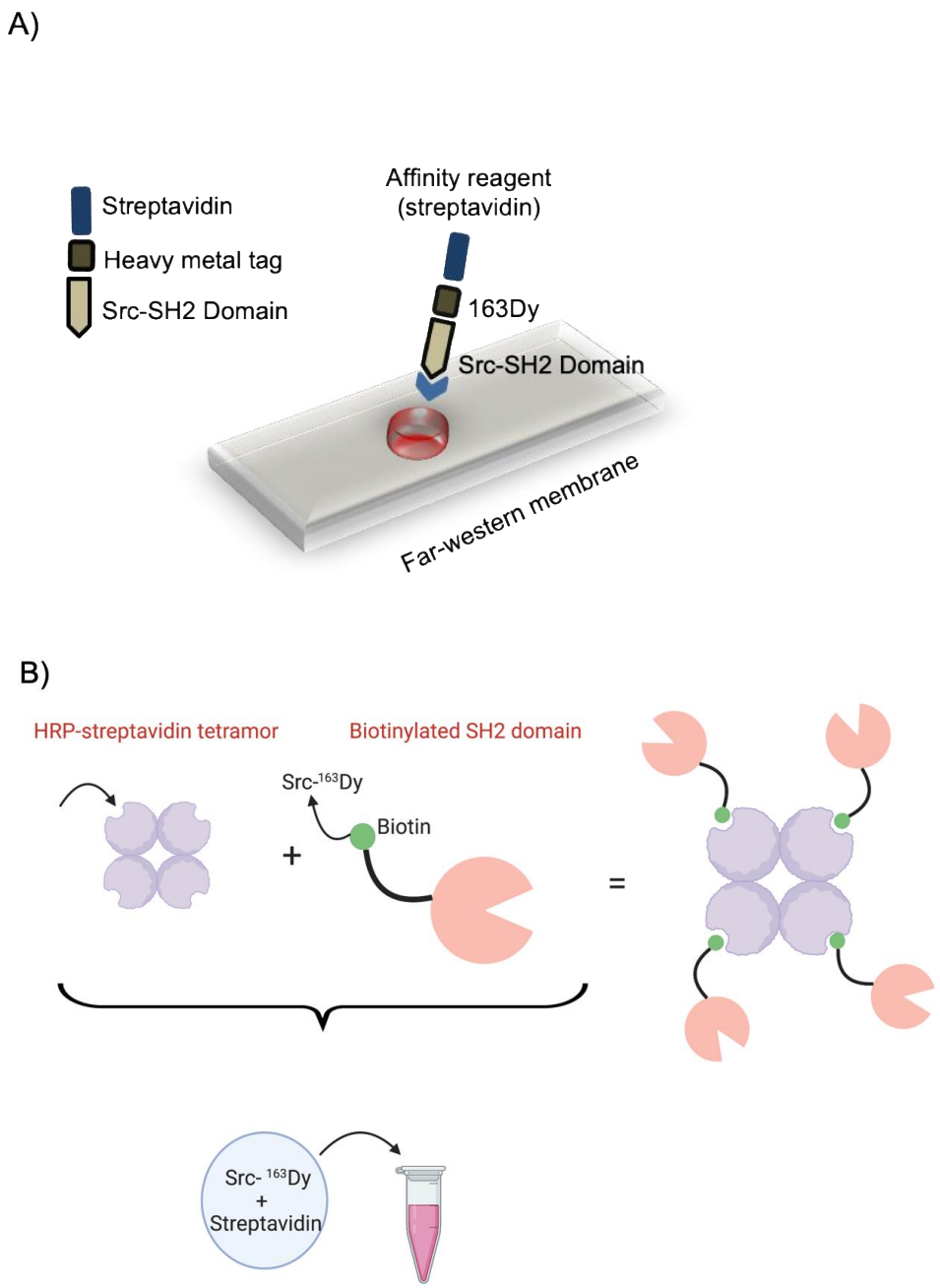


**Figure 4. 1 Concept of SH2 profiling assay in Far-Western and mass cytometry.** SH2 domains are labelled by heavy metals $^{163}$Dy,$^{176}$Yb,$^{169}$Tm and $^{153}$Eu that can be detected using approach by probing with HRP-streptavidin by molar ratio of 2:1 with final concentration 50ng/ml each domain 1-hour room temperature. **A.)** Far western and **B.)** diagram presentation of coupling HRP streptavidin tetramer with biotinylated SH2 domains on suspension fixed K562 cell lines for mass cytometry detection.

Cell lysates from K562 and Mec-1 cell lines were prepared as described in Materials and Methods section 2.1.15. K562 cell lines were treated with dasatinib (150nM, 24 h) in order to inhibit BCR-ABL activity and reduce tyrosine phosphorylation as much as possible in this cell line. In contrast, Mec-1 were treated with pervanadate (100mM,15mins) to inhibit protein phosphatases and increase tyrosine phosphorylation in these cells. To ensure that these respective treatments and cell lines responded in the way that should, I performed a Western blot where I probed the membranes with the anti-phosphotyrosine antibody (PY20). Figure 4.2 shows that dasatinib treatment of K562 cells resulted in decreased levels of PY20 reactivity compared to untreated cells, and pervanadate treatment of Mec1 cells showed an increase in PY20 reactivity. I could now probe the membranes with the SH2 domains. Figure 4.3 shows the reactivity of the 4 SH2 domains A) GRB2, B) NCK2, C) PI3KR1, and D) SRC I used in this thesis.

Although pervanadate treatment of Mec-1 cells showed an increase in phospho-tyrosine reactivity, there was no apparent change in the reactivity of the SH2 domains on the Far-Western blots (Figure 4.3). Moreover, where there were reactive bands, there seemed no difference between the blots in terms of the apparent size of the bands. For example, there was a band at 75kDa that was consistently present on all the blots regardless of the SH2 binding motif used. In contrast, with K562 cells there were distinctive differences, not only between treated and untreated cells, but also with the difference SH2 domains. Figure 4.3A shows the Far Western blot for the GRB2 SH2 domains where there appears to be specific reactivity with bands of ~49 kDa, ~37 kDa and 3 bands between 15 and 20 kDa. The reactivity of the SH2 domain was reduced in dasatinib treated cells. Figure 4.3B shows that NCK2 SH2 domains

identified bands at ~75, ~45 kDa and between ~25- 20 kDa. Figure 4.3C shows that PI3KR1 SH2 specifically and strongly recognised a band at ~150 kDa. Other lower molecular weight bands were also recognised, but the reactivity was not as strong. Figure 4.3D shows the reactivity of the SRC SH2 domain, where recognition of weak bands of ~70, and ~49 kDa was observed, and stronger reactivity observed with respect to a triplet of bands between ~25-~20 kDa. Together, these results show that the SH2 domains I used in this thesis had some of specificity in recognising phosphorylated proteins in cells.

Next I performed the same experiment but used heavy metal modified SH2 domains within the Far Western blots to see whether such modification changed their reactivity. Figure 4.4 shows the results for 3 of the SH2 domains, NCK, PI3KR1 and SRC, these results were largely similar to what was observed using the unlabelled SH2 domains, Because the membrane blots show no significant changes between labelled and unlabelled SH2 domain reactivity, it can be concluded that there is no interference of the heavy metals or the labelling procedure with the reactivity of the SH2 domains. The limitation of this experiment in both Western and far-Western blot did not have a loading controls total protein for each SH2 domain. Moreover, the model system employing K562 cells, where different epitopes are recognised by the SH2 domains, justified further experimentation and testing of the SH2 domains within a mass cytometry setting.

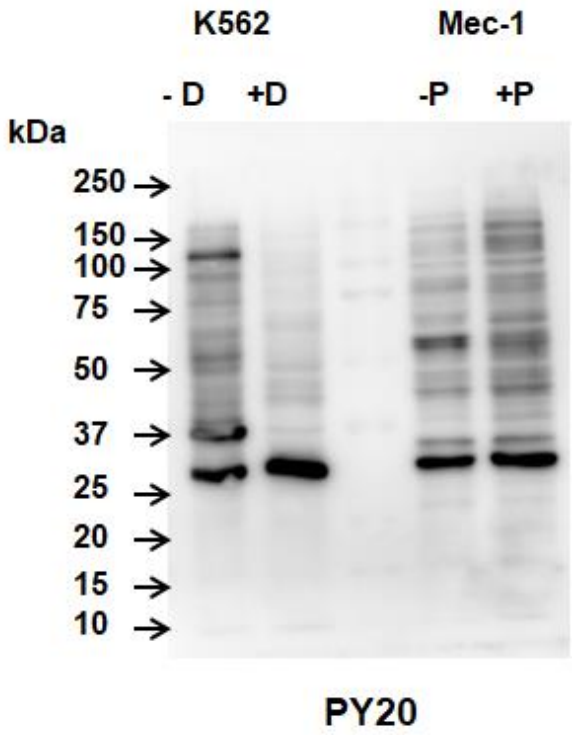


**Figure 4. 2 Western blot of phosphotyrosine following treatment of K562 and Mec-1 cell lines with dasatinib and pervanadate,** respectively. (4 x $10^6$) K562 and (4 x $10^6$) Mec-1 cells were treated, respectively, ± 150nM dasatinib for 24 hours, ± 1mM (100µM) pervanadate for 15min. Cells were harvested and lysed with SDS-PAGE buffer. 10µg of total protein from each cell line and condition were separated by SDS-PAGE using a 10% polyacrylamide gel and transferred to PVDF membranes. The membrane was probed with anti-phosphotyrosine antibody (PY20). The image was captured by using enhanced chemiluminescence (ECL) following treatment of the membrane with HRP-conjugated anti-mouse IgG.

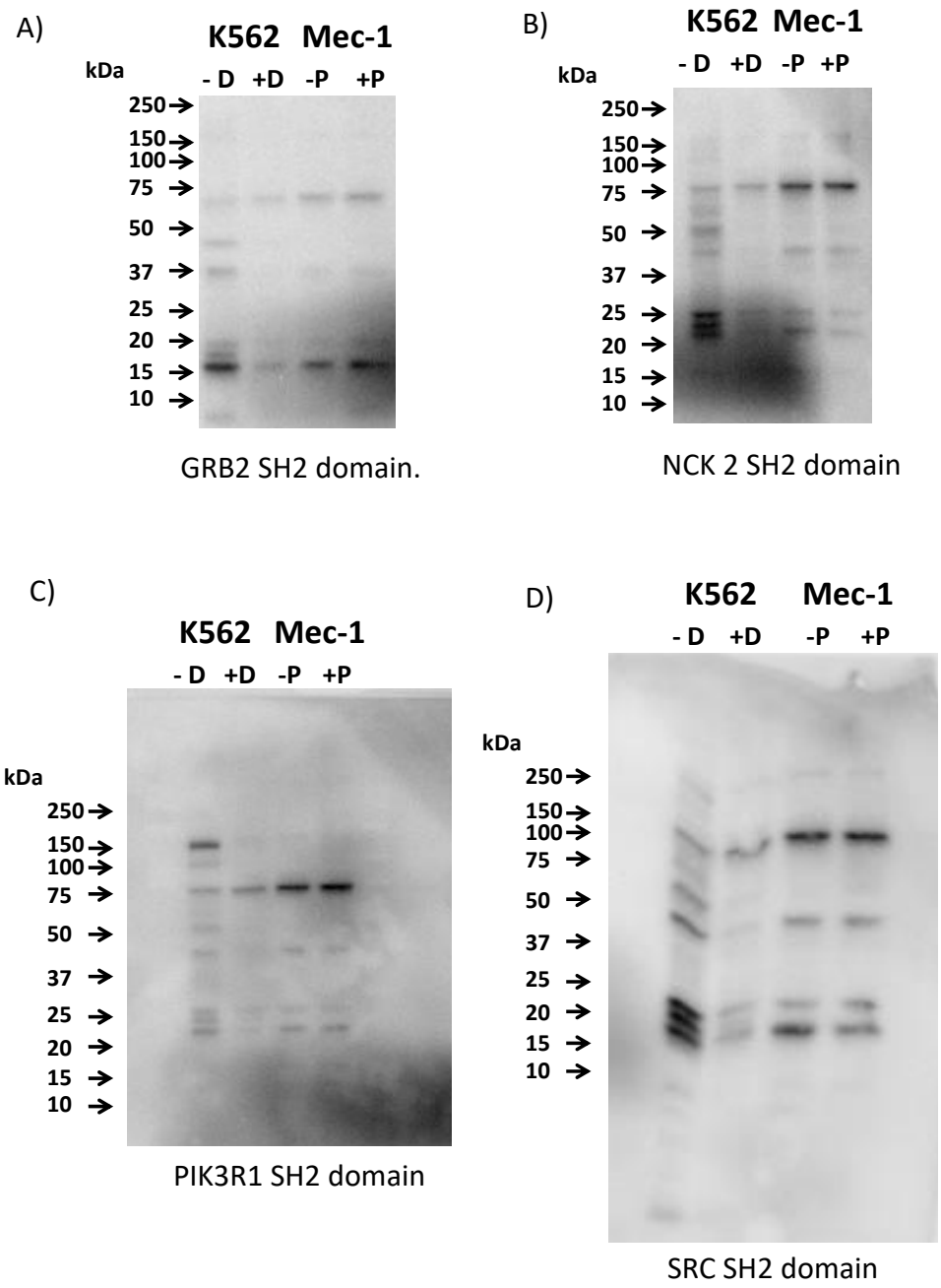


**Figure 4. 3 Far-western blot of unlabelled SH2 profiling of phosphotyrosine following treatment of K562 and Mec-1 cell lines with dasatinib and pervanadate**, respectively. (4 x $10^6$) K562 and (4 x $10^6$) Mec-1 cells were treated, respectively, ± 150nM dasatinib for 24 hours, ± 1mM (100µM) pervanadate for 15min. Cells were harvested and lysed with SDS-PAGE buffer. The membrane was probed with streptavidin-HRP antibody with unlabelled biotinylated SH2 domain at a final concentration of 50 ng/ml of each domain **A.)** GRB2, **B.)** NCK2, **C.)** PI3KR1 and **D.)** SRC. The image was captured by using enhanced chemiluminescence (ECL) for detection and binding reactions by streptavidin-HRP antibody with unlabelled SH2 domains.

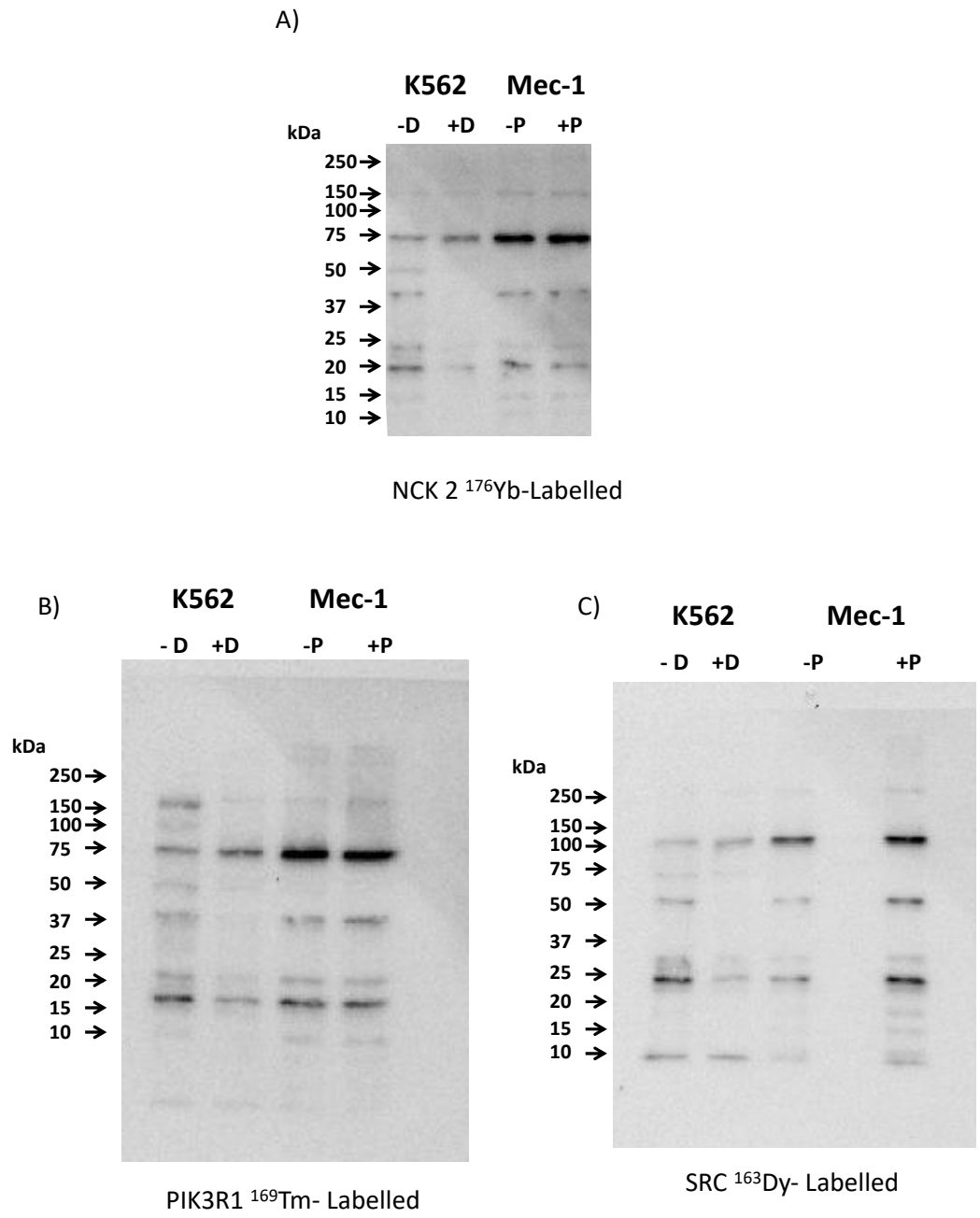


**Figure 4. 4 Far-Western blot of labelled SH2 profiling of phosphotyrosine following treatment of K562 and Mec-1 cell lines with dasatinib and pervanadate.** The membrane was probed with streptavidin-HRP antibody with labelled biotinylated SH2 domain at a final concentration of 50 ng/ml of each domain **A.)** NCK2 $^{176}$Yb, **B.)** PI3KR1 $^{169}$Tm and **C.)** SRC $^{163}$Dy. The image was captured by using enhanced chemiluminescence (ECL) for detection and binding reactions by streptavidin-HRP antibody with labelled SH2 domains.

Next, I tested whether my labelling of the SH2 domains resulted in efficient coupling of the chosen heavy metals to their respective SH2 domain (Table 4.2). Figure 4.5 shows the results of this test where the strong black bar on the rain plot from the mass spectrograph indicates the presence of the respective heavy metal lanthanide conjugated to its target SH2 domain. The GRB2 SH2 domain was conjugated separately and tested on a different day (data not shown).

The rain plot showing detection of the heavy metals I used. Successfully four tagged SH2 domains with their corresponding heavy metal lanthanides, was confirmed by mass cytometer. Figure 4.5 illustrates since my initial work using Far-Western blotting indicated that K562 cell were a good model, I used them to further investigate signaling using SH2 domains with mass cytometry. Figure 4.6 shows my attempts to optimize the cell permeabilization in order SH2 domain reactivity within the cells. Samples were permeabilised either with 0.1% triton X-100 at RT where a SH2 domain/Streptavidin concentration of 800ng/ml and incubation at room temperature were used (Figure 4.6A), or methanol at 4°C where, after washing, the cells were incubated with a SH2 domain/Streptavidin concentration of 2000ng/ml at RT (Figure 4.6B). Both methods of permeabilization allowed clear binding of GRB2- and PI3KR1-SH2 domains to cells. There was no binding of NCK-SH2 domains, and methanol permeabilization seemed to slightly increase SRC-SH2 domain binding. In Dasatinib treated samples, as was shown in Far Western blots, there was a complete reduction of SH2 domain reactivity, where the only difference between the two permeabilization methods is that residual binding of the GRB2 SH2 domain was observed in methanol permeabilised cells. In terms of reactivity the PI3KR1 SH2 domain was strongest followed by GRB2, SRC and then NCK2 which showed no reactivity. Taken together, these results show the usefulness of SH2 domains for the detection of intracellular signaling. I can conclude

that GRB2 and PI3KR1 SH2 domains can easily detect specific signals in K562 cells, whereas SRC and NCK 2 are less efficient. Whether this latter observation is due to lack of available motifs within K562 cells or to general non-reactivity of these domains remains to be determined. I next used phospho-specific antibodies to measure signaling in cells, testing how BCR signaling affected the reactivity of these antibodies with normal B and CLL cells.

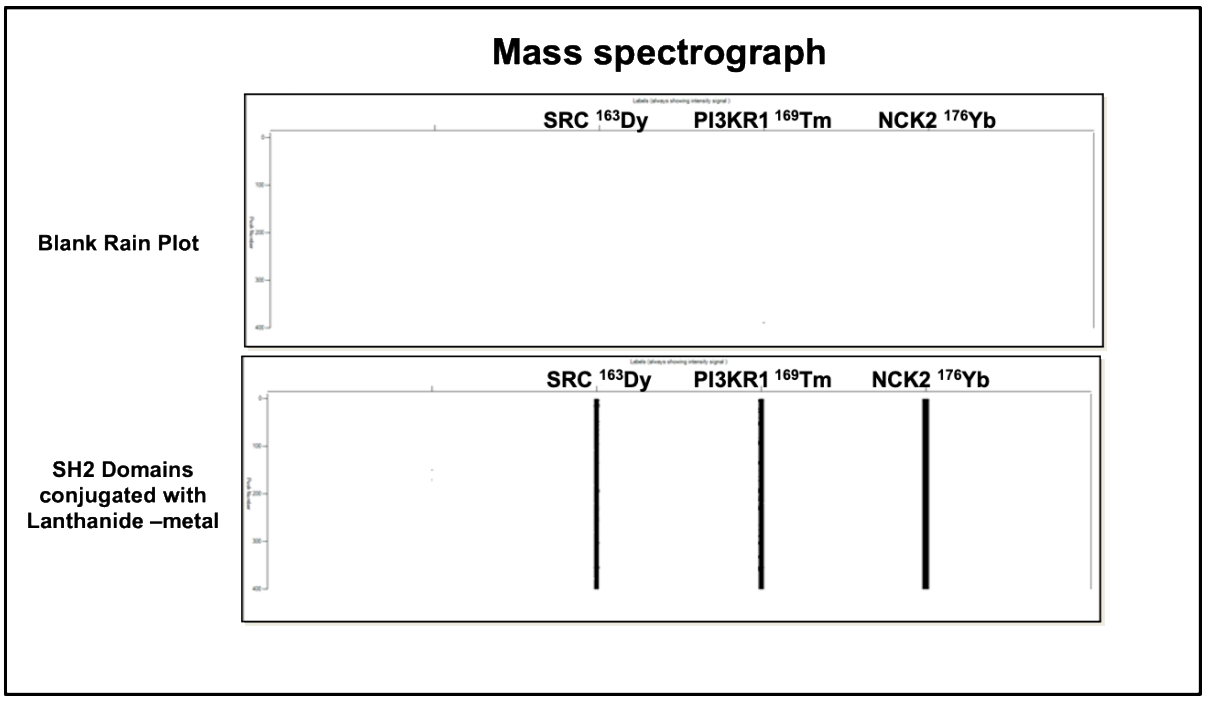


**Figure 4. 5 Mass spectrograph of 153Eu, 163Dy, 169Tm and 176Yb following Maxpar® labelling procedure of SH2 domain.** 100mg SRC, NCK2 and PI3KR1 SH2 domain was labelled with $^{163}$Dy, $^{169}$Tm, $^{176}$Yb following the Maxpar® labelling procedure. 10ml labelled SRC, NCK2 and PI3KR1 SH2 domain was then diluted in 400ml Maxpar® W-buffer and the presence of SRC $^{163}$Dy, PI3KR1 $^{169}$Tm, NCK2 $^{176}$Yb following the Maxpar® was detected using a Helios™ mass cytometer.

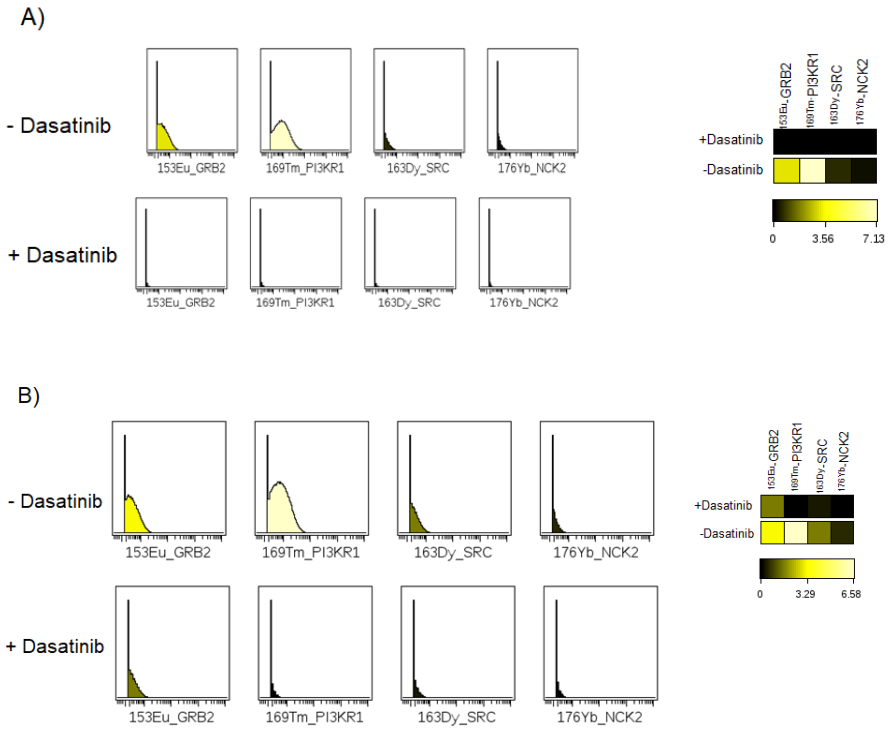


**Figure 4. 6 Labelled SH2 domains stained on K562 cell line by mass cytometry. A.)** shows a concentration of 800 ng of / Streptavidin ~~all mixed together~~ showing better permeabilising of the cells and there was better intracellular binding by using triton x-100 at 0.1%. **B.)** Samples were permeabilised with methanol at 4 °C at concentration 2000 ng of SH2/Streptavidin.

### 4.2.2 Measurement of BCR signaling using Western blot in model cell lines.

To begin exploring BCR signaling in CLL cells using mass cytometry and phospho-specific antibodies it was first necessary to establish optimal conditions using a model cell line. This is because CLL cells from different patients often respond to BCR stimulation in a heterogeneous way. In this first phase of method development, consistency of measurement was an important consideration. Maver-1 and Jeko-1 cells were used as model cell lines. These cell lines were derived from patients with Mantle Cell Lymphoma (MCL) and were suitable to these studies because these cells maintain a low baseline of signaling in their resting state, that then strongly changes when these cells are stimulated with BCR crosslinking

Table 4.4 shows the panel of phospho-specific antibodies chosen for mass cytometry, together with surface markers to identify cell phenotypes. To start choosing which phospho antibodies that I will need to include in my panel along with the surface antigens that I have designed according to its importance to CLL BCR signaling. At the beginning of this thesis the availability of phospho-specific antibodies targeting the BCR signaling pathway was restricted to: The panel antibodies I have chosen are listed in (table 4.4) are Phospho-p-38, which is a mitogen stress-activated protein kinase (MSAPK), that signals to induced differentiation or, apoptosis in cells [150]. The mitogen-activated protein kinase/extra cellular regulated kinase (MAPK/ERK) is known to have an important role in BCR signaling pathway in blood diseases and malignancies. This pathway plays a key role in cell survival, proliferation and gene expression [151]. In this chapter I chose p38, stress-activated protein kinase and studies have shown the main association of p38 is with an increase in proliferation and survival that can be due to induction of apoptosis mainly by stress cellular release in CLL [152, 153]. Moreover, Phospho-ERK1/2 (MAPK) regulates anti-apoptotic function

and cell cycle in cells *in vivo*, when phosphorylated constitutively activated is important in normal cell to facilitate cell entry in G1 to S phase progression [154]. In CLL cells p-ERK activation shown to be associated with anergic cells with increased expression of high basal levels of iCa2+ and p-ERK [155]. Inhibitors Ibrutinib and Idelalisib have shown to inhibit the MAPK/ERK kinase pathway signaling by blocking the surface levels of CXCR4 chemokine to prevent CLL cell cycle into circulation [156]. pERK in comes from one of group of kinases from eIF2a and with increased phosphorylation in cells can lead to disease progression in CLL and other cancer malignancies and can aid for drug resistance [157]. The next phosphoproteins I added, PI3K/AKT pathway, a protein kinase B, p-AKT is an oncogene that is responsible for sustaining cell survival, apoptosis and proliferation. Abnormality function to the PI3K/AKT pathway can lead to various of diseases including diabetes and cancer [158, 159].In CLL cells, p-AKT is often that has a strong connection with PI3K pathway highly activated due to its key role, AKT inhibitors are given to control haematological malignancies. Within the same line of pathway [160]. pS6 is site-specific ribosomal protein, a protein involved in RNA translation that can be phosphorylated by either AKT or ERK and is reported essential in CLL therapeutic responses [161]. The next phosphoantibodies I chose are pPLC$\gamma$2 (is a phospholipase C-$\gamma$2) is an essential component of BCR signaling pathway of BTK and is induced by epidermal growth factor (EGF) has an important role in BCR signaling activation and is a downstream of Bruton's tyrosine[162]. pZap-70/Syk phosphoprotein is from a tyrosine kinase family within the T cell and B cell receptor signaling pathways, respectively. It has an essential expression in CLL cells and is a diagnostic indicator of poor patient prognosis in this disease [42, 163].

Table 4. 4 Mass cytometry surface and intracellular panel antibodies

| Surface Human B cell panel antibodies | Heavy Metal | Clone |
|---|---|---|
| Anti-Human CD45 | 154Sm | H130 |
| Anti-Human CD49d | 141Pr | 9F10 |
| Anti-Human IgD | 146Nd | IA6-2 |
| Anti-Human CD5 | 143Nd | UCHT2 |
| Anti-Human CD20 | 147Sm | H1 |
| Anti-Human CD19 | 142Nd | H1B19 |
| Anti-Human IgM | 172Nd | MHM-88 |
| IgM UNLB goat anti-human | 148Nd | polyclonal |
| Anti-Human CD43 | 150Nd | 84-3C1 |
| Anti-Human CD21 | 152Sm | B1B |
| Anti-Human CD27 | 155Gd | L128 |
| Anti-Human CD22 | 159Tb | H1B22 |
| Anti-Human CD3 | 170Er | UCHT1 |
| Anti-Human CD184 [CXCR4] | 175Lu | 12G5 |
| Anti-FITC-160Gd | 160Gd | FIT-22 |
| **Intracellular panel antibodies** | **Heavy Metal** | **Clone** |
| Anti-p38 [T180/Y182] | 156Gd | D3F9 |
| Anti-pERK1/2 | 167Er | D13.14.43 |
| Anti-pTyrosine | 144Nd | p-Tyr100 |
| Anti-pAkt | 152Sm | D9E |
| Anti-pPLCg2 | 162Dy | [K89-689][PY759] |
| Anti-pZAP70 | 171Yb | 17a |
| Anti-pS6 | 172Yb | N7-548 |

First I wanted to establish the optimal time point in stimulated cells and so used lysates of BCR-stimulated Maver-1 and Jeko-1cells to generate Western blots that measured induction of signaling using the phospho-specific antibodies within my panel. Figure 4.7 shows the results of this experiment where Maver-1 and Jeko-1 cells were unstimulated or stimulated with BCR crosslinking antibody for 5 and 15 min. There was clear induction of p-PLC$\gamma$2, pBTK, pAKT & pERK1/2 in both Maver-1 and Jeko-1cells responding to BCR crosslinking (Figure 4.7A). Whereas significant induction of phosphorylation of some these proteins was observed at 5 min, it was only at 15min where statistical significance of induction was achieved for all (Figure 4.7B).

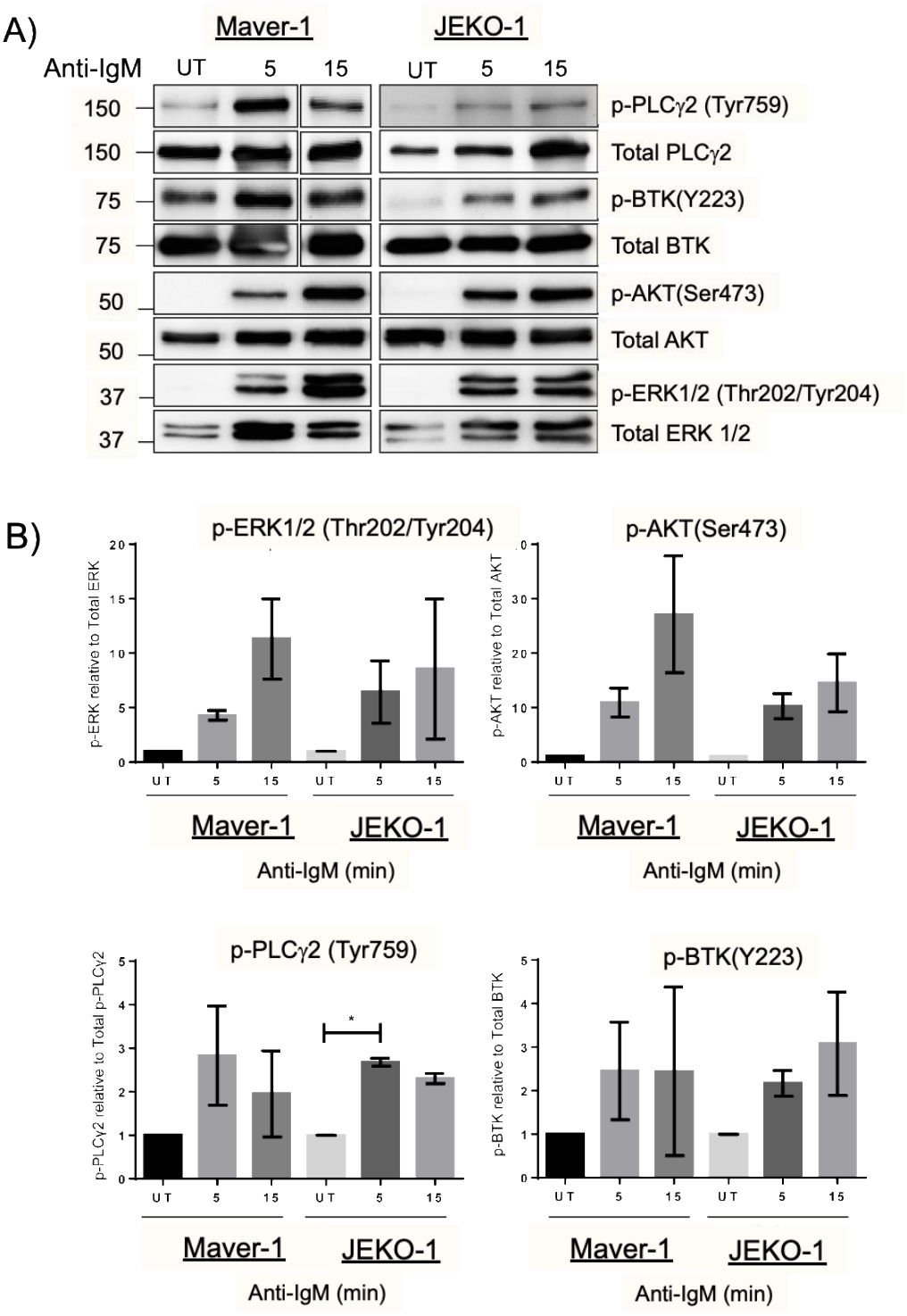


**Figure 4. 7 Induction of phospho antibodies in Maver-1 and Jeko-1cells by anti-IgM. A.)** Cells were stimulated with F(ab')$_2$ IgM antibody at a concentration of 20ug/mL with cell concentration 2x10$^6$ cells for 15 minutes 37ºC, run by 10% SDS-PAGE gel and probed by phospho-specific proteins 1:2000 dilution with 5 % BSA overnight at 4ºC. Total phospho were probed for 2 hour 1:3000 dilution with 5 % BSA at room temperature for loading control. **B.)** Densitometry analysis for Maver-1 and Jeko-1 n=3, One-way Anova was done for statistical analysis using GraphPad Prism™.

### 4.2.3 Measurement of induced signaling in BCR stimulated Maver-1 cells using mass cytometry.

Western blot analysis showed that Maver-1 and Jeko-1 cells responded in a similar way to BCR crosslinking. For this reason, I next chose to continue with Maver-1 cells for mass cytometry optimisation. Figure 4.8 shows the results of this optimisation, comparing unstimulated cells to those incubated with anti-IgM for 5, 10, 15, and 30 min. Figure 4.8A illustrates the reactivity of the phospho-specific antibodies I used at different time-points following stimulation with anti-IgM. Although induction was observed at 5 min for many of the phosphoproteins, the strongest change was observed in cells stimulated for 15min, which is then represented by the histogram plots in Figure 4.8B. Figure 4.8C shows the statistical analysis of four biological repeats comparting resting cells with those stimulated for 15min, significant induction of protein phosphorylation was observed for ERK, AKT, PLC$\gamma$2, and ZAP70/SYK and this seemed to correlate with an also significant appearance of pY epitopes in the stimulated cells. There was strong trend with regard to the induction p38 phosphorylation, but there seemed no significant difference with respect to phosphorylation of S6 kinase. This lack of significant difference with respect to S6K could be due to high basal levels of pS6 present in resting cells (Figure 4.8B). Taken together, these results show that BCR signaling can be measured using mass cytometry and phospho-specific antibodies.

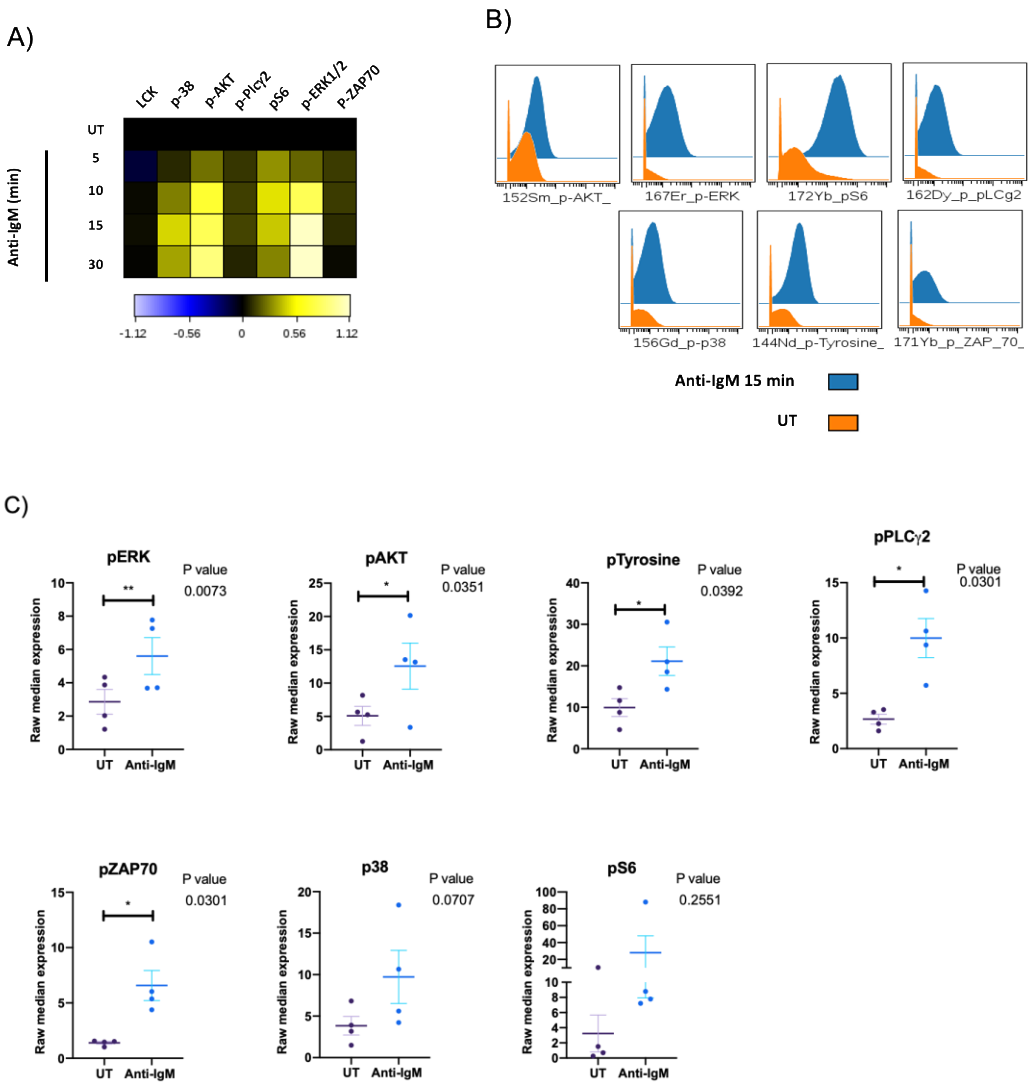


**Figure 4. 8 Induction of signaling in Maver-1 cells was achieved by crosslinking BCR with 20mg/mL F(ab')$_2$ anti-IgM antibody. A.)** Heat map generated by mass cytometry showing phospho-antibody binding to resting and BCR-stimulated cells, **B.)** Histogram representation of the data presented in part A. **C.)** Graphical representation of phospho-antibody binding to resting and BCR-stimulated cells after 15 mins. These graphs show the data generated for n=4 experiments. Statistical analysis was performed using a paired T-Test (GraphPad Prism™).

### 4.2.4 Mass cytometry allows observation of BCR signaling in normal B cells

I next applied the optimised panel of 13 surface antigen directed antibodies and 7 phospho-specific (internal antigen) antibodies to the study of normal PBMCs to identify the B cell subsets according to Figure 4.9A within the total B cell population. B cell subsets were gated according to CD27 and IgD to differentiate between Class switch memory, Memory IgM and Naïve IgM. Figure 4.9B a comparison of phospho-protein antibody reactivity in unstimulated and BCR-stimulated B cells from each of the identified subsets, and in the total T cell population. This latter population of cells showed no induction of protein phosphorylation which is not surprising because T cells do not express BCR and therefore cannot be stimulated by BCR crosslinking with anti-sIgM antibodies. Each B cell subset seemed to respond differently to BCR crosslinking; IgM memory cells responded more strongly than did naïve IgM+ B cells, and there was only a very weak response noted for the class switch B cells. This varied response is likely due to differences in sIgM expression on these different subpopulations of cells, and this is demonstrated by the significant positive relationship between this parameter and the intensity of phospho-PLC$\gamma$2 and S6 induction in analysis of 100 clusters of total B cells by FlowSOM (Figure 4.9C). Analysis of each B cell subset by SPADE shows that appearance of p-PLC$\gamma$2 is strongest in the memory B cell subset where sIgM is also strongest (Figure 4.9D). These data show clear evidence of differential B cell response to BCR engagement according to B cell subset.

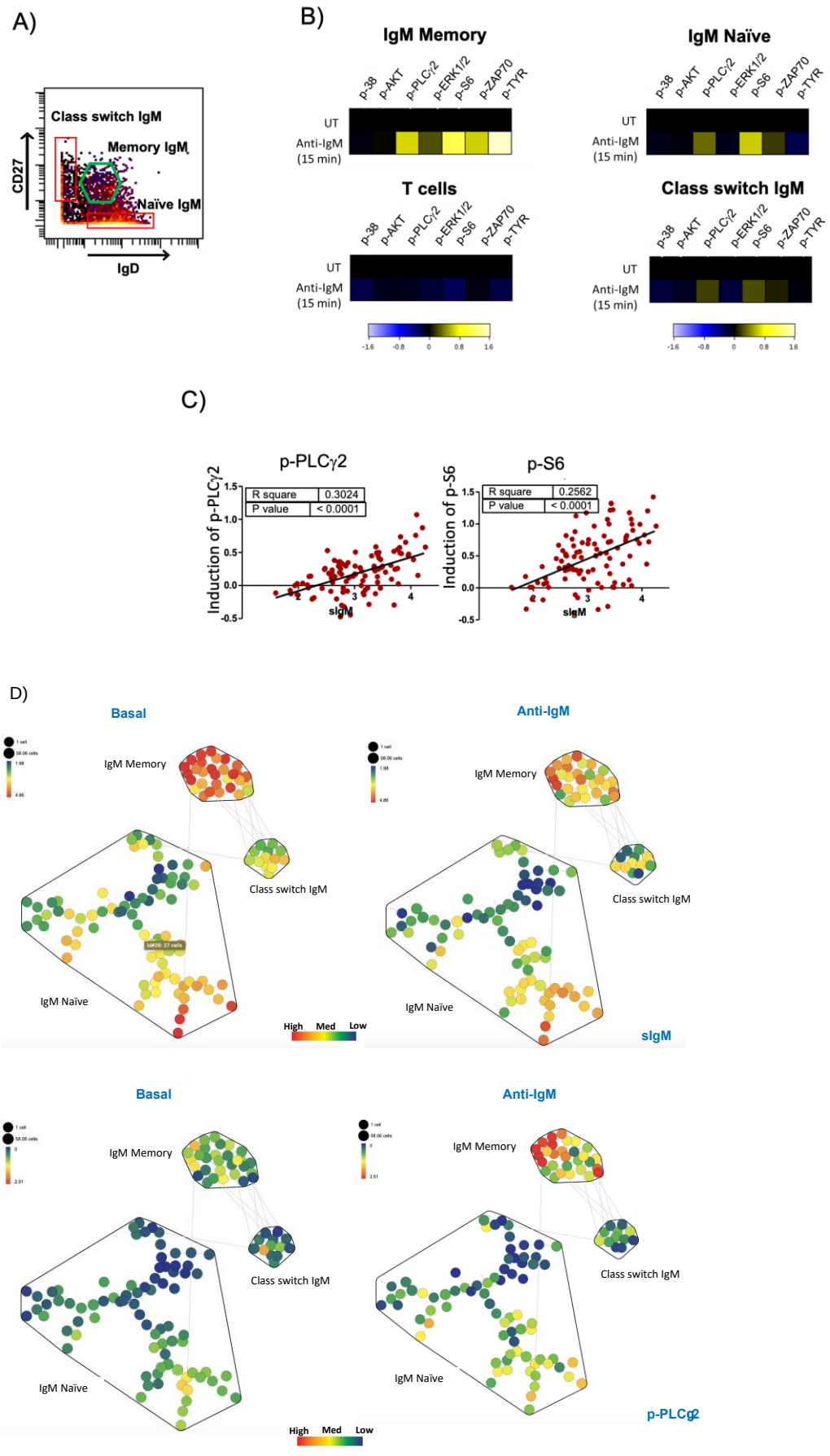
A)
Class switch IgM
Memory IgM
Naïve IgM
CD27
IgD
B)
IgM Memory
IgM Naïve
T cells
Class switch IgM
p-38
p-AKT
p-PLCγ2
p-ERK1/2
p-S6
p-ZAP70
p-TYR
UT
Anti-IgM (15 min)
C)
p-PLCγ2
p-S6
Induction of p-PLCγ2
Induction of p-S6
R square
P value
0.3024
< 0.0001
0.2562
< 0.0001
sIgM
D)
Basal
Anti-IgM
IgM Memory
Class switch IgM
IgM Naïve
High
Med
Low
sIgM
p-PLCg2

**Figure 4. 9 Induction of protein phosphorylation in B cell subtypes following BCR engagement. A.)** B cell populations were identified within PBMC suspensions by gating on CD19+/CD20+ cells. Memory, Naïve and class-switched B cells were further identified by CD27 and IgD expression. **B.)** B cells were stimulated with anti-IgM antibody (20µg/ml) for 15 min and then fixed with PFA. Cells were then prepared for mass cytometry where surface antigens were stained first, followed BS3 crosslinking and cell permeabilization and internal antigen staining. Mass cytometry analysis allowed generation of heat maps for each of the indicated cell subsets. **C.)** FlowSOM was used for further analysis of the total B cell population. Induced p-PLC$\gamma$2 and p-S6 was related to surface IgM expression on 100 clusters of individual cells. **D.)** SPADE tree analysis was generated to demonstrate signaling in B cell subsets. Linear regression and statistical analysis were performed using GraphPad Prism™. (n=1).

### 4.2.5 Mass cytometry allows observation of BCR signaling in different subpopulations of CLL cells.

This section introduces the measurement of BCR signaling in CLL cells. The results I presented in Chapter 3 show both interpatient and intraclonal heterogeneity of the malignant cell phenotypes in samples from CLL patients. While it can be expected that interpatient variability in phenotypes leads to differences in response to BCR engagement[38, 58, 164, 165], at the beginning of this thesis understanding of intraclonal differences in response to BCR engagement was poor. I began by relating sIgM expression with induction of protein phosphorylation using a similar approach to my analysis of this relationship in normal B cells (Figure 4.9C). In Figure 4.10 I show the results of this analysis; induction of pS6 showed the strongest correlation with sIgM and was followed by pPLC$\gamma$2, pTyrosine, pERK, and, finally, pAKT which showed the weakest relationship. These data largely agree with that reported by Coelho et al relating sIgM expression to induction of pPLC$\gamma$2 and pERK [164], my data extend this with the inclusion of the other phosphoprotein epitopes I include. Thus, my data supports suggest that the relationship between sIgM and induced signal intensity and demonstrates that this can also as be applied intraclonally in among CLL cells.

I next analysed this intraclonal variability of CLL cells using SPADE where designation between recognised subpopulations was achieved using CXCR4 and CD5 expression to classify resting phase “OQ” CLL cells and proliferative phase “NE” CLL cells[38] (Figure 4.11A). As is shown using normal PBMC in Figure 4.9D, SPADE analysis can be used to illustrate how different subpopulations of B cells respond to BCR crosslinking. I used the same approach to analyse the response of CLL cells to sIgM engagement, dividing these populations into the following categories: $CXCR4^-/CD5^-$, $CXCR4^+/CD5^-$ (OQ cells), $CXCR4^+/CD5^+$ and $CD5^+/CXCR4^-$ (NE cells). Figure 4.11B

shows the results of this analysis for each phospho-antibody used. I found that pAKT levels were consistent across the different subpopulations of CLL cells regardless of stimulation, suggesting that AKT is constitutively active in CLL and cannot be stimulated further. This finding agrees with established literature reporting constitutive activation of AKT [166], and explains why the correlation between pAKT and sIgM is so weak. . The other antibodies showed differences in reactivity not only between stimulated and resting cells, but also between different subpopulations. For example, the most dramatic change in phospho-protein induction between resting and stimulated cells was observed in $CXCR4^{+}/CD5^{+}$ and $CD5^{+}/ CXCR4^{-}$ (NE cells) populations. Interestingly, these populations also had higher baseline levels of phospho-antibody reactivity than did $CXCR4^{+}/CD5^{-}$ (OQ cells) and $CXCR4^{-}/CD5^{-}$ CLL cell populations. For this particular case of CLL sIgM expression varied slightly between the different cell populations, that is a known pan-CLL phenomenon (Figure 4.11C). $CXCR4^{+}/CD5^{+}$ and $CD5^{+}/ CXCR4^{-}$ (NE cells) populations had slightly higher expression of sIgM than did the $CXCR4^{-}/CD5^{-}$ population, suggesting the higher response of these cells to BCR engagement is due to higher levels of sIgM.

Application of statistical analysis across 5 CLL cases to compare the level of phospho-proteins as determined by SPADE between resting and stimulated CLL cells within each of the populations was then performed. My analysis is shown in Figure 4.12, significantly higher phosphorylation was observed in CLL cells within the $CXCR4^{+}/CD5^{+}$ and $CD5^{+}/ CXCR4^{-}$ (NE cells) populations. In general, BCR stimulation of CLL cells resulted in an overall increase in detected levels of phosphorylation, with cells in the $CXCR4^{+}/CD5^{+}$ and $CD5^{+}/ CXCR4^{-}$ (NE cells) populations seeming to respond more strongly than in the other two populations. Levels of pAKT are a notable exception, similar to the other phospho-antibodies where were significantly higher

levels of pAKT in $CXCR4^{+}/CD5^{+}$ and $CD5^{+}/ CXCR4^{-}$ (NE cells) populations, however, there was no effect of BCR crosslinking these levels, a result that is consistent with the notion that Akt is constitutively active in CLL cells [166]. Since $CXCR4^{+}/CD5^{+}$ and $CD5^{+}/ CXCR4^{-}$ (NE cells) populations have higher relative sIgM expression than do $CXCR4^{-}/CD5^{-}$, and $CXCR4^{+} /CD5^{-}$ (OQ cells) populations (Figure 3.19C), the data suggest that the relationship between sIgM expression and CLL cell response to BCR crosslinking can be extended to individual clones. Taken together, these data show that individual CLL cell response to BCR engagement can be measured to give information about intraclonal variability to this type of stimulation.

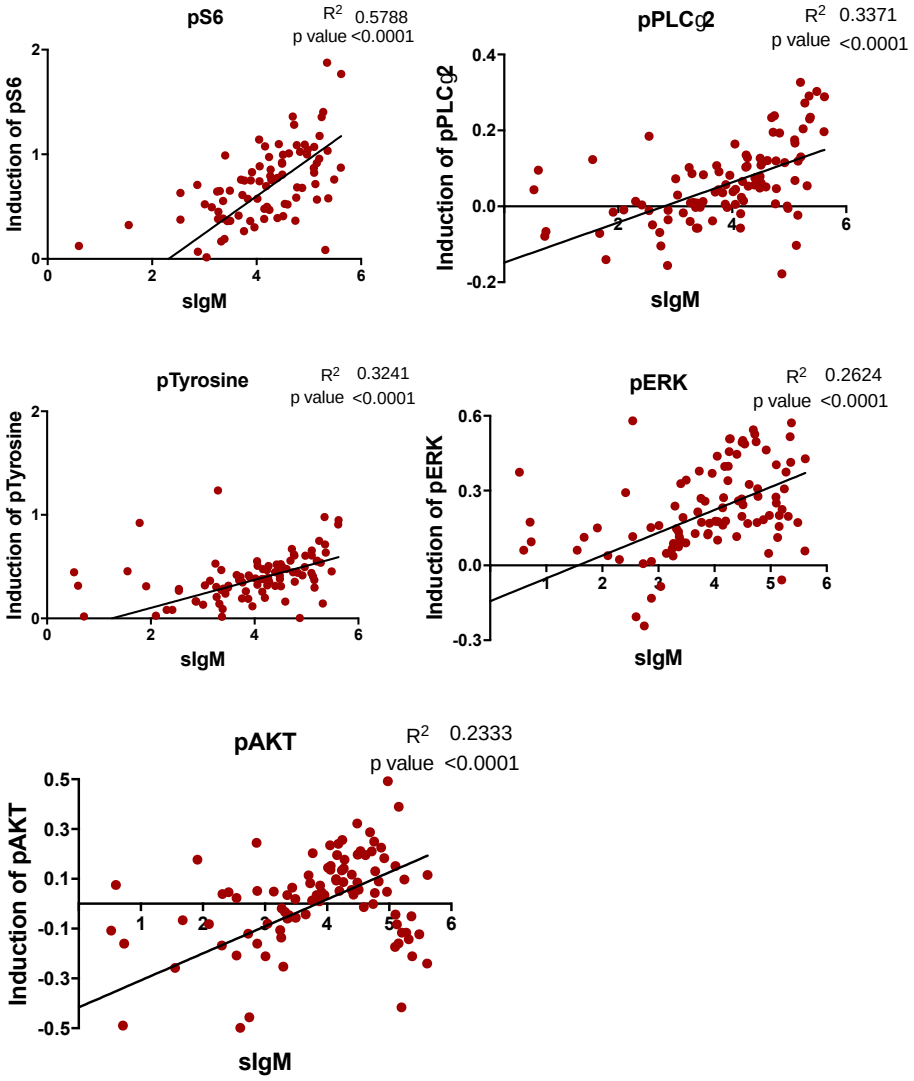


**Figure 4. 10 FlowSOM analysis for BCR signaling measurement in CLL population.** FlowSOM was used for analysis of the total CLL cell population. Induced phosphoproteins p-S6, p-PLCγ2, pTyrosine, pERK and, pAKT was related to surface IgM expression on 100 clusters of individual cells. Linear regression was performed using GraphPad Prism™.

A)

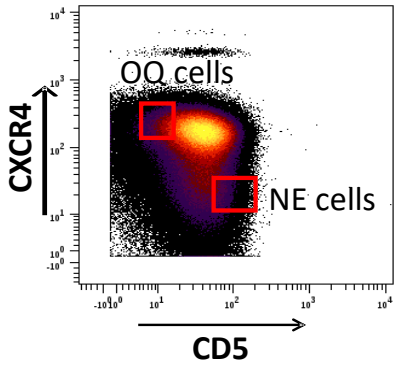
OQ cells
NE cells
CXCR4
CD5

B)

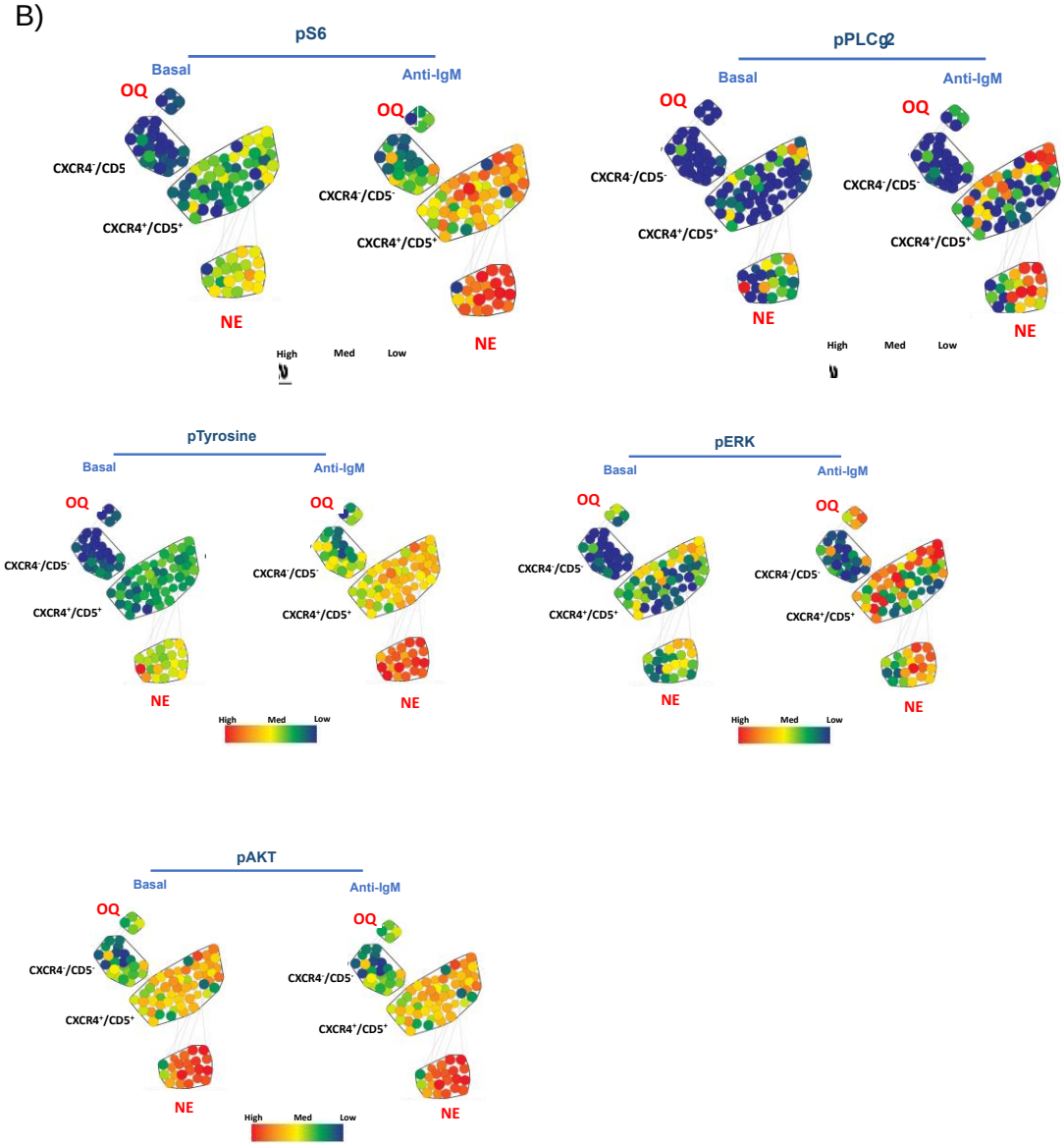
pS6
Basal
Anti-IgM
OQ
CXCR4⁻/CD5⁻
CXCR4⁺/CD5⁺
NE
High
Med
Low
pPLCg2
pTyrosine
pERK
pAKT

C)

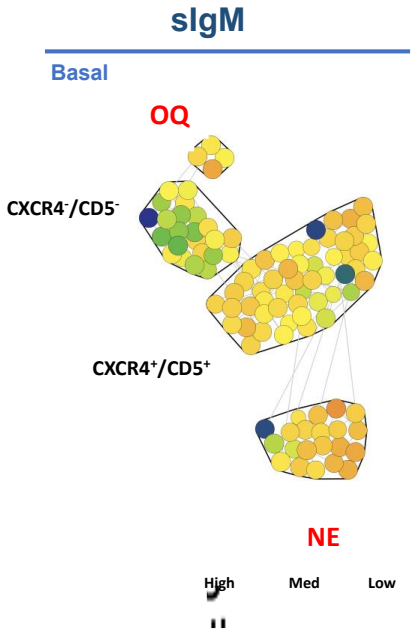


**Figure 4. 11 Expression of phosphoproteins in intraclonal CLL cells using SPADE. A.)** CLL cell gating strategy of "newly emerged cells" (NE $CD5^{+}$, $CXCR4^{-}$) and "older quiescent cells" (OQ, $CXCR4^{-}.CD5^{+}$)**. B.)** SPADE tree analysis for comparison of phospho-proteins in basal and anti-IgM-stimulated CLL cells in $CXCR4^{-}/CD5^{-}$, $CXCR4^{+}$ /$CD5^{-}$ (OQ cells), $CXCR4^{+}/CD5^{+}$ and $CD5^{+}$/ $CXCR4^{-}$ (NE cells). **C.)** level of sIgM expression in the basal condition in all 4 CLL cells.

Basal

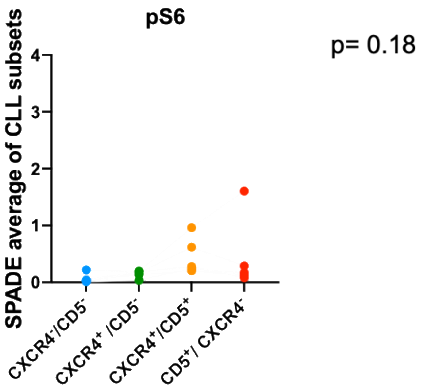


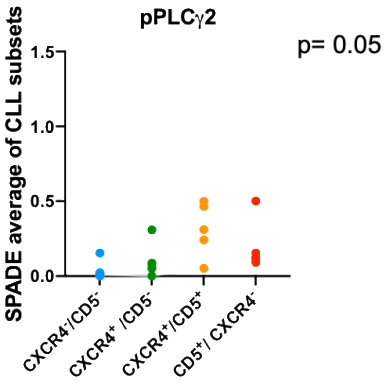


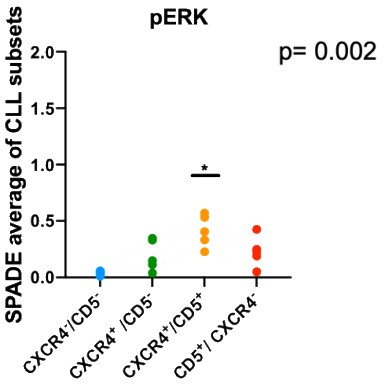


Anti-IgM

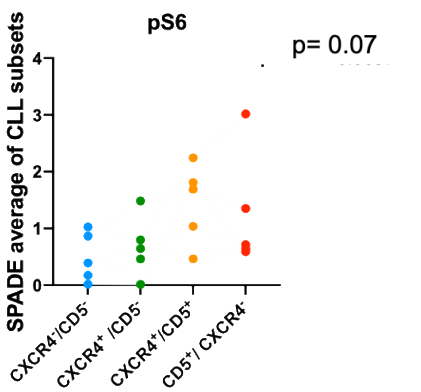


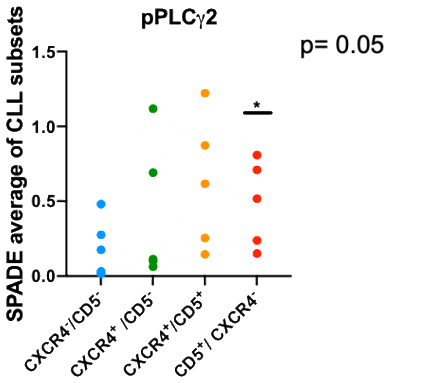


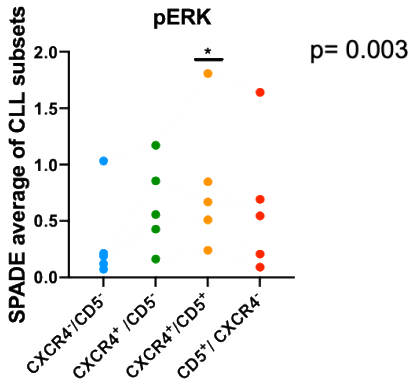

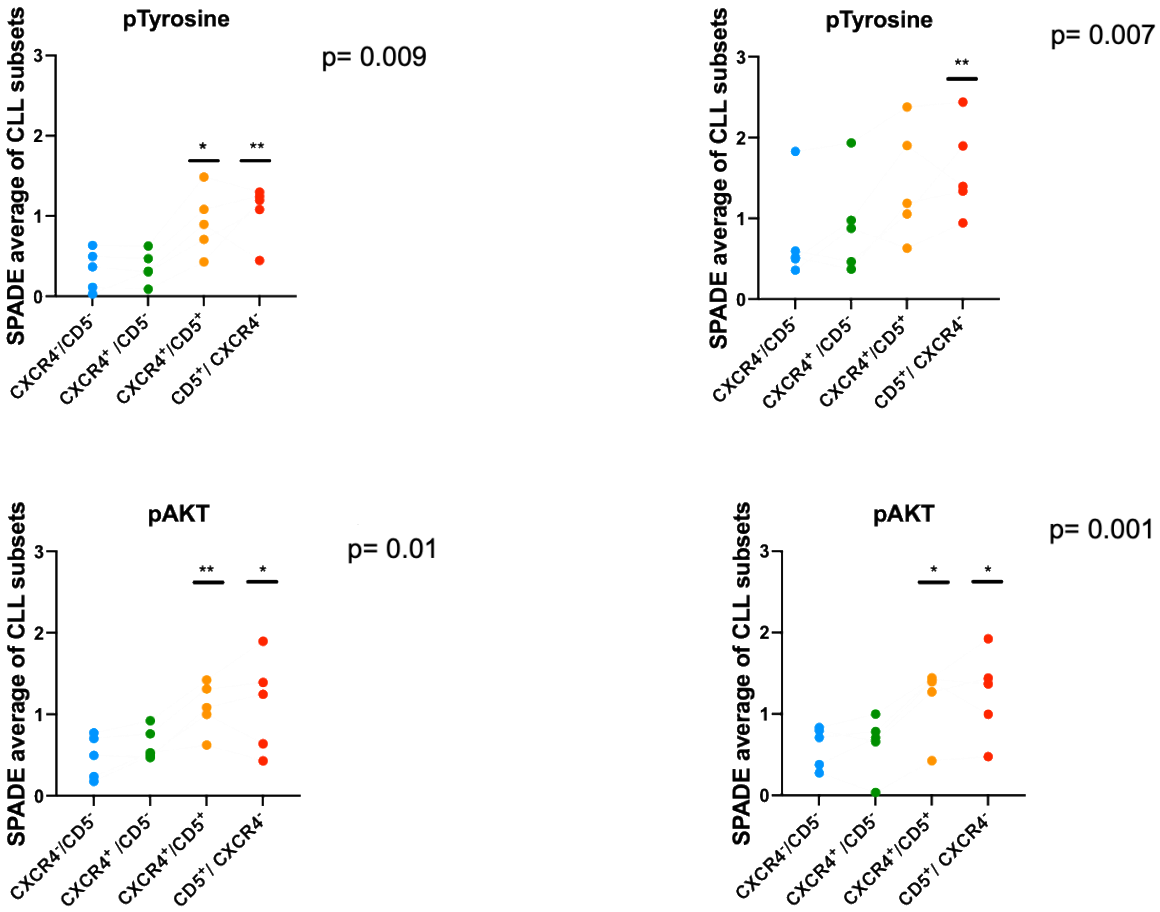


**Figure 4. 12 Graphical representation of the SPADE data for identified cell types.** Average nodal expression for each phospho-protein basal and after stimulation with anti-IgM is taken for $CXCR4^-/CD5^-$, $CXCR4^+/CD5^-$, $CXCR4^+/CD5^+$ and $CD5^+/CXCR4^-$ CLL cell subtypes where each dot represents a single CLL case. The graphs represent n=5 experiments using CLL cells from different patient samples. p values were calculated using a one-way Anova, and where statistical significance was found followed up with multiple comparison analysis. Columns with * or ** record significance below a p value of 0.05 or 0.01 respectively.

### 4.2.6 Effect of ibrutinib and idelalisib on BCR induced signaling in primary CLL at single cell resolution.

Ibrutinib [an inhibitor of Bruton's tyrosine kinase (BTK)] and idelalisib [an inhibitor of phosphatidylinositol 3 kinase δ (PI3Kδ)] are compounds that are used to treat CLL based on their ability to affect BCR signaling [167]. It is approved for clinical use, but not shown, that all CLL cells are affected by these compounds. However, this assumption might be unfounded considering that the inhibitory effects of these on induced signaling can be overcome by pre-treatment of CLL cells with IL4 to raise surface expression levels of IgM [64]. Considering the intraclonal relationship between sIgM expression and BCR signaling that can be studied using mass cytometry, it next seemed appropriate to use this technology to investigate how these inhibitors affect the BCR response of the different CLL subsets.

#### 4.2.6.1 Determination of optimal concentrations of ibrutinib and idelalisib to inhibit BCR signaling using a model cell line (Maver-1).

In this section optimisation was conducted using different dose concentrations of ibrutinib and idelalisib to determine their effect on BCR signaling. Figures 4.13A and B show the results associated with ibrutinib. Maver-1 cells were treated with increasing dose concentrations of ibrutinib, 100nM, 200nM, 500nM and 1000nM, for 1h, and then followed by BCR stimulation with anti-IgM for 5 minutes. Western blot was then performed on cell lysates, analysing for the presence of pSyk, pERK, p38, pAKT, pBKT and pPLCγ2. Figure 4.13A and B illustrate that ibrutinib treatment inhibited pBTK at a concentration of 100nM, and complete inhibition was observed at 200nM. Ideally, I should have observed inhibition of pPLCγ2 as well, and in the

Western blot illustrated in Figure 4.13A there is a distinct reduction of this band in MAVER-1 cells treated with 200nM ibrutinib, but we were unable to consistently repeat this experiment with the same result (Figure 4.13B). As expected pSYK was unaffected by ibrutinib treatment because SYK is upstream of BTK in the BCR signaling pathway (Figure 1.4). BCR induction of pERK and pp38 were also unaffected by ibrutinib treatment of Maver-1 cells. The $Y^{223}$ site in BTK is a target for autophosphorylation, and reduction of the reactive band in a Western blot using the pBTK antibody in our experiments indicates that kinase activity is inhibited. This therefore suggests that a concentration of 200nM can be used for ibrutinib to achieve complete kinase inhibition despite not observing consistent reduction in phosphorylation of the downstream target of BTK, namely PLC$\gamma$2.

Figures 4.13 C and D show the results for our optimization experiments using Idelalisib. The same approach was used for idelalisib as was used for ibrutinib; Maver-1 cells were incubated with 100nM, 200nM, 500nM and 1000nM idelalisib for 1h, and then stimulated with anti-IgM for 5 mins. We found that BCR induction of pAKT was consistently inhibited by treating Maver-1 cells with 100nM idelalisib (Figure 4.13A and B). The other phospho-epitopes, pSYK, pERK were unaffected by idelalisib, even when concentrations as high as 1$\mu$M were used. The 100nM concentration for idelalisib needed for inhibition of PI3K$\delta$ that I observed was inconsistent with values reported in the literature where concentrations of 1$\mu$M have been used [168]. For my thesis I selected the optimal dose concentration for idelalisib is 1$\mu$M for use in mass cytometry experiments.

After choosing the optimal drug concentration for each B cell receptor inhibitor (BCRI), the next step was to see the effect of these inhibitors within mass cytometry

experiments. In these experiments I use only one concentration each of Ibrutinib (200nM) and Idelalisib (1μM) to investigate their effect on BCR-stimulated Maver-1 cells with the panel of phospho-specific antibodies available. Idelalisib treatment of Maver-1 cells reduced BCR induction of pAKT to near unstimulated levels indicating the effectiveness of this BCRI in inhibiting PI3Kδ (Figure 4.14). As expected because of its place within the PI3K signaling pathway (Figure 1.4), there was a partial reduction of BCR-induced pS6 levels (Figure 4.14). Inhibition of PI3Kδ also resulted in partial reduction of BCR-induced pERK and pp38, but had little, if any, effect on pSYK and overall pTyrosine levels. The effects of ibrutinib treatment on BCR-inducing were largely similar to those observed for idelalisib, with the exception of pAKT and pS6 which were unaffected by this drug (Figure 4.14). The measurement of pPLCγ2 levels in these experiments was problematic from the point of view that they showed a large variability between repeat measurements. Clear induction was observed in Maver-1 cells responding to BCR crosslinking, however, a clear effect of either idelalisib or ibrutinib could be discerned [169]. Nevertheless, taken together these results show that mass cytometry can potentially be used to measure the effects of BCRI on signaling in cells.

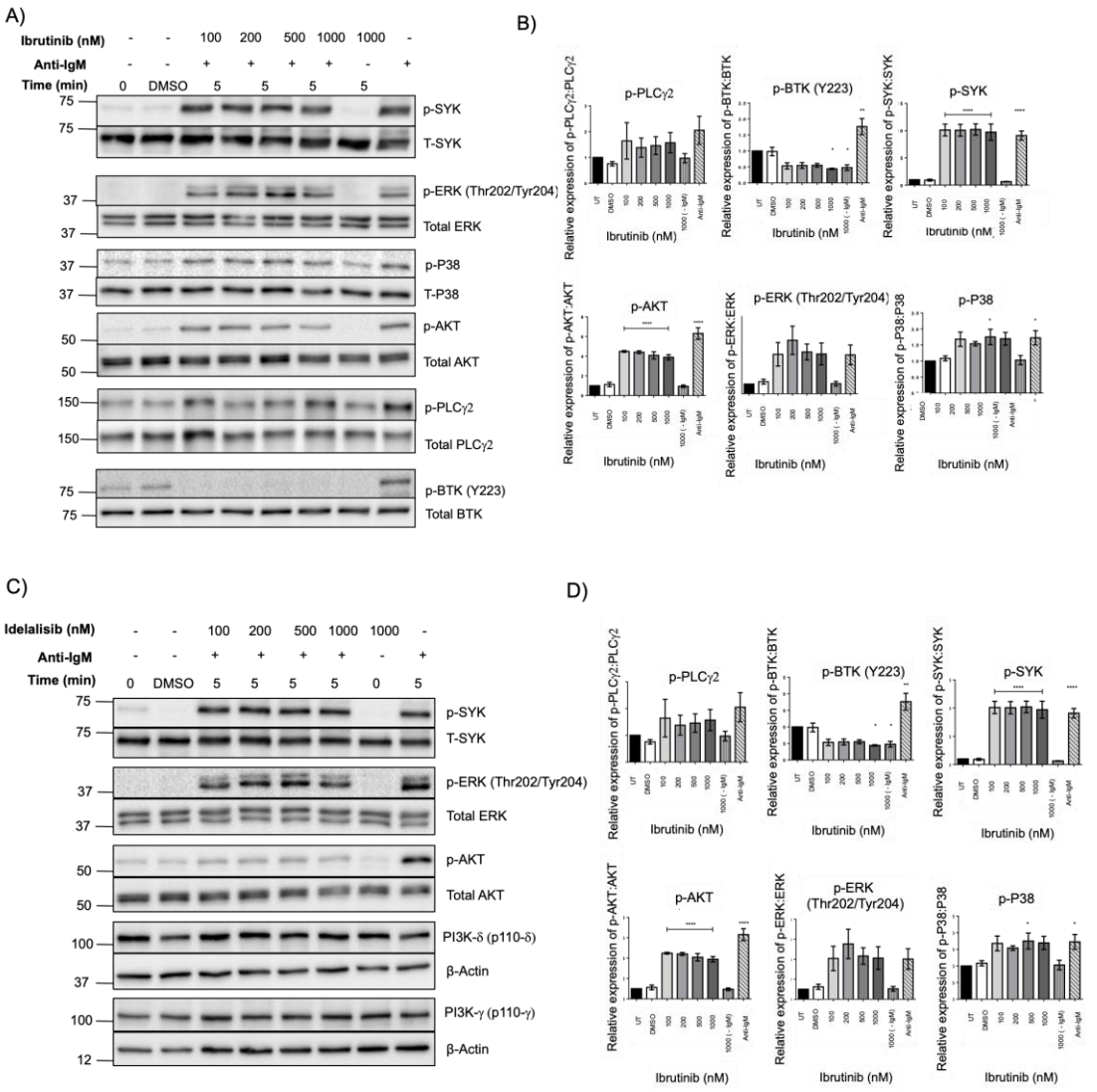


**Figure 4. 13 Dose concentration optimization of MAVER-1 cells with BCRI.** Western blot of phosphoproteins investigated following stimulation of Maver-1 cell line with F(ab') $_2$ IgM antibody at a concentration of 20ug/mL for 5 minutes **A.)** Ibrutinib at different drug concentrations for one hour 37°C. **B.)** densitometry analysis of Ibrutinib for each phosphoprotein. **C.)** Idelalisib treatment at different drug concentration one hour 37°C. **D.)** densitometry analysis of effect of Idelalisib on each phosphoprotein. Cells were harvested and lysed with SDS-PAGE buffer, respectively (5 x $10^6$) in Maver-1 cells. 10µg of cellular lysate from each condition were separated by SDS-PAGE using a 10% polyacrylamide gel and transferred to PVDF membranes. The membrane was probed with different phosphoprotein with 1:2000 dilution with 5 % BSA overnight at 4ºC.Total phospho were probed for 2 hour 1:3000 dilution with 5 % BSA at room temperature for loading control. The image was captured by using enhanced chemiluminescence (ECL). One-way Anova was done for statistical analysis using GraphPad Prism™.

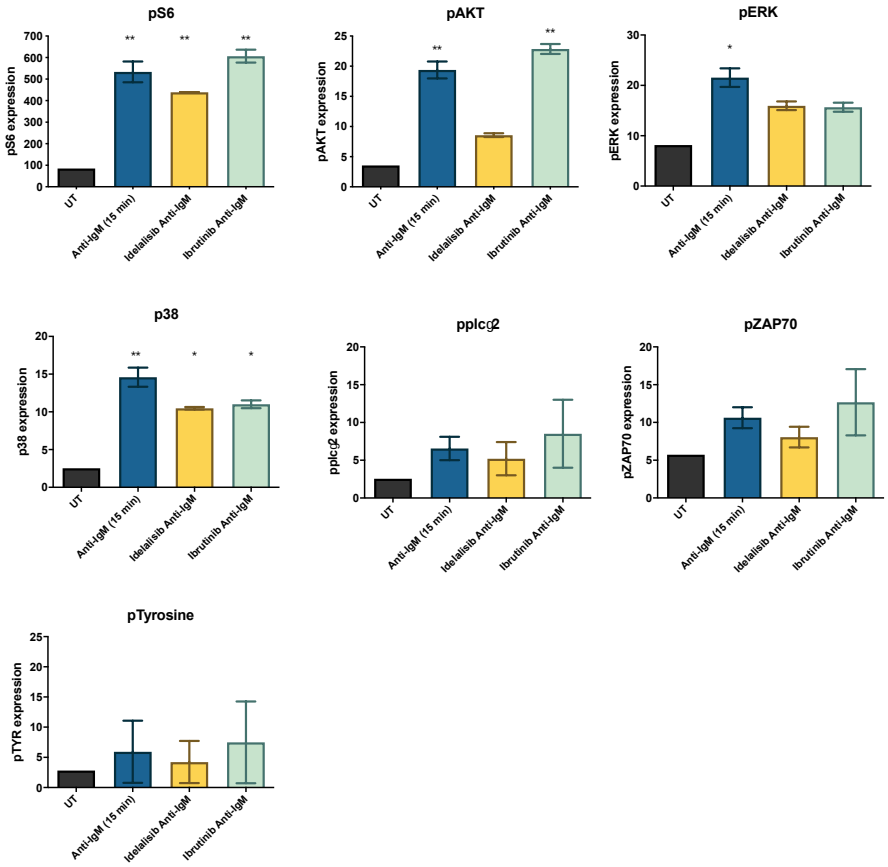


**Figure 4. 14 Single-Cell analysis of BCR inhibitors on signaling effect on Maver-1 cells.** Cells were stimulated with anti-IgM followed with Ibrutinib (200nM) and Idelalisib (1μM) treatment for one hour at 37°C, cells were fixed and permeabilised with methanol -80°C overnight followed with phosphoprotein staining 1:100 dilution for 30 minutes at 37°C on heat block with gentle vortex. The phosphoprotein analysed pS6, pAKT, pERK, p38, p-PLCγ2 and pZAP70 were investigated. These graphs show the data generated for n=2 experiments. One-way Anova was performed and statistical analysis by GraphPad Prism™.

### 4.2.6.2 Measurement of ibrutinib and idelalisib inhibition of BCR signaling in primary CLL cells.

My experiments using Maver-1 cells showed the potential of doing the same in primary CLL cells. Therefore, I next applied this approach to test the BCRI on primary CLL cases by western blot analysis of whole populations of cells, and by mass cytometry analysis of single cells. The main aim is to see the intraclonal variability of response to BCRI in terms of phosphoprotein expression within CLL cell subpopulations. In Figure 4.15 we probed 6 CLL cell lysates with p-SYK, pBTK, p-PLCγ2, pAKT , pERK and LCK antibodies by Western blot, screening for the effect of anti-IgM in the presence or absence of 200nM Ibrutinib. Each CLL case investigated responded differently to anti-IgM crosslinking of surface BCR. For example, case 3711 did not respond to anti-IgM and BCRI treatment (Figure 4.15). This inability to respond was similar to case 3712 where no response was due to surface expression of IgG instead of IgM but could not be attributed to the same reason because case 3711 is IgM positive and the reason for this case it is an indolent case mutated CLL. In contrast, case 3380 showed a strong response to surface IgM crosslinking where induction of pERK, pSyk, pBTK, p-PLCγ2 and pAKT could be clearly observed. We found that these CLL cells were similar to Maver-1 in that ibrutinib treatment resulted in profound reduction of pBTK, partial reduction of p-PLCγ2, but had no effect on pERK, pAKT, and pSyk.

I next analysed these cells by mass cytometry to investigate whether any intraclonal variation could be observed. This analysis was performed only for CLL case 3380 and are shown in 5 SPADE tree illustrations, one for each phospho-antibody, where the total population of cells is segregated into similar sub-groups of cells as was previously done (Figures 4.16 - 4.20). Each figure illustrates antibody reactivity in $CXCR4^{-}/CD5^{-}$

, $CXCR4^+$ /$CD5^-$, $CXCR4^+$/$CD5^+$ and $CD5^+$/ $CXCR4^-$ populations of unstimulated and BCR stimulated CLL cells that were either left untreated or were treated with Ibrutinib and Idelalisib.

With respect to pS6 (Figure 4.16), antibody reactivity with unstimulated cells was low across all subpopulations regardless of treatment. BCR crosslinking resulted in increased pS6 antibody reactivity across all populations, but $CXCR4^+$/$CD5^+$ and $CD5^+$/ $CXCR4^-$ cells seemed to show a greater increase than was observed in $CXCR4^-$/$CD5^-$ and $CXCR4^+$ /$CD5^-$ populations. CLL treatment with Ibrutinib resulted in a reduction in BCR-induced pS6 reactivity across all populations, a reduction that was more profound if CLL cells had been treated with Idelalisib. These results are in keeping with the ability of idelalisib to inhibit the PI3K pathway. Interestingly, select nodes within the $CXCR4^+$/$CD5^+$ and $CD5^+$/ $CXCR4^-$ populations showed an ability to respond to BCR crosslinking despite the presence of idelalisib, an observation that was as clearly visible in $CXCR4^-$/$CD5^-$ and $CXCR4^+$ /$CD5^-$ populations. This suggests the presence of particular subclones of CLL cells that are at least partially resistant to the idelalisib.

In a similar way pPLC$\gamma$2 levels also increased in BCR-stimulated CLL cells, where it seemed that $CXCR4^+$/$CD5^+$ and $CD5^+$/ $CXCR4^-$ populations show a greater increase than that in $CXCR4^-$/$CD5^-$ and $CXCR4^+$ /$CD5^-$ populations (Figure 4.17). However, in contrast to pS6, pPLC$\gamma$2 reactivity was more distinctly affected by ibrutinib treatment. pPLC$\gamma$2 reactivity was also affected by idelalisib treatment, but the level of inhibition was not as great as what was observed with ibrutinib. It is important to note here that select nodes within the $CXCR4^+$/$CD5^+$ and $CD5^+$/ $CXCR4^-$ populations showed an ability to respond to BCR crosslinking despite the presence of ibrutinib, again

suggesting the presence of subclones of CLL cells able to resist the effects of this kinase inhibitor.

Although pTyrosine antibody reactivity was induced by BCR stimulation (Figure 4.18), neither idelalisib nor ibrutinib treatment seemed to affect this induction. No increase was observed for pERK (Figure 4.19) and pATK (Figure 4.20) reactivity in BCR stimulated CLL cells. In my experiments it is likely that the pERK and pATK antibodies did not work as they had in previous experiments.

Taken together, these results support the main aim of this thesis that mass cytometry can be used to identify and observe different CLL cell subclones and their response to stimulation and different kinase inhibitors.

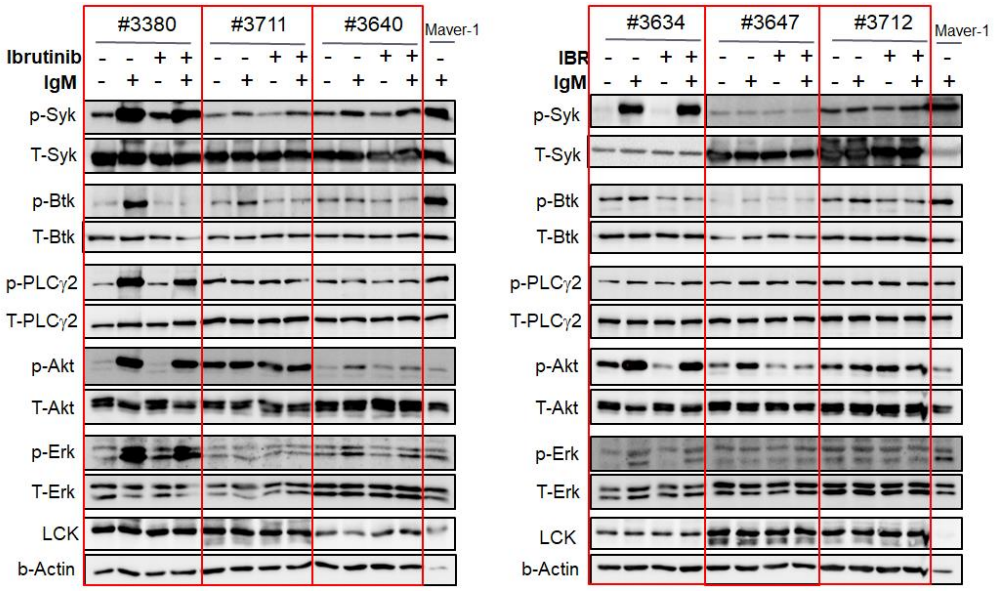


**Figure 4. 15 Comparative of phosphoproteins in different CLL patients by western blot analysis.** Cells were treated with F(ab')$_2$ IgM antibody at a concentration of 20ug/mL for 5 minutes with cell concentration and ibrutinib 200nM for one hour at 37°C .10µg of cellular lysate from each condition were separated by SDS-PAGE using a 10% polyacrylamide gel and transferred to PVDF membranes. The membrane was probed with different phosphoprotein with 1:2000 dilution with 5 % BSA overnight at 4ºC.Total phospho were probed for 2 hour 1:3000 dilution with 5 % BSA at room temperature for loading control. The image was captured by using enhanced chemiluminescence (ECL).

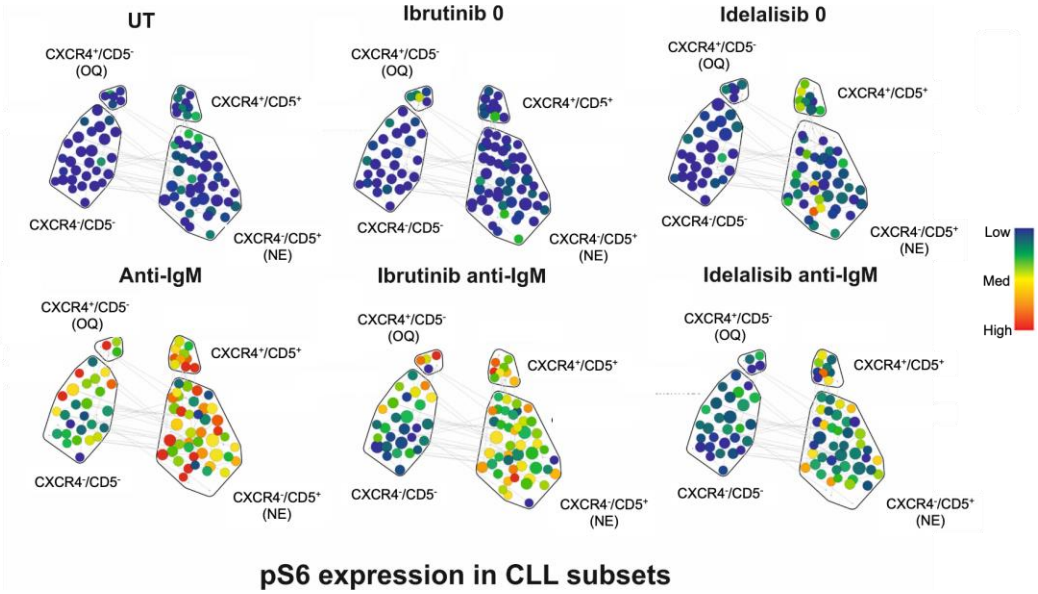


**Figure 4. 16 Unsupervised clustering of pS6 phosphoprotein expression in CLL subpopulations using SPADE tool in different conditions.** pS6 phosphoprotein expression in 4 CLL subpopulation. The CLL subpopulation are divided into unstimulated, stimulated with anti-IgM (15 mins), ibrutinib (200nM) and Idelalisib (1μM) with and without anti-IgM stimulation.

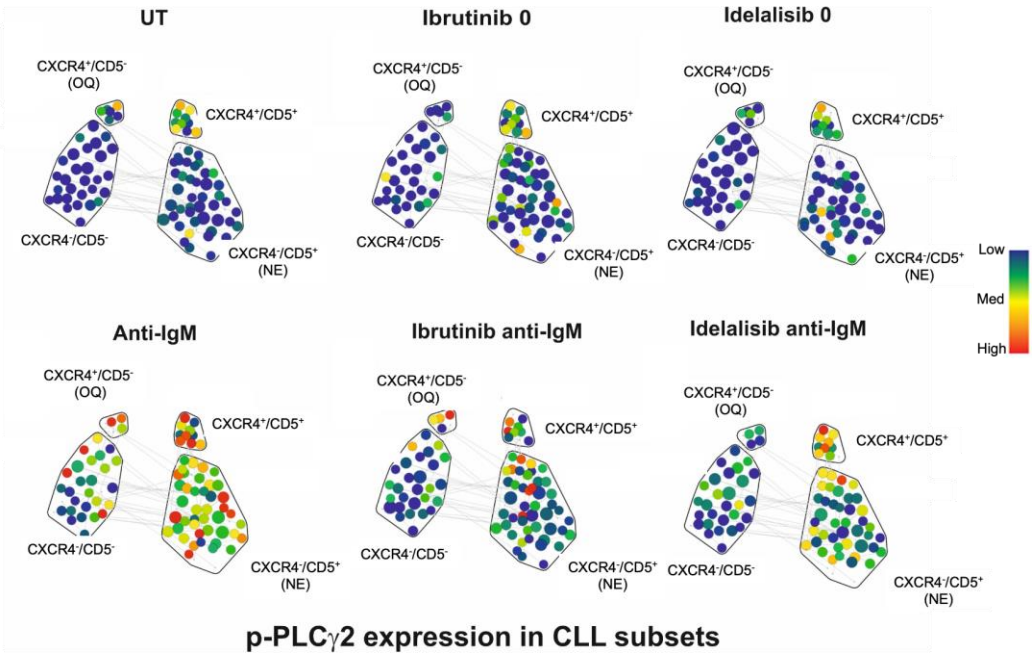


**Figure 4. 17 Unsupervised clustering of pPLCγ2 phosphoprotein expression in CLL subpopulations using SPADE tool in different conditions.** pPLCγ2 phosphoprotein expression in 4 CLL subpopulation. The CLL subpopulation are divided into unstimulated, stimulated with anti-IgM (15 mins), ibrutinib (200nM) and Idelalisib (1μM) with and without anti-IgM stimulation.

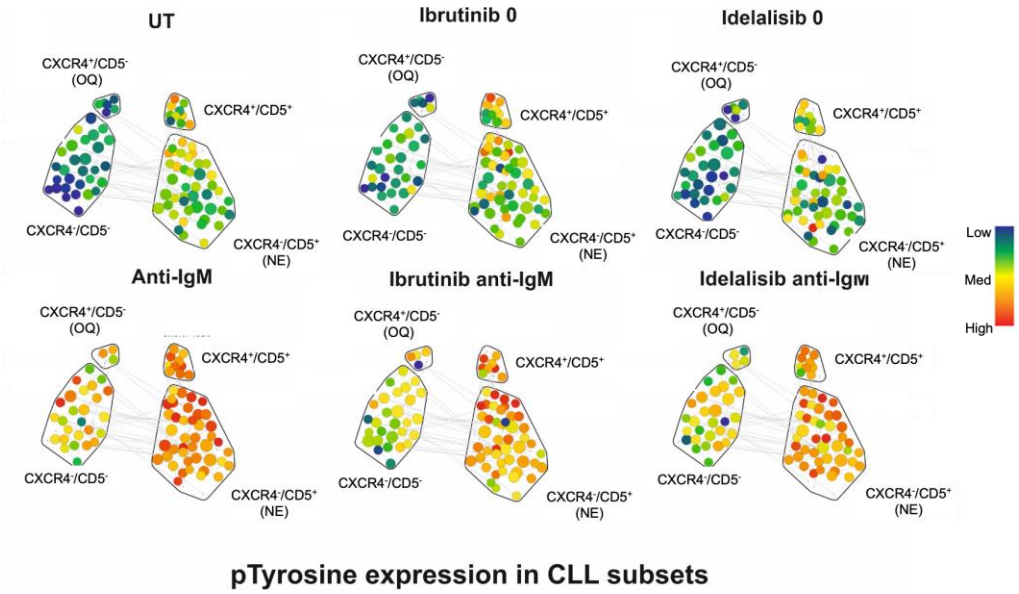


**Figure 4. 18 Unsupervised clustering of pTyrosine phosphoprotein expression in CLL subpopulations using SPADE tool in different conditions.** pTyrosine phosphoprotein expression in 4 CLL subpopulation. The CLL subpopulation are divided into unstimulated, stimulated with anti-IgM (15 mins), ibrutinib (200nM) and Idelalisib (1μM) with and without anti-IgM stimulation.

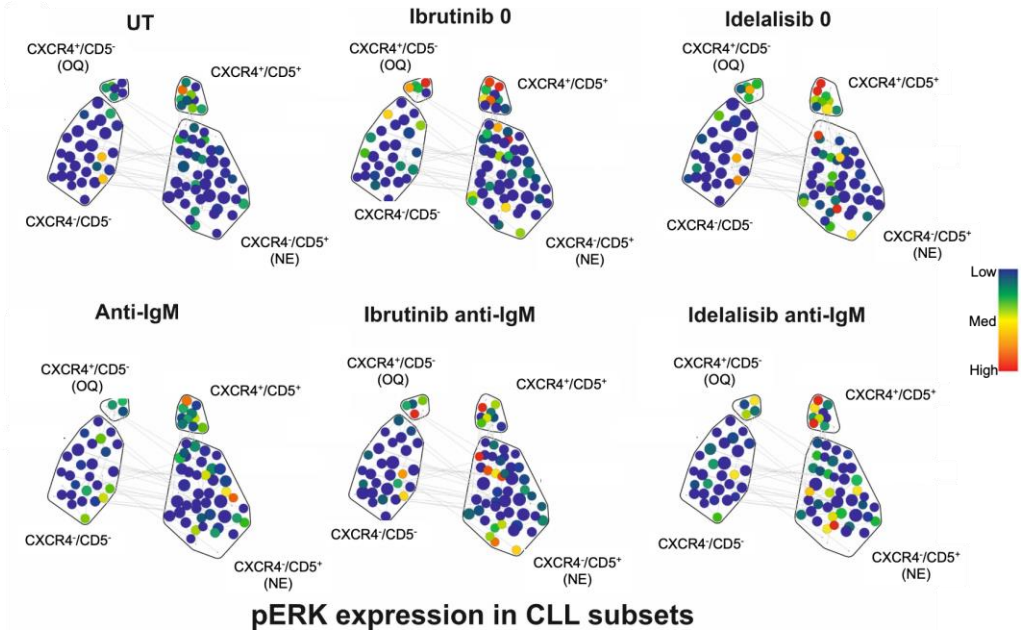


**Figure 4. 19 Unsupervised clustering of pERK phosphoprotein expression in CLL subpopulations using SPADE tool in different conditions.** pERK phosphoprotein expression in 4 CLL subpopulation. The CLL subpopulation are divided into unstimulated, stimulated with anti-IgM (15 mins), ibrutinib (200nM) and Idelalisib (1μM) with and without anti-IgM stimulation.

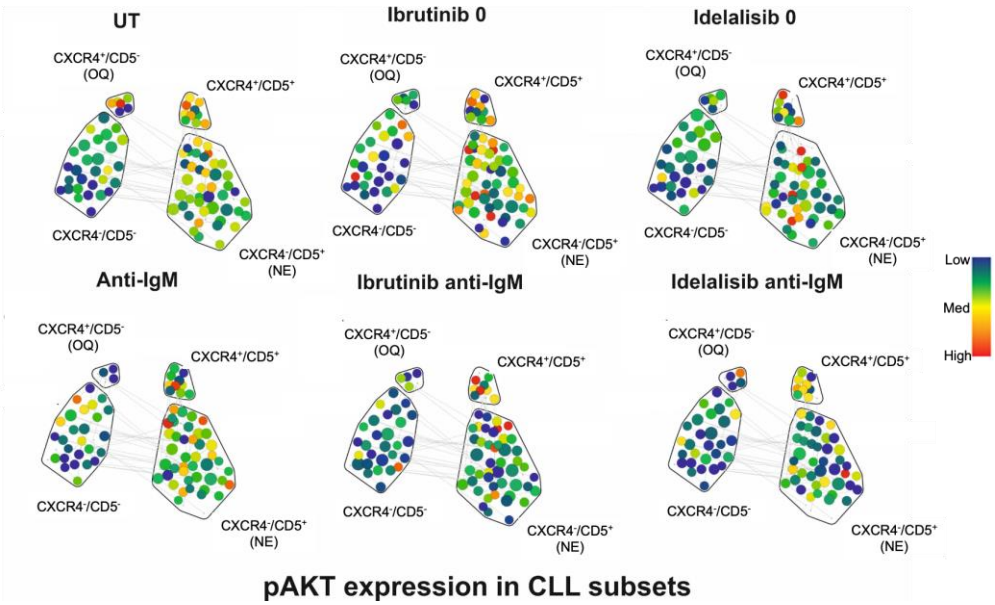


**Figure 4. 20 Unsupervised clustering of pAKT phosphoprotein expression in CLL subpopulations using SPADE tool in different conditions.** pAKT phosphoprotein expression in 4 CLL subpopulation. The CLL subpopulation are divided into unstimulated, stimulated with anti-IgM (15 mins), ibrutinib (200nM) and Idelalisib (1μM) with and without anti-IgM stimulation.

### 4.3 Discussion

Novel techniques have applied a clear knowledge to CLL pathobiology to understand the heterogeneity of this disease. CLL biology depends on its microenvironment where it promotes continuous survival and proliferation [121]. This is due to continuous BCR signaling and chemokine receptors, CXCR4-CXCL12 that facilitate cells migration from the periphery into lymphoid organs to create a favourable survival microenvironment [65].

The aim of this chapter was to investigate the measurement of B cell receptor signaling in CLL and normal PBMC cells using mass cytometry. I use two methods to interrogate signaling; SH2 profiling and antibodies to detect phospho-proteins. I found that SH2 profiling can be used but was unsatisfactory within the confines of this thesis because of sensitivity. Use of phospho-specific antibodies yielded better results, and when combined with antibodies recognising antigen-defined phenotype, yielded information on signaling within different subpopulations of normal B cells and CLL cells.

I began this chapter with development of the SH2 profiling assay. This involved using purified SH2 domains of PI3KR1, GRB2, SRC and NCK2, coupling to heavy metals and using streptavidin to create quaternary structures that enhance the binding of these domains to their phospho-tyrosine targets within proteins. In a cell line model, my results show that the PI3KR1 SH2 domain seems to be useful to detect signaling. Far-Western blot analysis detected a band of approximately 150kDa that was not there when cells were treated with dasatinib. K562 cells are derived from a patient suffering from chronic myeloid leukaemia and are positive for the reciprocal translocation t(9;22)(q34;q11) yielding expression of the BCR-ABL oncogene[170]. Class Ia PI3K isoforms bind to phosphotyrosine motifs within activated receptor tyrosine kinases and other proteins via tandem a SH2 domains within their p85 subunit [171]. PI3K is

constitutively activated by BCR-ABL+ cells such as K562 [172, 173] possibly mediated by direct interaction with BCR-ABL or other intermediary proteins such as Gab2, it is likely that this is what the PI3KR1 SH2 domain recognises in the Far-Western blots[174]. The PI3KR1 SH2 domain also showed specific reactivity in assays using mass cytometry, suggesting that this could be used to assess signaling in cells as is proposed by Peter Nollau who has described application of oligonucleotide-tagged SH2 profiling (using PI3K and other SH2 domains) to the analysis of signaling in cells [106]. In contrast to the PI3KR1 SH2 domain, the other reagents, SH2 domains of GRB2, SRC and NCK2 were not as sensitive or specific in the mass cytometry assay as shown in Figure 4.6, suggesting a severe limitation to this approach and supporting the decision to not follow this line of research further.

The second approach for signal pathway interrogation in this thesis was the use of phospho-specific antibodies. This approach has been widely used to measure BCR signaling in many cell types, including primary CLL cells, and is considered a hallmark to understand the complexity of CLL biology and behaviour. Phospho-specific antibodies are useful in flow cytometry and western blot applications, and I use these applications in this thesis for cross validation of these techniques. These applications produced largely similar results, and are in agreement with studies performed by Krutzik *et al* [6] where comparison between flow cytometry with traditional Western blotting showed that both were comparable, but that flow cytometry was better because of the increased number of parameters that could be investigated on a simultaneous basis.

However, I found there were differences. The antibodies I used in Western blot were not always effective in mass cytometry. One example in Figure 4.7, is $pS^{473}$-AKT, this antibody works extremely well in Western blot where it easily detects activated AKT in

both Maver-1 and primary CLL cells. However, this antibody weakly detected activated AKT by mass cytometry, and reliably only in Maver-1 cells, because idelalisib treatment of CLL cells failed to affect baseline and BCR-stimulated $pS^{473}$-AKT levels detected by mass cytometry despite inhibiting induction of this epitope as measured by Western blot. This observation is similar to that made by Blix *et al* [102] who used $pS^{473}$-AKT antibodies to measure active AKT in CLL cells and found only very weak reactivity. The difference between CLL and Maver-1 cells in terms of this reliability could be dependent on cell size, Maver-1 cells are larger than CLL cells. Added to this is copy number of AKT itself within cells, it has been estimated that the cytoplasmic concentration of this kinase is a third of the concentration of ERK and a tenth the concentration of S6 [175]. Nevertheless, mass cytometry can be used to measure signaling in cells.

The real power of mass cytometry is the ability to measure signaling in single cells, or in cell subpopulations, without first purifying the cells. Thus, I was able to combine a panel of 13 surface markers together with 7 intracellular markers for a total of 20 parameters of measurement. This is a distinct advantage over the conventional flow cytometry technologies I had available (Becton Dickinson LSR Fortessa) where maximal number of parameters available is limited to 18. Conventional flow cytometry is also complicated by the need to perform compensation for each fluorochrome because of spectral overlap. With mass cytometry this problem is largely overcome by using highly purified isotopes so that spillover on to other measurement channels is minimized. I used my panel of antibodies to measure BCR signaling in subpopulations of healthy B cells and in CLL cells. I found that a common feature of the response of these cells to BCR engagement is the relationship between signaling intensity and surface expression of BCR. This finding agrees with those of others, and, in particular,

studies of CLL where surface IgM expression is linked to induction of $Ca^{2+}$ flux and disease prognosis[164]. The advantage of my study is the ability to investigate this relationship in different subpopulations of cells from a single patient. I found that signaling seemed more intense in memory B than in naïve B cells where pS6, pPLCγ2 and pTyrosine all seemed to be more strongly induced according to higher levels of surface IgM expression. My results in Figure 4.9 show that this induction was specific for surface IgM-expressing cells, because memory B cells negative for this epitope and T cells showed no change in the levels of these markers.

In a similar way, I could also investigate the response of different subpopulations of CLL cells to BCR engagement. The subpopulations I investigated were defined by expression of CXCR4 and CD5, which describes CLL cells that are either newly emerged or older quiescent according to the paradigm set by Calissano *et al* [38] . I found within these subpopulations that higher basal levels of pS6, PLCγ2, pTyrosine, pERK and pAKT were observed in the $CXCR4^{+}/CD5^{+}$ and $CXCR4^{-}/CD5^{+}$ (NE) cells. This observation is in agreement with those reported by Blix et al. where p-SFKs, p-PLCγ2, p-ERK, p-p38, p-p65 (NF-κB), p-STAT5 and p-STAT6 levels were investigated within whole populations of CLL and SLL cells [102]. However, in my study I am able to bring in extra dimension to this understanding, by being able to differentiate between subclones of CLL cells, findings that are largely in agreement with those reported in an abstract published by Damle *et al*, showing similar high levels of pAkt, pErk, p38MAPK and pSyk in the same subclone[143]. The results I reported in Chapter 3 show that $CXCR4^{+}/CD5^{+}$ and $CXCR4^{-}/CD5^{+}$ (NE) CLL cells express higher levels of surface IgM than do $CXCR4^{-}/CD5^{-}$ and $CXCR4^{+}/CD5^{-}$ (OQ) cells, and it can be expected that the former subpopulations of CLL cells respond better to BCR crosslinking. Unfortunately, direct measurement of surface IgM in BCR-stimulated CLL

cells was not easy to perform within the experiments listed in this thesis. I used 2 different approaches to attempt this; one using a FITC-conjugated anti-IgM antibody where a second layer heavy metal-conjugated anti-FITC antibody was used to detect the first, and a second approach where I directly conjugated heavy metals to the anti-IgM antibody. While both approaches yielded results, further optimisation is required before a full interpretation can be attempted.

My ability to measure BCR signaling in different subclones of CLL cells allowed investigation of the effect different BCR pathway inhibitors have on these subclones. I treated the cells from a single CLL case with ibrutinib and idelalisib, respectively inhibitors of BTK and PI3K$\delta$, and looked see whether all cells were affected equally, or there was subclonal variation. I know that these inhibitors were effective in my experiments from the Western blot analysis I performed, and to a certain extent within the mass cytometry experiments. In particular I could only observe effects of these inhibitors on induced pS6 levels (idelalisib) and pPLC$\gamma$2 levels (ibrutinib) in Figure 4.16 and Figure 4.17. pERK and pAKT were not working as expected and I could not see change in the levels of these epitopes between BCR-stimulated and/or inhibitor treated cells. Nevertheless, mass cytometry appeared to identify subclones of CLL cells that did respond to BCR crosslinking despite the presence of ibrutinib and idelalisib, indicating a potential to detect inhibitor-resistant clones. With further optimisation, such a goal might be achievable.

In conclusion, Mass cytometry allows in-depth characterisation of normal and CLL B cells, allowing simultaneous investigation of phenotype and signaling within these cells. The limitations are availability of antibodies to detect intracellular signaling, future studies focussing on this aspect could possibly employ a range of reagents that include SH2 domain detection of phosphorylated tyrosine motifs and phospho-specific

antibodies. The power of these studies is in the resolution that is achievable. I employed a panel of 20 antibodies to perform these studies. This panel can easily be expanded and include additional technologies such as proximity ligation assay for RNA (PLAYR) to detect signal-induced gene transcription [176]. My results from this chapter show that different normal and CLL B cell populations respond to BCR engagement in a way that is dependent upon individual cell expression of surface immunoglobulin (in this case sIgM). This potentially has ramifications in the way KI inhibitors, such as ibrutinib, affect BCR signaling in CLL cells because I was able to detect small populations of cells which appeared resistant to the effects of this drug. In total, mass cytometry will be a useful tool to understand clonal evolution in CLL.

# Chapter 5: Main Discussion

In this thesis the main aim was to use mass cytometry to study the role of B cell receptor signaling in subsets of normal B cells and CLL cells. Up until now there are no studies that directly compare BCR signaling between naïve and memory B cells, and only a few which investigate intraclonal response of CLL cells to BCR engagement [38, 164]. My thesis sets a foundation upon which further studies can be based. This will be important for understanding known clonal heterogeneity of the malignant cells of CLL, and potentially give insight into clonal evolution during disease resistance to therapy, a phenomenon that has only been studied at the genetic level [177]. Thus, on a broad basis, the work of my thesis is applicable to the study of clonal evolution in CLL and other cancers as it applies to the phenotype of the malignant cells.

CLL is an incurable disease that when treated goes through cycles of remission and relapse. At the beginning of this thesis typical frontline therapy relied on chemoimmunotherapy, and new second line therapies that target the BCR signaling pathway, ibrutinib and idelalisib. However, disease resistance to these new therapies was observed, and it was noted that patients who developed resistance did so through clonal evolution of cells bearing mutation within the target kinases of these inhibitors (particularly ibrutinib)[178]. It seemed logical that ibrutinib-resistant clones would maintain BCR signaling and that these clones should be visible within whole populations of CLL cells.

To understand CLL subclone characterisation and the reason of selective resistant CLL subclones that can result from an outgrowth of more aggressive genetic characterisation by understanding first the CLL life cycle that occurs in the peripheral blood and lymphoid organs. CLL cells are characterised by expression of multiple

chemokine receptors that include CXCR4 and CXCR5 [179]. In CLL, CXCR4 binds to CXCL12 that is essential and is produced in mesenchymal stromal cells and bone marrow [180, 181]. The combination of CXCR4/CXCL12 chemokine interaction allows cells to migrate from the peripheral blood into the lymphoid organs to maintain survival and sustaining viability within the lymph node or less viable cells undergo apoptosis. This showed changes of surface phenotype of CXCR4/CD5 within the total clone of B cells that were further divided into older quiescent cells (OQ) $CXCR4^{bright}$/CD5dim or newly emerged cells (NE), $CXCR4^{dim}/CD5^{bright}$ [38]. Each fraction of CLL subclone have been investigated to understand the immunophenotype expression and internal BCR pathway expression to analyse intraclonal heterogeneity in CLL biology.

To build the tools to investigate this I designed an antibody panel that could discriminate CLL B cell subsets based on the expression of CXCR4 and CD5. Here I could distinguish 4 different subpopulations; $CXCR4^-/CD5^-$, $CXCR4^+$ $/CD5^-$ (OQ cells as characterised by [38]), $CXCR4^+/CD5^+$ and $CD5^+$/ $CXCR4^-$ (NE cells). I found that the CLL B cell subpopulations that were $CXCR4^+/CD5^+$ and $CD5^+$/ $CXCR4^-$ (NE cells) seemed to express higher levels of other surface markers compared to the whole population. This led to the results I report in Chapter 4 where BCR signaling in these CLL B subpopulations is investigated. I used phospho-specific antibodies to measure BCR signaling and found that the CXCR4+/CD5+ and CD5+/ CXCR4- (NE cells) CLL subclones show higher induction of pERK, pPLC$\gamma$2, pS6, and pTyrosine after surface IgM crosslinking. This result agrees with existing studies [143] and confirms that mass cytometry can be used as a tool to investigate intraclonal heterogeneity of BCR-mediated signal transduction in populations of CLL cells. Further investigation of the effects of ibrutinib on BCR signaling in CLL cells showed most clones are affected by this inhibitor, but a small of proportion of cells appear to suppress the ability to induce

pS6 and pPLCγ2 in response to BCR crosslinking. This experiment suggests that mass cytometry can be used to identify ibrutinib-resistant clones of CLL, however, because not all the antibodies worked reproducibly this will require further work and optimisation for a firmer conclusion to be made.

In my thesis, the analysis on OQ/NE CLL cells, I have done on frozen samples I identified a range of novel features where each CLL case has shown heterogeneity in some cases that have indolent course of disease and shows insensitive to IgM BCR stimulation. This clonal anergy can as well be the main contributor to not respond to full inhibition to ibrutinib and idelalisib as shown in Figure 4.16-20, where some CLL subclones have not achieved total treatment of CLL subclones that are resistant and shows that BCR signalling inhibitors can control the disease and not fully affect all CLL cells that can lead to relapse of patients. This explains clonal outgrowth in developed mutations in PLCγ2 and BTK after treatment of Ibrutinib and emerged into clonal evolution. However, CLL patient's stratification is based on clinical characterisation to identify genetic abnormalities, IGHV mutational status and karyotypic abnormalities leading to clinical trials in the near future for therapeutic targeting of CLL clones to prevent subclone development.

I also investigated BCR signaling in populations of normal B cells. Mass cytometry is clearly an excellent tool to characterise B cell populations, and I was able to distinguish between naïve and memory B cells. One goal of the thesis was to identify normal CD5+ B cells, however, this was not satisfactorily achieved because the numbers of these cells in peripheral blood is less than 1%, which the results I generated agree with. For further study of this population, particularly with respect to signaling properties, I would have needed to purify B cells from peripheral blood in order to enhance my ability to analyse them. Nevertheless, I did investigate response of naïve

and memory B cells to BCR engagement. I found that IgM+ memory B cells induce greater levels of pS6, pPLCγ2 and pTyrosine than do naïve B cells, indicating that mass cytometry can be used to investigate this phenomenon in B cell populations, however, I was not able to study the effects of ibrutinib on these subsets owing to time and reagent constraints. Taken together with the results I generated using primary CLL cells, these results confirm that mass cytometry is a useful tool for interrogating populations of malignant and normal B cells.

For the purpose of this thesis, I used phospho-specific antibodies to detect signal transduction in CLL cells. The results I generated were not optimal, potentially because of the detection limit associated with these reagents. Moreover, full appreciation of intracellular signaling was not achieved because of the limiting number of phospho-specific antibodies that are available. I attempted to create new tools for the study of signal transduction and employed the approach described by Dierck *et al*, where they used purified SH2 domains to measure cellular signaling. I conjugated SH2 domains from PI3KR1, GRB2, NCK and SRC to lanthanide mass tags. I found that although the conjugation method did not affect the binding of these reagents to phospho-tyrosine containing proteins by Western blot analysis, only 2 of the 4 SH2 domains seemed to work by mass cytometry, PI3KR1 and GRB2. However, the signal was weak, and I felt that better results would be generated using phospho-specific antibodies. Further work will need to be performed with this technique in order to optimise it for application in mass cytometry.

My work using mass cytometry to study CLL and normal B cells provides a pathway with which to understand the physiology of disease. Further development of this technology, such as application of lanthanide labelled SH2 domains to study signal transduction, could lead to increased understanding of signaling in CLL subclones

yielding insight to their heterogeneity and expansion during therapy. Additional tools, such as detection of mRNA species can also be achieved, and although not a part of this thesis, I was involved in the development of an adaptation of an *in-situ* hybridization (ISH) approach that uses transcript-specific oligonucleotide sequences within a rolling circle amplification, called **P**roximal **L**igation **A**ssa**y** for **R**NA (PLAYR), to detect specific mRNA transcripts [176]. In particular, PLAYR was optimised for use in combination with antibodies for surface phenotype determination, allowing for single cell analysis of gene expression within whole populations of cells. The PLAYR protocol developed uses detector oligonucleotides that are conjugated with heavy metal mass tags, and we were able to detect 27 different mRNA species in primary CLL cells and a mantle cell lymphoma cell line. Figure 5.1 shows how the PLAYR assay works within a single cell. This developed tool, together with surface Ag analysis, allows to investigation of BCR-induced expression of prognostic genes within CLL subclones. This technology can now be applied to the analysis of other cell types in other physiological and pathological situations to provide insight into disease.

In conclusion, I have demonstrated in this thesis that mass cytometry (CyTOF-3) can be used to characterise B cell subpopulations in peripheral blood from normal individuals and patients with CLL. I show that this technique can be used to measure BCR expression and relate this to signaling intensity in single cells, and demonstrate that normal B cells, (IgM memory, IgM naïve, class switch IgM) differentially respond to BCR engagement and that different CLL subclones do the same. Finally, my results suggest that mass cytometry can be used to understand how CLL cell subclones respond to therapies such as ibrutinib, potentially providing understanding of clonal evolution as a mechanism of disease resistance. My work therefore shows that mass

cytometry will be a particularly useful tool for future studies, such as looking at blood cells in CLL.

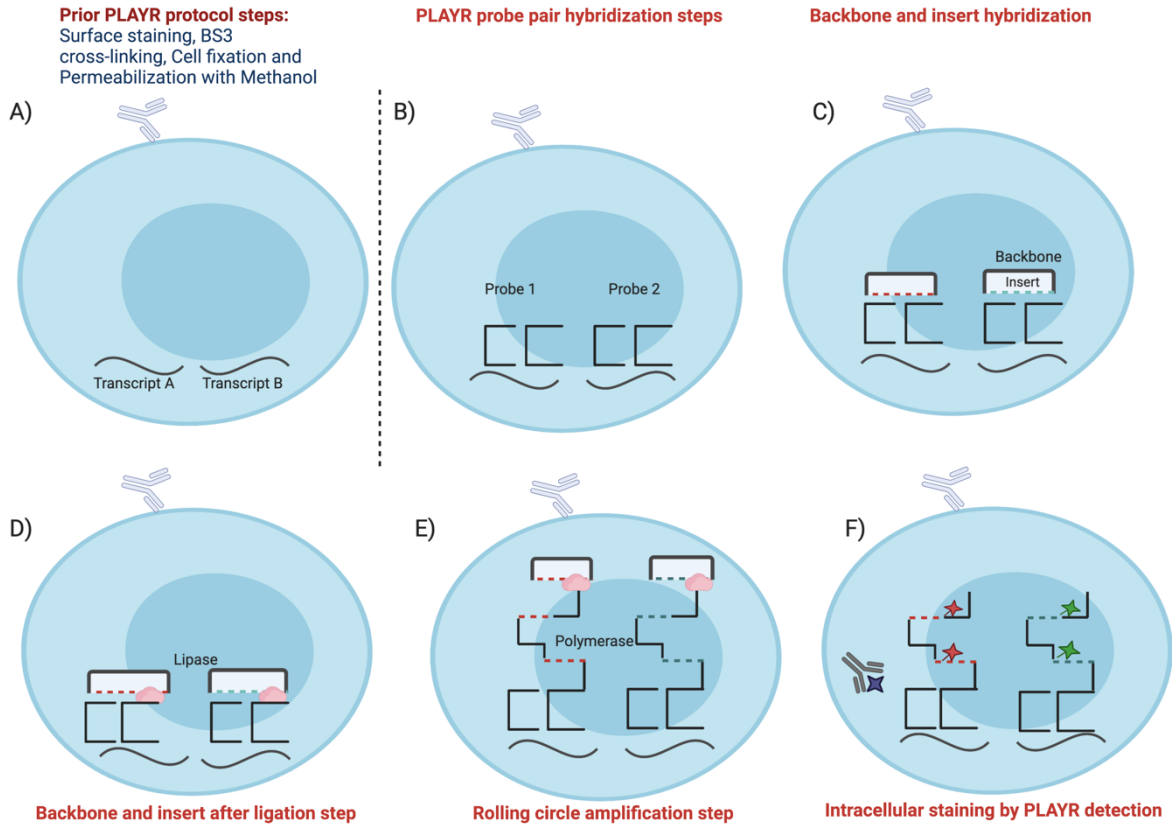


**Figure 5. 1 PLAYR assay steps representation diagram. A.)** At the beginning of the PLAYR assay, several steps should follow as an initial stages prior the assay. Staining cells with surface antibodies followed with BS3 cross-linker a chemical agent that crosslinks cells by covalently binding to cells that helps them to attach into the surface antibodies.This is then followed up by cell fixation with paraformaldehyde and cells are ready to be permeabilized with methanol and can be stored in -80ºC. This step does not affect the RNA integrity and surface antibodies. **B.)** PLAYR probe pairs are enhanced for proximal hybridization to cognate transcripts. **C.)** Backbone and insert region contains oligonucleotides that form a circle for hybridization to form single stranded DNA to bind to the transcripts. **D.)** Backbone and insert region containing oligonucleotides are ligated with lipase. **E.)** Polymerization starts by rolling circle amplification of the DNA circle. **F.)** PLAYR detection of the labelled oligonucleotides intracellular staining that were bonded to the insert regions. This figure was created by Biorender.com [176].

# References


1. Marjanovic, N.D., R.A. Weinberg, and C.L. Chaffer, *Cell plasticity and heterogeneity in cancer.* Clinical chemistry, 2013. **59**(1): p. 168-179.
2. Guo, M., et al., *Epigenetic heterogeneity in cancer.* Biomarker research, 2019. **7**: p. 23-23.
3. Turajlic, S., et al., *Resolving genetic heterogeneity in cancer.* Nature Reviews Genetics, 2019. **20**(7): p. 404-416.
4. Hientz, K., et al., *The role of p53 in cancer drug resistance and targeted chemotherapy.* Oncotarget, 2017. **8**(5): p. 8921-8946.
5. Gutierrez, C. and C.J. Wu, *Clonal dynamics in chronic lymphocytic leukemia.* Blood advances, 2019. **3**(22): p. 3759-3769.
6. Krutzik, P.O., et al., *Analysis of protein phosphorylation and cellular signaling events by flow cytometry: techniques and clinical applications.* Clin Immunol, 2004. **110**(3): p. 206-21.
7. Lucas, J.S., et al., *Chapter 1 - The Structure and Regulation of the Immunoglobulin Loci*, in *Molecular Biology of B Cells (Second Edition)*, F.W. Alt, et al., Editors. 2015, Academic Press: London. p. 1-11.
8. Nussenzweig, M.C. and F.W. Alt, *Antibody diversity: one enzyme to rule them all.* Nature Medicine, 2004. **10**: p. 1304.
9. Hoffbrand, A.V. and D.P. Steensma, *Hoffbrand's essential haematology*. 2019: John Wiley & Sons.
10. Rothenberg, E.V., *Transcriptional control of early T and B cell developmental choices.* Annual review of immunology, 2014. **32**: p. 283-321.
11. Blom, B. and H. Spits, *Development of human lymphoid cells.* Annu. Rev. Immunol., 2006. **24**: p. 287-320.
12. Melchers, F., *Checkpoints that control B cell development.* The Journal of clinical investigation, 2015. **125**(6): p. 2203-2210.
13. Rolink, A.G., J. Andersson, and F. Melchers, *Molecular mechanisms guiding late stages of B-cell development.* Immunological Reviews, 2004. **197**(1): p. 41-50.
14. Early, P., et al., *An immunoglobulin heavy chain variable region gene is generated from three segments of DNA: VH, D and JH.* Cell, 1980. **19**(4): p. 981-92.
15. Ikawa, T., et al., *Long-Term Cultured E2A-Deficient Hematopoietic Progenitor Cells Are Pluripotent.* Immunity, 2004. **20**(3): p. 349-360.
16. Osmond, D.G., A. Rolink, and F. Melchers, *Murine B lymphopoiesis: towards a unified model.* Immunology Today, 1998. **19**(2): p. 65-68.
17. Hardy, R.R., et al., *Resolution and characterization of pro-B and pre-pro-B cell stages in normal mouse bone marrow.* The Journal of Experimental Medicine, 1991. **173**(5): p. 1213-1225.
18. Grawunder, U., et al., *Down-regulation of RAG1 and RAG2 gene expression in PreB cells after functional immunoglobulin heavy chain rearrangement.* Immunity, 1995. **3**(5): p. 601-608.
19. Rush, J.S., J. Hasbold, and P.D. Hodgkin, *Cross-linking surface Ig delays CD40 ligand- and IL-4-induced B cell Ig class switching and reveals evidence for independent regulation of B cell proliferation and differentiation.* J Immunol, 2002. **168**(6): p. 2676-82.

20. Pieper, K., B. Grimbacher, and H. Eibel, *B-cell biology and development.* J Allergy Clin Immunol, 2013. **131**(4): p. 959-71.
21. Baumgarth, N., *A Hard(y) Look at B-1 Cell Development and Function.* The Journal of Immunology, 2017. **199**(10): p. 3387.
22. Herzenberg, L.A. and A.B. Kantor, *B-cell lineages exist in the mouse.* Immunol Today, 1993. **14**(2): p. 79-83; discussion 88-90.
23. Ochsenbein, A.F., et al., *Control of Early Viral and Bacterial Distribution and Disease by Natural Antibodies.* Science, 1999. **286**(5447): p. 2156-2159.
24. Baumgarth, N., *The double life of a B-1 cell: self-reactivity selects for protective effector functions.* Nat Rev Immunol, 2011. **11**(1): p. 34-46.
25. Baumgarth, N., *Innate-Like B Cells and Their Rules of Engagement*, in *Crossroads Between Innate and Adaptive Immunity IV*, P.D. Katsikis, S.P. Schoenberger, and B. Pulendran, Editors. 2013, Springer New York: New York, NY. p. 57-66.
26. Baumgarth, N., *B-Cell Immunophenotyping*, in *Methods in Cell Biology*. 2004, Academic Press. p. 643-662.
27. Seifert, M., et al., *Cellular origin and pathophysiology of chronic lymphocytic leukemia.* The Journal of experimental medicine, 2012. **209**(12): p. 2183-2198.
28. Rothstein, T.L., et al., *Human B-1 cells take the stage.* Annals of the New York Academy of Sciences, 2013. **1285**(1): p. 97-114.
29. Griffin, D.O., N.E. Holodick, and T.L. Rothstein, *Human B1 cells are CD3-: A reply to "A human equivalent of mouse B-1 cells?" and "The nature of circulating CD27+CD43+ B cells".* The Journal of experimental medicine, 2011. **208**(13): p. 2566-2569.
30. Griffin, D.O. and T.L. Rothstein, *Human b1 cell frequency: isolation and analysis of human b1 cells.* Frontiers in immunology, 2012. **3**: p. 122-122.
31. Strati, P. and T.D. Shanafelt, *Monoclonal B-cell lymphocytosis and early-stage chronic lymphocytic leukemia: diagnosis, natural history, and risk stratification.* Blood, 2015. **126**(4): p. 454-462.
32. Kalpadakis, C., et al., *New insights into monoclonal B-cell lymphocytosis.* BioMed research international, 2014. **2014**: p. 258917-258917.
33. Darwiche, W., et al., *Chronic Lymphocytic Leukemia B-Cell Normal Cellular Counterpart: Clues From a Functional Perspective.* Frontiers in immunology, 2018. **9**: p. 683-683.
34. Duty, J.A., et al., *Functional anergy in a subpopulation of naive B cells from healthy humans that express autoreactive immunoglobulin receptors.* The Journal of experimental medicine, 2009. **206**(1): p. 139-151.
35. Quách, T.D., et al., *Anergic responses characterize a large fraction of human autoreactive naive B cells expressing low levels of surface IgM.* Journal of immunology (Baltimore, Md. : 1950), 2011. **186**(8): p. 4640-4648.
36. Nabhan, C. and S.T. Rosen, *Chronic lymphocytic leukemia: a clinical review.* Jama, 2014. **312**(21): p. 2265-2276.
37. Dighiero, G. and T. Hamblin, *Chronic lymphocytic leukaemia.* The Lancet, 2008. **371**(9617): p. 1017-1029.
38. Calissano, C., et al., *Intraclonal complexity in chronic lymphocytic leukemia: fractions enriched in recently born/divided and older/quiescent cells.* Mol Med, 2011. **17**(11-12): p. 1374-82.
39. Hallek, M., et al., *iwCLL guidelines for diagnosis, indications for treatment, response assessment, and supportive management of CLL.* Blood, 2018. **131**(25): p. 2745-2760.

40. Hamblin, T.J., et al., *Unmutated Ig V(H) genes are associated with a more aggressive form of chronic lymphocytic leukemia.* Blood, 1999. **94**(6): p. 1848-54.
41. Rosenwald, A., et al., *Relation of gene expression phenotype to immunoglobulin mutation genotype in B cell chronic lymphocytic leukemia.* Journal of Experimental Medicine, 2001. **194**(11): p. 1639-1648.
42. Crespo, M., et al., *ZAP-70 expression as a surrogate for immunoglobulin-variable-region mutations in chronic lymphocytic leukemia.* New England Journal of Medicine, 2003. **348**(18): p. 1764-1775.
43. Rassenti, L.Z., et al., *ZAP-70 compared with immunoglobulin heavy-chain gene mutation status as a predictor of disease progression in chronic lymphocytic leukemia.* New England Journal of Medicine, 2004. **351**(9): p. 893-901.
44. Ibrahim, S., et al., *CD38 expression as an important prognostic factor in B-cell chronic lymphocytic leukemia.* Blood, The Journal of the American Society of Hematology, 2001. **98**(1): p. 181-186.
45. Ghia, P., et al., *The pattern of CD38 expression defines a distinct subset of chronic lymphocytic leukemia (CLL) patients at risk of disease progression.* Blood, The Journal of the American Society of Hematology, 2003. **101**(4): p. 1262-1269.
46. Orchard, J.A., et al., *ZAP-70 expression and prognosis in chronic lymphocytic leukaemia.* Lancet, 2004. **363**(9403): p. 105-11.
47. Pepper, C., et al., *Defining the prognosis of early stage chronic lymphocytic leukaemia patients.* Br J Haematol, 2012. **156**(4): p. 499-507.
48. Stevenson, F.K., et al., *B-cell receptor signaling in chronic lymphocytic leukemia.* Blood, 2011. **118**(16): p. 4313-20.
49. Ten Hacken, E., et al., *The importance of B cell receptor isotypes and stereotypes in chronic lymphocytic leukemia.* Leukemia, 2019. **33**(2): p. 287-298.
50. Messmer, B.T., et al., *The pattern and distribution of immunoglobulin VH gene mutations in chronic lymphocytic leukemia B cells are consistent with the canonical somatic hypermutation process.* Blood, 2004. **103**(9): p. 3490-3495.
51. Chiorazzi, N., K.R. Rai, and M. Ferrarini, *Chronic lymphocytic leukemia.* New England Journal of Medicine, 2005. **352**(8): p. 804-815.
52. Radaev, S., et al., *Structural and functional studies of Igalphabeta and its assembly with the B cell antigen receptor.* Structure (London, England : 1993), 2010. **18**(8): p. 934-943.
53. Slupsky, J.R., *Does B cell receptor signaling in chronic lymphocytic leukaemia cells differ from that in other B cell types?* Scientifica, 2014. **2014**: p. 208928-208928.
54. Yao, X., et al., *Immunoreceptor tyrosine-based activation motif is required to signal pathways of receptor-mediated growth arrest and apoptosis in murine B lymphoma cells.* The Journal of Immunology, 1995. **155**(2): p. 652-661.
55. Tedder, T.F., L.-J. Zhou, and P. Engel, *The CD19/CD21 signal transduction complex of B lymphocytes.* Immunology today, 1994. **15**(9): p. 437-442.
56. Pleiman, C.M., W.M. Hertz, and J.C. Cambier, *Activation of phosphatidylinositol-3'kinase by Src-family kinase SH3 binding to the p85 subunit.* Science, 1994. **263**(5153): p. 1609-1612.
57. Werner, M., E. Hobeika, and H. Jumaa, *Role of PI3K in the generation and survival of B cells.* Immunological reviews, 2010. **237**(1): p. 55-71.
58. Packham, G., et al., *The outcome of B-cell receptor signaling in chronic lymphocytic leukemia: proliferation or anergy.* Haematologica, 2014. **99**(7): p. 1138.

59. Knies, N., et al., *Lymphomagenic CARD11/BCL10/MALT1 signaling drives malignant B-cell proliferation via cooperative NF-κB and JNK activation.* Proceedings of the National Academy of Sciences, 2015. **112**(52): p. E7230-E7238.
60. Das, J., et al., *Digital signaling and hysteresis characterize ras activation in lymphoid cells.* Cell, 2009. **136**(2): p. 337-351.
61. Datta, S.R., et al., *Akt Phosphorylation of BAD Couples Survival Signals to the Cell-Intrinsic Death Machinery.* Cell, 1997. **91**(2): p. 231-241.
62. Wiestner, A., *The role of B-cell receptor inhibitors in the treatment of patients with chronic lymphocytic leukemia.* Haematologica, 2015. **100**(12): p. 1495.
63. Burger, J.A., et al., *Clonal evolution in patients with chronic lymphocytic leukaemia developing resistance to BTK inhibition.* Nature communications, 2016. **7**(1): p. 1-13.
64. Aguilar-Hernandez, M.M., et al., *IL-4 enhances expression and function of surface IgM in CLL cells.* Blood, 2016. **127**(24): p. 3015-25.
65. Burger, J.A., *Nurture versus nature: the microenvironment in chronic lymphocytic leukemia.* Hematology 2010, the American Society of Hematology Education Program Book, 2011. **2011**(1): p. 96-103.
66. Herishanu, Y., et al., *The lymph node microenvironment promotes B-cell receptor signaling, NF-κB activation, and tumor proliferation in chronic lymphocytic leukemia.* Blood, 2011. **117**(2): p. 563-574.
67. Landau, D.A., et al., *Evolution and impact of subclonal mutations in chronic lymphocytic leukemia.* Cell, 2013. **152**(4): p. 714-726.
68. Messmer, B.T., et al., *In vivo measurements document the dynamic cellular kinetics of chronic lymphocytic leukemia B cells.* J Clin Invest, 2005. **115**(3): p. 755-64.
69. Haselager, M.V., A.P. Kater, and E. Eldering, *Proliferative Signals in Chronic Lymphocytic Leukemia; What Are We Missing?* Frontiers in oncology, 2020. **10**: p. 592205-592205.
70. Oppezzo, P. and G. Dighiero, *"Role of the B-cell receptor and the microenvironment in chronic lymphocytic leukemia''.* Blood Cancer Journal, 2013. **3**(9): p. e149-e149.
71. Stetler-Stevenson, M. and C.M. Yuan, *Flow cytometry*, in *Diagnostic Techniques in Hematological Malignancies*, W.N. Erber, Editor. 2010, Cambridge University Press: Cambridge. p. 51-70.
72. Szalóki, G. and K. Goda, *Compensation in multicolor flow cytometry.* Cytometry Part A, 2015. **87**(11): p. 982-985.
73. Spitzer, M.H. and G.P. Nolan, *Mass Cytometry: Single Cells, Many Features.* Cell, 2016. **165**(4): p. 780-791.
74. Haas, K.L. and K.J. Franz, *Application of metal coordination chemistry to explore and manipulate cell biology.* Chemical reviews, 2009. **109**(10): p. 4921-4960.
75. Han, G., et al., *Metal-isotope-tagged monoclonal antibodies for high-dimensional mass cytometry.* Nature Protocols, 2018. **13**(10): p. 2121-2148.
76. Majonis, D., et al., *Curious results with palladium-and platinum-carrying polymers in mass cytometry bioassays and an unexpected application as a dead cell stain.* Biomacromolecules, 2011. **12**(11): p. 3997-4010.
77. Lou, X., et al., *Polymer-Based Elemental Tags for Sensitive Bioassays.* Angewandte Chemie International Edition, 2007. **46**(32): p. 6111-6114.
78. Ornatsky, O., et al., *Highly multiparametric analysis by mass cytometry.* J Immunol Methods, 2010. **361**(1-2): p. 1-20.

79. Krutzik, P.O. and G.P. Nolan, *Fluorescent cell barcoding in flow cytometry allows high-throughput drug screening and signaling profiling.* Nature methods, 2006. **3**(5): p. 361-368.
80. Li, L., M. Dong, and X.-G. Wang, *The Implication and Significance of Beta 2 Microglobulin: A Conservative Multifunctional Regulator.* Chinese medical journal, 2016. **129**(4): p. 448-455.
81. Zunder, E.R., et al., *Palladium-based mass tag cell barcoding with a doublet-filtering scheme and single-cell deconvolution algorithm.* Nature protocols, 2015. **10**(2): p. 316.
82. De Stefano, C., et al., *Palladium (II) complexes of aminopolycarboxylic ligands in aqueous solution.* Journal of Chemical & Engineering Data, 2011. **56**(12): p. 4759-4771.
83. Liechti, T. and M. Roederer, *OMIP-058: 30-parameter flow cytometry panel to characterize iNKT, NK, unconventional and conventional T cells.* Cytometry Part A, 2019. **95**(9): p. 946-951.
84. Park, L.M., J. Lannigan, and M.C. Jaimes, *OMIP-069: Forty-Color Full Spectrum Flow Cytometry Panel for Deep Immunophenotyping of Major Cell Subsets in Human Peripheral Blood.* Cytometry Part A, 2020. **n/a**(n/a).
85. Diggins, K.E., P.B. Ferrell, and J.M. Irish, *Methods for discovery and characterization of cell subsets in high dimensional mass cytometry data.* Methods, 2015. **82**: p. 55-63.
86. Kotecha, N., P.O. Krutzik, and J.M. Irish, *Web-based analysis and publication of flow cytometry experiments.* Current protocols in cytometry, 2010. **53**(1): p. 10.17. 1-10.17. 24.
87. Chester, C. and H.T. Maecker, *Algorithmic Tools for Mining High-Dimensional Cytometry Data.* J Immunol, 2015. **195**(3): p. 773-9.
88. Amir, E.-a.D., et al., *viSNE enables visualization of high dimensional single-cell data and reveals phenotypic heterogeneity of leukemia.* Nature biotechnology, 2013. **31**(6): p. 545-552.
89. Amir el, A.D., et al., *viSNE enables visualization of high dimensional single-cell data and reveals phenotypic heterogeneity of leukemia.* Nat Biotechnol, 2013. **31**(6): p. 545-52.
90. Kimball, A.K., et al., *A Beginner's Guide to Analyzing and Visualizing Mass Cytometry Data.* Journal of immunology (Baltimore, Md. : 1950), 2018. **200**(1): p. 3-22.
91. Maaten, L.v.d., *Visualizing Data using t-SNE.* Journal of Machine Learning Research, 2008. **9**.
92. Shekhar, K., et al., *Automatic classification of cellular expression by nonlinear stochastic embedding (ACCENSE).* Proceedings of the National Academy of Sciences, 2014. **111**(1): p. 202-207.
93. Bendall, S.C., et al., *Single-cell trajectory detection uncovers progression and regulatory coordination in human B cell development.* Cell, 2014. **157**(3): p. 714-725.
94. Anchang, B., et al., *Visualization and cellular hierarchy inference of single-cell data using SPADE.* Nat Protoc, 2016. **11**(7): p. 1264-79.
95. Bendall, S.C., et al., *Single-cell mass cytometry of differential immune and drug responses across a human hematopoietic continuum.* Science (New York, N.Y.), 2011. **332**(6030): p. 687-696.

96. Qiu, P., et al., *Extracting a cellular hierarchy from high-dimensional cytometry data with SPADE.* Nat Biotechnol, 2011. **29**(10): p. 886-91.
97. Van Gassen, S., et al., *FlowSOM: Using self-organizing maps for visualization and interpretation of cytometry data.* Cytometry Part A, 2015. **87**(7): p. 636-645.
98. Bruggner, R.V., et al., *Automated identification of stratifying signatures in cellular subpopulations.* Proceedings of the National Academy of Sciences, 2014. **111**(26): p. E2770.
99. Gaudillière, B., et al., *Clinical recovery from surgery correlates with single-cell immune signatures.* Science Translational Medicine, 2014. **6**(255): p. 255ra131.
100. Vartanov, A.R., et al., *Mass cytometry identifies T cell populations associated with severe hepatotoxicity in CLL patients on upfront idelalisib.* Blood, 2018. **132**(Supplement 1): p. 4413-4413.
101. Wierz, M., et al., *High-dimensional mass cytometry analysis revealed microenvironment complexity in chronic lymphocytic leukemia.* Oncoimmunology, 2018. **7**(8): p. e1465167.
102. Blix, E.S., et al., *Phospho-specific flow cytometry identifies aberrant signaling in indolent B-cell lymphoma.* BMC Cancer, 2012. **12**(1): p. 478.
103. Chiorazzi, N., S.-S. Chen, and K.R. Rai, *Chronic lymphocytic leukemia.* Cold Spring Harbor perspectives in medicine, 2021. **11**(2): p. a035220.
104. Kipps, T.J., et al., *Chronic lymphocytic leukaemia.* Nature reviews. Disease primers, 2017. **3**: p. 16096-16096.
105. Machida, K., B.J. Mayer, and P. Nollau, *Profiling the global tyrosine phosphorylation state.* Mol Cell Proteomics, 2003. **2**(4): p. 215-33.
106. Dierck, K., et al., *Quantitative multiplexed profiling of cellular signaling networks using phosphotyrosine-specific DNA-tagged SH2 domains.* Nat Methods, 2006. **3**(9): p. 737-44.
107. Sigal, A., et al., *Generation of a fluorescently labeled endogenous protein library in living human cells.* Nature Protocols, 2007. **2**: p. 1515.
108. Bjornson, Z.B., G.P. Nolan, and W.J. Fantl, *Single-cell mass cytometry for analysis of immune system functional states.* Curr Opin Immunol, 2013. **25**(4): p. 484-94.
109. Bendall, S.C., et al., *A deep profiler's guide to cytometry.* Trends Immunol, 2012. **33**(7): p. 323-32.
110. Bendall, S.C. and G.P. Nolan, *From single cells to deep phenotypes in cancer.* Nature Biotechnology, 2012. **30**: p. 639.
111. Naeim, F., et al., *Chapter 2 - Principles of Immunophenotyping*, in *Atlas of Hematopathology (Second Edition)*, F. Naeim, et al., Editors. 2018, Academic Press. p. 29-56.
112. Seifert, M., et al., *Cellular origin and pathophysiology of chronic lymphocytic leukemia.* J Exp Med, 2012. **209**(12): p. 2183-98.
113. Schroeder, H.W., A. Radbruch, and C. Berek, *7 - B-Cell Development and Differentiation*, in *Clinical Immunology (Fifth Edition)*, R.R. Rich, et al., Editors. 2019, Content Repository Only!: London. p. 107-118.e1.
114. MoyrOn-QuirOz, J.E., et al., *Expression and Function of CD22, a B-cell Restricted Molecule*.* Scandinavian Journal of Immunology, 2002. **55**(4): p. 343-351.
115. Mak, T.W. and M.E. Saunders, *14 - T Cell Activation*, in *The Immune Response*, T.W. Mak and M.E. Saunders, Editors. 2006, Academic Press: Burlington. p. 373-401.

116. Schiött, A., et al., *CD27- CD4+ memory T cells define a differentiated memory population at both the functional and transcriptional levels.* Immunology, 2004. **113**(3): p. 363-370.
117. Naeim, F., et al., *27 - Chronic Lymphocytic Leukemia/Small Lymphocytic Lymphoma*, in *Atlas of Hematopathology*, F. Naeim, et al., Editors. 2013, Academic Press. p. 335-350.
118. Brachtl, G., et al., *The pathogenic relevance of the prognostic markers CD38 and CD49d in chronic lymphocytic leukemia.* Annals of Hematology, 2014. **93**(3): p. 361-374.
119. Malavasi, F., et al., *Evolution and Function of the ADP Ribosyl Cyclase/CD38 Gene Family in Physiology and Pathology.* Physiological Reviews, 2008. **88**(3): p. 841-886.
120. Rose, D.M., J. Han, and M.H. Ginsberg, *α4 integrins and the immune response.* Immunological Reviews, 2002. **186**(1): p. 118-124.
121. Awan, F.T. and J.C. Byrd, *Chapter 77 - Chronic Lymphocytic Leukemia*, in *Hematology (Seventh Edition)*, R. Hoffman, et al., Editors. 2018, Elsevier. p. 1244-1264.
122. Nie, Y., et al., *The Role of CXCR4 in Maintaining Peripheral B Cell Compartments and Humoral Immunity.* The Journal of Experimental Medicine, 2004. **200**(9): p. 1145-1156.
123. Mei, H.E., M.D. Leipold, and H.T. Maecker, *Platinum-conjugated antibodies for application in mass cytometry.* Cytometry Part A, 2016. **89**(3): p. 292-300.
124. Dasari, S. and P.B. Tchounwou, *Cisplatin in cancer therapy: molecular mechanisms of action.* European journal of pharmacology, 2014. **740**: p. 364-378.
125. Morbach, H., et al., *Reference values for B cell subpopulations from infancy to adulthood.* Clinical and experimental immunology, 2010. **162**(2): p. 271-279.
126. Seifert, M., et al., *Functional capacities of human IgM memory B cells in early inflammatory responses and secondary germinal center reactions.* Proceedings of the National Academy of Sciences, 2015. **112**(6): p. E546.
127. Clavarino, G., et al., *Novel Strategy for Phenotypic Characterization of Human B Lymphocytes from Precursors to Effector Cells by Flow Cytometry.* PLOS ONE, 2016. **11**(9): p. e0162209.
128. Sims, G.P., et al., *Identification and characterization of circulating human transitional B cells.* Blood, 2005. **105**(11): p. 4390-8.
129. Nagel, A., et al., *CD3-Positive B Cells: A Storage-Dependent Phenomenon.* PLOS ONE, 2014. **9**(10): p. e110138.
130. Lee, J., et al., *Identification and Characterization of a Human CD5<sup>+</sup> Pre-Naive B Cell Population.* The Journal of Immunology, 2009. **182**(7): p. 4116.
131. Qiu, P., et al., *Extracting a cellular hierarchy from high-dimensional cytometry data with SPADE.* Nature Biotechnology, 2011. **29**(10): p. 886-891.
132. Chen, K. and A. Cerutti, *The function and regulation of immunoglobulin D.* Current opinion in immunology, 2011. **23**(3): p. 345-352.
133. Gutzeit, C., K. Chen, and A. Cerutti, *The enigmatic function of IgD: some answers at last.* Eur J Immunol, 2018. **48**(7): p. 1101-1113.
134. Bartholdy, B.A., et al., *CLL intraclonal fractions exhibit established and recently acquired patterns of DNA methylation.* Blood Advances, 2020. **4**(5): p. 893-905.

135. Jovanovic, D., et al., *Possible role of CD22, CD79b and CD20 expression in distinguishing small lymphocytic lymphoma from chronic lymphocytic leukemia.* Contemporary oncology (Poznan, Poland), 2014. **18**(1): p. 29-33.
136. Klein, U., K. Rajewsky, and R. Küppers, *Human Immunoglobulin (Ig)M+IgD+ Peripheral Blood B Cells Expressing the CD27 Cell Surface Antigen Carry Somatically Mutated Variable Region Genes: CD27 as a General Marker for Somatically Mutated (Memory) B Cells.* Journal of Experimental Medicine, 1998. **188**(9): p. 1679-1689.
137. Morbach, H., et al., *Reference values for B cell subpopulations from infancy to adulthood.* Clin Exp Immunol, 2010. **162**(2): p. 271-9.
138. Wong, S.-C., et al., *Peritoneal CD5+ B-1 Cells Have Signaling Properties Similar to Tolerant B Cells.* Journal of Biological Chemistry, 2002. **277**(34): p. 30707-30715.
139. Saeko, F., et al., *Cryopreservation of human lymphocytes for assessment of lymphocyte subsets and natural killer cytotoxicity.* Journal of Immunological Methods, 1986. **90**(2): p. 265-273.
140. Matrai, Z., et al., *CD38 expression and Ig VH gene mutation in B-cell chronic lymphocytic leukemia.* Blood, The Journal of the American Society of Hematology, 2001. **97**(6): p. 1902-1902.
141. Schuh, A., et al., *Monitoring chronic lymphocytic leukemia progression by whole genome sequencing reveals heterogeneous clonal evolution patterns.* Blood, 2012. **120**(20): p. 4191-4196.
142. Bashford-Rogers, R.J., et al., *Dynamic variation of CD5 surface expression levels within individual chronic lymphocytic leukemia clones.* Exp Hematol, 2017. **46**: p. 31-37.e10.
143. Damle, R.N., et al., *Reciprocal Densities of CXCR4 and CD5 Define Subfractions of Chronic Lymphocytic Leukemia Clones Differing in Phenotype and Response to Environmental Stimuli: Towards a Better Definition of Targetable Components of Leukemic Clones.* Blood, 2014. **124**(21): p. 3322-3322.
144. Myhrvold, I.K., et al., *Single cell profiling of phospho-protein levels in chronic lymphocytic leukemia.* Oncotarget, 2018. **9**(10): p. 9273-9284.
145. Caligaris-Cappio, F. and T.J. Hamblin, *B-cell chronic lymphocytic leukemia: a bird of a different feather.* Journal of Clinical Oncology, 1999. **17**(1): p. 399-399.
146. Krutzik, P.O., et al., *Analysis of protein phosphorylation and cellular signaling events by flow cytometry: techniques and clinical applications.* Clinical immunology, 2004. **110**(3): p. 206-221.
147. Liu, B.A. and K. Machida, *Introduction: History of SH2 Domains and Their Applications.* Methods Mol Biol, 2017. **1555**: p. 3-35.
148. Karimiani, E.G., et al., *Single-cell analysis of K562 cells: An imatinib-resistant subpopulation is adherent and has upregulated expression of BCR-ABL mRNA and protein.* Experimental Hematology, 2014. **42**(3): p. 183-191.e5.
149. Rasul, E., et al., *The MEC1 and MEC2 lines represent two CLL subclones in different stages of progression towards prolymphocytic leukemia.* PloS one, 2014. **9**(8): p. e106008-e106008.
150. Obata, T., G.E. Brown, and M.B. Yaffe, *MAP kinase pathways activated by stress: the p38 MAPK pathway.* Crit Care Med, 2000. **28**(4 Suppl): p. N67-77.
151. Siegfried, Z., et al., *Regulation of the Ras-MAPK and PI3K-mTOR Signalling Pathways by Alternative Splicing in Cancer.* International journal of cell biology, 2013. **2013**: p. 568931-568931.

152. Feng, Y., J. Wen, and C.-C. Chang, *p38 Mitogen-Activated Protein Kinase and Hematologic Malignancies.* Archives of Pathology & Laboratory Medicine, 2009. **133**(11): p. 1850-1856.
153. Zarubin, T. and J. Han, *Activation and signaling of the p38 MAP kinase pathway.* Cell Research, 2005. **15**(1): p. 11-18.
154. Meloche, S. and J. Pouysségur, *The ERK1/2 mitogen-activated protein kinase pathway as a master regulator of the G1- to S-phase transition.* Oncogene, 2007. **26**(22): p. 3227-39.
155. Packham, G., et al., *The outcome of B-cell receptor signaling in chronic lymphocytic leukemia: proliferation or anergy.* Haematologica, 2014. **99**(7): p. 1138-48.
156. Chen, S.S., et al., *BTK inhibition results in impaired CXCR4 chemokine receptor surface expression, signaling and function in chronic lymphocytic leukemia.* Leukemia, 2016. **30**(4): p. 833-43.
157. Kusio-Kobialka, M., et al., *The PERK-eIF2α phosphorylation arm is a pro-survival pathway of BCR-ABL signaling and confers resistance to imatinib treatment in chronic myeloid leukemia cells.* Cell cycle (Georgetown, Tex.), 2012. **11**(21): p. 4069-4078.
158. Fruman, D.A., et al., *The PI3K Pathway in Human Disease.* Cell, 2017. **170**(4): p. 605-635.
159. Huang, X., et al., *The PI3K/AKT pathway in obesity and type 2 diabetes.* International journal of biological sciences, 2018. **14**(11): p. 1483-1496.
160. Hart, J.R. and P.K. Vogt, *Phosphorylation of AKT: a mutational analysis.* Oncotarget, 2011. **2**(6): p. 467-476.
161. Roux, P.P., et al., *RAS/ERK signaling promotes site-specific ribosomal protein S6 phosphorylation via RSK and stimulates cap-dependent translation.* The Journal of biological chemistry, 2007. **282**(19): p. 14056-14064.
162. Kim, Y.J., et al., *Mechanism of B-cell receptor-induced phosphorylation and activation of phospholipase C-gamma2.* Mol Cell Biol, 2004. **24**(22): p. 9986-99.
163. Dürig, J., et al., *ZAP-70 expression is a prognostic factor in chronic lymphocytic leukemia.* Leukemia, 2003. **17**(12): p. 2426-34.
164. Coelho, V., et al., *Identification in CLL of circulating intraclonal subgroups with varying B-cell receptor expression and function.* Blood, 2013. **122**(15): p. 2664-2672.
165. Ziegler, C.G.K., et al., *Constitutive Activation of the B Cell Receptor Underlies Dysfunctional Signaling in Chronic Lymphocytic Leukemia.* Cell Reports, 2019. **28**(4): p. 923-937.e3.
166. Zhuang, J., et al., *Akt is activated in chronic lymphocytic leukemia cells and delivers a pro-survival signal: the therapeutic potential of Akt inhibition.* Haematologica, 2010. **95**(1): p. 110.
167. Sanford, D.S., et al., *Three Newly Approved Drugs for Chronic Lymphocytic Leukemia: Incorporating Ibrutinib, Idelalisib, and Obinutuzumab into Clinical Practice.* Clinical Lymphoma Myeloma and Leukemia, 2015. **15**(7): p. 385-391.
168. Lannutti, B.J., et al., *CAL-101, a p110delta selective phosphatidylinositol-3-kinase inhibitor for the treatment of B-cell malignancies, inhibits PI3K signaling and cellular viability.* Blood, 2011. **117**(2): p. 591-594.
169. Wang, L., et al., *Advances in targeted therapy for malignant lymphoma.* Signal Transduction and Targeted Therapy, 2020. **5**(1): p. 15.
170. Kang, Z.-J., et al., *The Philadelphia chromosome in leukemogenesis.* Chinese journal of cancer, 2016. **35**: p. 48-48.

171. Arcaro, A. and A.S. Guerreiro, *The phosphoinositide 3-kinase pathway in human cancer: genetic alterations and therapeutic implications.* Current genomics, 2007. **8**(5): p. 271-306.
172. Varticovski, L., et al., *Activation of phosphatidylinositol 3-kinase in cells expressing abl oncogene variants.* Mol Cell Biol, 1991. **11**(2): p. 1107-13.
173. Skorski, T., et al., *Phosphatidylinositol-3 kinase activity is regulated by BCR/ABL and is required for the growth of Philadelphia chromosome-positive cells.* Blood, 1995. **86**(2): p. 726-36.
174. Sattler, M., et al., *Critical role for Gab2 in transformation by BCR/ABL.* Cancer Cell, 2002. **1**(5): p. 479-92.
175. Adlung, L., et al., *Protein abundance of AKT and ERK pathway components governs cell type-specific regulation of proliferation.* Mol Syst Biol, 2017. **13**(1): p. 904.
176. Duckworth, A.D., et al., *Multiplexed profiling of RNA and protein expression signatures in individual cells using flow or mass cytometry.* Nat Protoc, 2019. **14**(3): p. 901-920.
177. Guièze, R. and C.J. Wu, *Genomic and epigenomic heterogeneity in chronic lymphocytic leukemia.* Blood, 2015. **126**(4): p. 445-453.
178. Burger, J.A., et al., *Clonal evolution in patients with chronic lymphocytic leukaemia developing resistance to BTK inhibition.* Nature communications, 2016. **7**: p. 11589-11589.
179. Furusato, B. and J.S. Rhim, *CXCR4 and cancer.* Chemokine Receptors in Cancer, 2009: p. 31-45.
180. Sun, X., et al., *CXCL12 / CXCR4 / CXCR7 chemokine axis and cancer progression.* Cancer metastasis reviews, 2010. **29**(4): p. 709-722.
181. Shaim, H., et al., *The CXCR4–STAT3–IL-10 Pathway Controls the Immunoregulatory Function of Chronic Lymphocytic Leukemia and Is Modulated by Lenalidomide.* Frontiers in Immunology, 2018. **8**(1773).